



核融合炉固体増殖ブランケット用セラミックス材料 に関する研究

メタデータ	言語: English 出版者: 公開日: 2021-06-23 キーワード (Ja): キーワード (En): 作成者: 金, 鍾壹 メールアドレス: 所属:
URL	https://doi.org/10.15118/00010400

核融合炉の固体増殖ブランケット用
セラミックス材料に関する研究

Study on the ceramics materials of solid-
breeding blanket for fusion reactor

Jong-II Kim

核融合炉の固体増殖ブランケット用
セラミックス材料に関する研究

**Study on the ceramics materials of solid-
breeding blanket for fusion reactor**

指導教官：岸本 弘立 教授

工学専攻

金 鍾壹

2020年12月

室蘭工業大学・学位論文

Acknowledgement

I would like to extend my appreciation to the many people who have contributed to this research both directly and indirectly, many of who are not included here.

I would like to give my sincere thanks to Prof. Hirotatsu Kishimoto. He has greatly influenced my learning and my life since I became a student in his laboratory. I have been able to investigate what I would like to do with his appropriate advice had a lot of precious experiences in my life. I was given a lot of chances to present my work at domestic and at international conferences and those experiences enlarged my knowledge and point of view. I consider myself fortunate to have been on of Prof. Hirotatsu Kishimoto.

I would like to appreciate to Dr. Joon-Soo Park. I was always surprised by his innovative ideas came up from his unique sight on things. He always helped my study, I totally respect his toughness and attitude to research. My engineering knowledge and skills truly improved by working with him.

I would like to express my deep gratitude to Dr. Yi-Hyun Park. He has given me many interesting subjects and precious chances for my study. When I study the Korea Institute of Fusion Energy (KFE), he had been continuously encouraging and guiding me as a teacher. I respect not only wide knowledge on fusion materials and fusion technology, but also his gentle, kind, and patient personality. I could not have completed this work without his kind and proper guidance.

I appreciate very much the discussion with assistant Prof, Nakazato Naofumi. His detailed suggestions and advices often help me make sense out of my studying and solve the problems that might have troubled me several days.

Many people have been involved in this research through various collaborations: Dr. Seungyon Cho, Dr. Mu-Yong Ahn, Dr. Changsuk-Kim, Dr. Youngmin Lee, Dr. Hyosung Kwon of KFE in South Korea, and Dr. Hiroyasu Tanigawa, Dr. Takashi Nozawa, Dr. Jae-Hwan Kim, Dr. Ju-Hyeon Yu of Quantum and Radiological science and Technology (QST) in Japan, and Prof. Akira Kohyama of Kyoto University and Mr. Byung-Min Kim of Muroran Institute of Technology.

I would like to thank the committee for being generously flexible in regard to scheduling of the defense times for both the ‘proposal’ of this work as well as the dissertation defense.

Finally, as a personal note, I would like to show my appreciation to my family for sacrificing to allow me to pursue my education.

December 2020, Jong-II Kim

Table of Contents

1. Introduction	1
1.1 Motivation	3
1.2 Objective and outline of research	6
References	10
2. Background	11
2.1 Functional & structure materials for breeding blanket in fusion reactor	18
2.1.1 SiC_f/SiC composites	20
2.1.2 Tritium Breeding Materials	28
References	35
3. Mechanical properties of NITE-SiC/SiC composites with different fiber architecture	39
3.1 Introduction	39
3.2 Experimental	40
3.2.1 Materials	40
3.2.2 Testing method	41
3.3 Results & Discussion	42
3.3.1 Mechanical properties depending on the architecture	42
3.3.2 Shear elastic modulus depending on the architecture	48
3.4 Summary	50
References	52
4. Oxidation behavior of NITE-SiC/SiC composites	53
4.1 Introduction	53
4.2 Experimental	54

4.2.1	Materials	54
4.2.2	Oxidation test	55
4.3	Results & Discussion	59
4.3.1	Oxidation rate of carbon in atmosphere.....	59
4.3.2	Oxidation of NITE-SiC/SiC composite with/without CVD-SiC outer coating	61
4.4	Summary.....	67
	References.....	69
5.	Improvement of Slurry Droplet Wetting method for Li_2TiO_3 Pebbles	71
5.1	Introduction	71
5.2	Experimental	72
5.2.1	Initial Material & Mixing Condition.....	73
5.2.2	Dynamic Interactions between Slurry and Glycerin with Boric acid.....	74
5.2.3	Surface Tension.....	75
5.2.4	Penetration of Slurry into the Glycerin with Boric acid	76
5.2.5	Optimization of heat-treatment conditions	77
5.3	Results & Discussion	82
5.3.1	Effects of surface tension on the shaping of Li_2TiO_3 pebbles	82
5.3.2	Pebbles shaping with different conditions of liquid bath or injection method	84
5.3.3	Penetration of slurry into the glycerin with boric acid.....	85
5.3.4	Proposal of suitable heat-treatment conditions for Li_2TiO_3 pebbles.....	94
5.4	Summary.....	101
	References.....	103
6.	Proposal maximum operating temperature of Li_2TiO_3 pebble bed.....	106
6.1	Introduction.....	106

6.2	Experimental	107
6.3	Results & Discussion	109
6.3.1	Sintering phenomena of Li_2TiO_3 pebble bed	109
6.3.2	Creep phenomena of Li_2TiO_3 pebble bed	112
6.4	Summary	114
	Reference	115
7.	Chemical Compatibility between Conceptual Design of Li_2TiO_3 Pebbles bed and Structure Materials	116
7.1	Introduction	116
7.2	Experimental	118
7.2.1	Materials	118
7.2.2	Method	119
7.3	Results & Discussion	120
7.3.1	Compatibility between SiC & SiC/SiC composites and Li_2TiO_3 Pebble Bed	120
7.4	Summary	122
	References	123
8.	Summary and conclusions	125
	Research Activity	127

1. Introduction

“Science has been a contribution to the human progress a lot, and in the future, it will be continued to make numerous progress from the ethics studies”

The human has made numerous developments since it has advent on the earth. This development not only improves the creature’s comfort such as food, clothing, and shelter but also guarantees welfare, convenience and so on. Continuously, human will make a great effort for sustainable development (SD) [1,2].

The human life is closely connected with energy. The foods we consume are our body energy source, which allows us to maintain body temperature, walk, and some exercise. Further being primitive, the vegetation has be photosynthesis on the primary earth by the solar. Heterotrophs such as Homo sapiens could use more energy evolved to exploit. Indeed, the ability to use energy extrasomatically (outside the body) allows humans enables human beings to use far more energy than any other heterotroph that has evolved. The control of fire and the exploitation of fossil fuels have made it possible for Homo sapiens to release, in a short time, vast amounts of energy that accumulated long before the species appeared.

From the view point of the energy, the history human can be recorded by deformation of the main source of fuel for energy. The Neolithic era has historical value in that humanity began to grow grain, a stable energy supply. The Neolithic era has historical value in that humanity began to grow grain, a stable supply available energy. Hence, humanity can accumulate surplus products by harvest crops compared to the previous era survived by foraging. In addition, a national system is created to maintain surplus products, while a war of aggression occurs.

By using extrasomatic energy to modify more and more of its environment to suit human needs, the human population effectively expanded its resource base so that for long periods it has exceeded contemporary requirements. The world's present population of over 5.5 billion is sustained and continues to grow through the use of extrasomatic energy [3].

With the course of time, the history of human faced revolutionary a changeover period through the industrial revolution. At the close of the 17th century, the breaking down feudalism of England, and the wool industry developed centered on farmers. The first industrial revolution began in the 18th century

when a steam engine improved by James Watt based on abundant underground resources (coal, iron) that in England. Machines were invented to replace humans or horses and cattle. The power to move them came from the coal. The driving force of the industrial revolution was coal. However, an engine with a new internal combustion engine was developed instead of the steam engine, which used to occupy most of the power with the continuous development of technology. After a developed internal combustion engine using coal gas was applied in the light industry, Gottlieb Daimler & Wilhelm Maybach developed a gasoline engine in 1885. The revolution of conveyance, which is the starting point of today's automobile industry, took place. Indeed, a world in which the main energy is changed from coal to oil has begun.

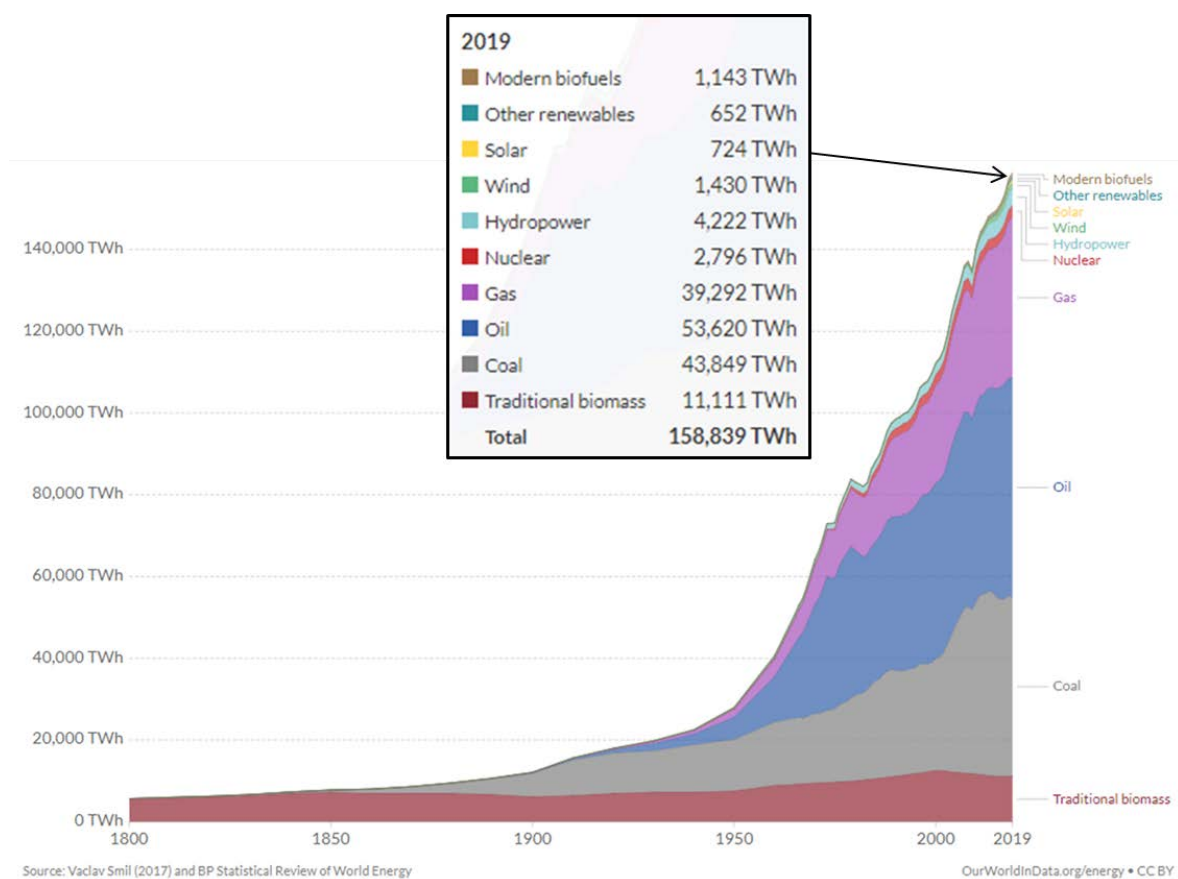


Figure 1.1 Global primary energy consumption [4]

Source: ourworldindata.org/grapher/global-primary-energy

With the continuous industrial revolution and the advancement of science, the human needs more energy with overtime. Consumption of energy and mineral resources has been increasing sharply with world economic growth over the past half century. The fossil fuels supply more than 90% of all the energy consumed today [5]. This rapid burst in energy and mineral resources consumption has been

induced the global problems of depletion of resources and destruction of the environment.

Geologists estimate that the only 210~340T/ of petroleum resources deposited in the earth [6]. It means that petroleum resources of the world will be depleted at 41 years later. In the case of natural gas and coal. Their resources are also extremely limited.

The effects of two oil crises, caused by the Arab oil embargo of 1973-1974 and Iran/Iraq war in 1979, raised ten times the oil price of 1973. The lack of fossil fuels will bring about the third oil shock in near future. In addition, the extravagant amount of CO₂ (40 billion ton per year), SO_x, NO_x and etc. has been generated by the combustion of fossil fuels. It leads to serious environmental problems such as the greenhouse effect, the breakdown of O₃ layer, and the acid rain. The reduction of the greenhouse gas emission is achieved by greater use of renewable energy and nuclear power and improved energy efficiency.

1.1 Motivation

Humanity continues to form an advanced society, it is assured that there will be developing civilizations and inventions in the future. The energy source used has changed according to the developed society. Until now, energy sources are highly dependent on the earth's underground resources. These underground resources are limited cause many ecosystem disturbances with environmental destruction in their use. These problems will worsen over time, which is recognized to the populace more than in the past. Most people prefer using recycle and working on energy saving for the environment. Targeting public awareness, commercial companies are also aiming to grow and leap forward through the development of eco-friendly products. In addition, the expansion of renewable energy is being encouraged by the state and organizations. The expansion of renewable energy is desirable. It is eco-friendly above all, a sustainable energy source. However, many problems remain to be solved. Solar energy cannot generate electricity at night and it is strongly affected by sunlight during the day. Wind power also has jagged power generation depending on the season and weather. To compensate for such intermittent, electricity is stored in an energy storage system (ESS) and used when needed, but it is still unstable and expensive. Another problem with renewable energy is an enormous site. In countries with a small area and a large population, securing a site for generating renewable energy is difficult. Both problems are not easy to solve simple, they stand out as problems of cost and efficiency. However, safety is the focus of public opinion due to the connection with fission energy, which cannot be overlooked. Fusion has a clear advantage over fission at this point. Fusion is in principle safe. It is neither exploding nor out of control. Fission plants must contain significant amounts

of fuels such as uranium or plutonium to last for several years, fusion plants only need very little deuterium or tritium fuel. Usually, about 1 gram of fuel can hold the reaction for a few seconds. If fuel is not supplied continuously, the fusion power plant shuts down or knock-off. The second safety issue is the radioactive waste problem. There are two types of waste produced by fission reactors. The most difficult is the treatment and store of waste from the fission fuel cycle. The fusion fuel cycle does not generate such radioactive waste. The helium gas generated from the fusion fuel cycles, which is neither toxic nor radioactive. Tritium used as a fuel itself has radioactivity, but its half-life is 12.3 years, decaying relatively quickly [7]. In addition, all of the generated tritium is rapidly burned in the power plant through supporting system. Therefore, it is safe for a fusion power plant that there is no need to move radioactive fuel or take it out of the power plant. The raw materials for making fusion fuel are lithium and water, both of which are not completely radioactive. Lithium is enough to last thousands of years, and deuterium exists in seawater to an infinite degree. These raw materials are widely distributed in almost every location on the ground, making it impossible for a single country to monopolize. The second source of waste from nuclear power plants is the structure materials that make up the reactor. Structure materials take radioactive by neutrons emitted during nuclear reactions. Fusion & Fission are similar in this respect in a broad sense, certain parts of the materials of a fusion power plant may have very strong radioactivity. The work on the parts that need to be stored, repaired, or replaced is carried out by a remotely controlled robot-arm. The collected materials are stored in a thick concrete shield. However, the disposal time of the waste of structure materials from fusion energy is much shorter than that of fission waste. A nuclear fusion power plant can be safely disposed of if it is shielded for about 100 years after the end of its life. Furthermore, this waste can be reduced by selecting materials with considered design. The radiation level remaining about 100 years after a fusion plant shuts down can be made close to the amount left by a coal plant with careful design and material selection. It will be surprising that radiation is also emitted from coal power plants. When coal is burned, no new radiation is emitted, but coal contains uranium in addition to many other toxic factors, and that uranium is released into the environment when it is burned. The proportion of uranium in the coal is relatively small, but it is a significant amount considering the total content. Considering the amount of electricity used in a typical industrial city, 3.5 million barrels of coal must be burned to obtain energy that uses 1 gigawatt of electricity for a year, which the uranium contained in it exceeds 5 tons. This amount is actually more than the amount of uranium that must be used in a fission reactor to supply the stated amount of electricity. Some of the uranium is released into the air, but most of it remains as ash. It is buried in landfills.

Ceramics are defined as ‘artificially made non-metallic inorganic solid materials’. The etymology of ceramics is the Greek word *keramikos*, which is derived from the ancient Sanskrit word meaning ‘burning’. Ceramics are old and new material from the beginning of humankind to the present [8-9]. It was made as earthenware in the age of stone tools and earthenware and has supported the text of each

country as pottery of arts and crafts according to the progress of civilization. When the modern industry started, it has supported the modern industry in Japan as a material with excellent material properties such as heat resistance, wear resistance, voltage resistance, and chemical resistance. Today's ceramics, which are given more functionality, have become an indispensable industrial material in many situations.

Currently, ceramics are an indispensable industrial material along with metal materials such as iron and organic materials such as plastics. Among them, ceramics, which use high-purity refined raw materials and artificially adjust the composition and microstructure in order to maximize the characteristics of the materials, often use natural raw materials, such as ceramics, cement, and glass. In contrast to traditional ceramics such as these, they are called fine ceramics. Silicon carbide used in this study is also one of the fine ceramics. Fine ceramics, which have various chemical bonds such as ionic bonds and covalent bonds, have great expectations for future development and development as advanced materials that exhibit properties different from those of other materials.

Years	Developed fine ceramics
1920s	Cobalt ferrite (ferrite magnetic)
1940s	Barium titanate
1950s	Zirconate titanate Semiconductor thermistor Translucent ceramics Artificial diamond
1960s	C/C composites
1970s	Non-oxide ceramics Zinc oxide varistor Titanium oxide catalyst
1980s	High-temperature superconducting ceramics High quality gallium nitride crystal fullerenes for blue light emitting diodes
1990s	carbon nanotube

Table 1.1 History of development of fine ceramics

Electronics-related materials have made particularly significant progress in fine ceramics. By increasing the purity, the electromagnetic properties of many substances have been clarified, and materials with good properties have become available. As an example, an oxide having a perovskite crystal structure contains many substances having different components. From these substances, barium

titanate ferroelectrics, which have an extremely large relative permittivity compared to conventional materials, were discovered in the 1940s, and new materials that exhibit superconductivity at high temperatures were discovered in the 1980s. Table 1-1 [8-9] shows an example of the development of fine ceramics. From a lot of research, not only in the field of electronics, but also in the fields of structural materials, biomaterials, etc., many fine-ceramic products support modern society, and in order to further expand the range of applications, stability as an industrial product is required. Improving reliability is an issue to be solved. One way to solve this problem is the compounding described in the section.

One of the important achievements in fusion reactor is the improvement of generation energy [10]. The energy is generated the transition from kinetic energy of neutron to thermal energy in fusion reactor. Therefore, the generation energy is important the thermal energy. Namely, the fusion reactor is need the operation at high temperature. Generally, the fusion reactor such as JT-60, TFTK, JET, and ITER is conducted the steels to the structure materials. However, the steels such as stainless steel and reduced activation ferritic martensitic steel are have weak-point at high temperature, which is connected the limit of operation conditions. The ceramic materials can be increasing the operation parameter such as operation temperature.

1.2 Objective and outline of research

At present, fusion reactor are used the deuterium (D) - tritium (T) reaction because it occurs relatively at low-temperature with high reactivity. A part of breeding blanket is important in fusion reactor, which is located between the fusion plasma and vacuum vessel. The main functions of breeding blanket are the generation and transport of heat from the neutron of kinetic energy, the tritium breeding from the nuclear reaction of neutrons and lithium, the neutron shielding and so on. The goals for fusion power plant are to produce energy in as safe, economical, and benign a manner as possible. This thesis includes that the study of ceramic materials for application as structure/functional materials in solid-breeding blanket for generation of energy in as safe, economical.

The SiC/SiC composites have many desirable characteristics when compared to metals. One of the most attractive characteristics of SiC/SiC composites is high strength at high temperatures with light weight. Typically, the operating temperatures of metals such as reduced activity ferritic metals do not exceed 550 °C, while the temperature ceramics can potentially be expected between 1000 and 1500 °C. It is expected that the enable operation of the plant and efficient energy production compared to metals.

Despite advantages of SiC/SiC composites over metals, composites with complicated shapes have own properties depending on their fiber reinforcing architectures.

A tritium breeding material demands to withstand several radiation-induced damage and high temperatures, as well as to be compatible with the structural material. Lithium metatitanate (Li_2TiO_3) has been chosen as the ceramic material in solid-breeding blanket. Li_2TiO_3 has reasonable lithium density, high melting temperature, low activation, good chemical stability, and excellent tritium release performance, relative to all other candidates such as Li_2O , Li_4SiO_4 , Li_2ZrO_3 , LiAlO_2 , and so on. However, the development such as fabrication method and compatibility test with ceramic structure of Li_2TiO_3 is not enough in terms of tritium breeding ratio (TBR).

In this paper, a development of ceramic materials that can be applied to the structural/functional materials of the solid-breeding blanket was conducted to effectively increase the in terms of energy production efficiency of nuclear fusion reactors. In order to understand the mechanical properties change according to the fiber reinforced architecture of SiC/SiC composite that can be applied as a structural material, the inter-laminar shear strength and the fracture mechanism were examined. In the case of tritium breeding material, a manufacturing method for Li_2TiO_3 breeder was developed for improving the physical properties. And the operating conditions of Li_2TiO_3 breeder are proposed in a solid-breeding blanket of the fusion reactor. A details are as follows.

Chapter 1 is an introduction, where the importance of fusion energy toward the continued growth of a sustainable society on earth is emphasized. The motivation and objective of this study are also explained. Chapter 2 presents the background of study on SiC/SiC composites, Li_2TiO_3 breeder, and the fusion energy by referring to the literatures. Chapter 3 cares about the mechanical properties of SiC/SiC composites with different fiber reinforced architectures. Though the mechanical strength values such as in-plane and inter-laminar shear strength were not to be significantly modified, but the elastic modulus was affected by the fiber reinforced architecture. Intersections of the fiber bundles are suggested to behave as obstacles for deformation and crack propagation according to the comparison of fracture surface and load-displacement curves. Chapter 4 discusses the oxidation behavior of SiC/SiC composites. The weight change of the composites was confirmed at 600 °C in oxidizing environment. Because the carbon exists at the matrix/fiber interface in SiC/SiC composites, the degradation of mechanical properties is considered to be caused by the oxidation of carbon. The SiC coating for the composites is suggested to be necessary as an oxidation barrier.

Chapter 5 describes the improvement of a slurry droplet wetting method for Li_2TiO_3 breeder to obtain good physical properties. The fabricated Li_2TiO_3 pebbles were satisfied the properties such as spherical shape with 1mm diameter, suitable grain boundaries (5~10um), and a homogeneous microstructure. The carbon exists in the Li_2TiO_3 breeder because the organic binder is added to the

slurry for the shaping. Because the residual carbon is expected to cause the discoloration of the sintered body during the sintering in the He + 1% H₂ atmosphere, the pebbles need to be thermally treated at 600 °C for 20h before the sintering process. Chapter 6 proposes optimal operation conditions of the Li₂TiO₃ pebble bed based on the sintering and creep behavior during the operation. Chapter 7 discusses the compatibility between SiC/SiC composites and Li₂TiO₃ tritium breeding materials. The optimal operation conditions of the blanket made by the SiC/SiC composites and Li₂TiO₃ breeders are suggested.

A design with the improved structural integrity of the breeding blanket is expected from the evaluation of the mechanical properties of the SiC/SiC composite material with a different fiber reinforcing architecture. Furthermore, the Li₂TiO₃ tritium breeding materials with suitable physical properties were fabricated by improvement fabrication method, which is expected to increase the efficiency of the fusion power reactor applied to the breeding blanket concept.

<p style="text-align: center;">Chapter 1 Motivation and objective</p>	
<p style="text-align: center;">Chapter 2 Functional & Structure materials based on the ceramics for solid-breeding blanket of fusion reactor</p>	
<p style="text-align: center;">Chapter 3 Mechanical properties of NITE-SiC/SiC composites with different fiber reinforcing architecture</p>	<p style="text-align: center;">Chapter 5 Improvement of fabrication method for Li_2TiO_3 tritium breeding materials</p>
<p style="text-align: center;">Chapter 4 Oxidation behavior of NITE-SiC/SiC composites</p>	<p style="text-align: center;">Chapter 6 Proposal maximum operating temperature of Li_2TiO_3 pebble bed</p>
<p style="text-align: center;">Chapter 7 Compatibility between conceptual design of Li_2TiO_3 pebble bed and structure materials blanket of fusion reactor</p>	
<p style="text-align: center;">Summary</p>	

Figure 1.2 Layout of dissertation

References

- [1] Justice Mensah, Sustainable development: Meaning, history, principles, pillars, and implications for human action: literature review, 5 (2019) 1.
- [2] Shafayet Ullah Sabuj, Syed Mithun Ali, Kazi Wahadul Hasan, Sanjoy Kumar Paul, Contextual relationships among key factors related to environmental sustainability: Evidence from an emerging economy, Sustainable Production and Consumption, 27 (2021) 86-99.
- [3] David Price, Energy and Human Evolution, Population and Environment, 16 (1995) 301-319.
- [4] ourworldindata.org/grapher/global-primary-energy
- [5] www.erca.go.jp
- [6] IEA, CO2 Emissions from Fuel Combustion Highlights 2011 Edition
- [7] A. V. Grosse, W. M. Johnston, R. L. Wolfgang, and W. F. Libby, Tritium in nature, Science, 113 (1951) 1-2.
- [8] M.F. Ashby 著, 金子純一, 大塚正久 訳, 機械設計のため材料選定, 内田老鶴園 (1997)
- [9] 日本セラミックス協会編, トコンやさしいセラミックスの本, 日刊工業新聞社 (2009)
- [10] M. Kikuchi, Steady state tokamak reactor based on the bootstrap current, Nuclear Fusion 30 (1990) 265-276.

2. Background

The mass defect can be explained to the Einstein's equation $E=mc^2$, and represents the energy that was released when the nucleus was formed. This is the basic principle of nuclear fusion energy, the process of fusion of light atoms such as hydrogen into the heavy atoms. For the understanding, the average binding energy per nucleon according to the total number of protons and neutrons in the nucleus (i.e. atomic mass) is shown in figure 2.1 [4]. Where the x-axis the nucleons number of 56 is presented the maximum value of the y-axis, it means that the corresponding elements are the most stable elements. Elements located on both end areas have excess mass, which can be moved to the center of the curve from that the excess mass is released in the form of energy. Indeed, two light atoms react with each other to form a heavy atom (nuclear fusion). On the other hand, a heavy atom is divided split into two light atoms (nuclear fission).

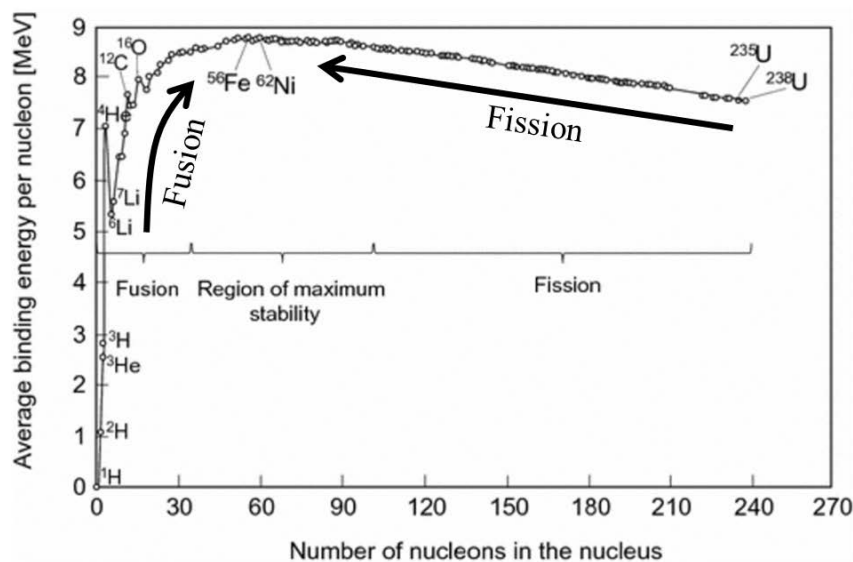


Figure 2.1 Experimental values of the average binding energy per nucleon as a function of the mass number, which adopted from Ref. [4]

The various fusion reaction can occur as shown in Figure 2.2, however, the Deuterium (D) - Tritium (T) reaction is the most viable reaction among them because it has relatively high reactivity at the low temperature. Deuterium can be extracted by electrolysis of seawater (0.03g/1L), and tritium can be obtained through the reaction of lithium and neutrons. Lithium is buried in an amount that can be used for about 15 million years on the earth. About specific of how can obtained tritium is described in

section 2.1.2. In the case of the D-T reaction, the energy generated per number of times is 17.6 MeV. This is enormous energy even compared to fission power generation. In the case of fusion power generation, the reactor system is automatically stopped when the fuel supply is interrupted. Even if there is a malfunction of equipment or something it is immediately extinguished without risk of explosion. In addition, there is no high-level radio-waste just a small amount of radio-waste with a very short half-life exists. Based on this, the reduction of radio-waste is expected in about 50 years compared to coal-fired power plants.

Fusion energy is attracting attention as an inevitable alternative energy source in the future due to its large capacity and eco-friendly characteristics for the development of fusion into a sustainable energy source, there are two primary requirements. First one is that it must be economically competitive and second, it must have public acceptance. Decisions regarding the viability of fusion energy will depend on the alternatives and competition for energy generation, and the risk associated with the implementation of a new technology. It is widely recognized that fusion offers a potential for significant safety and environmental advantages as an energy source. However, it is generally concluded that it will be a major challenge to make fusion energy economically competitive. It is also clear that the first-wall/blanket system will have a dominant impact on both the economic and the safety/environmental issues. Since most of the fusion energy is recovered in this system, it will operate at the highest temperature and will be exposed to the highest radiation levels [1].

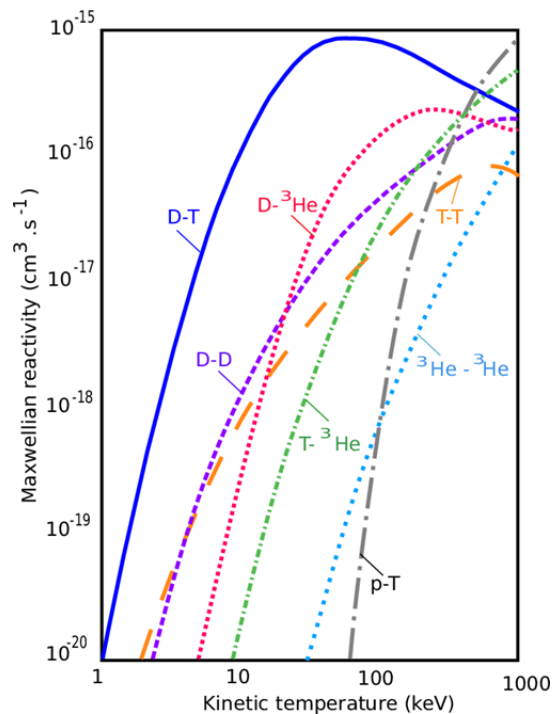


Figure 2.2 Fusion reactivity depending on the temperature, which adopted from Ref. [3].

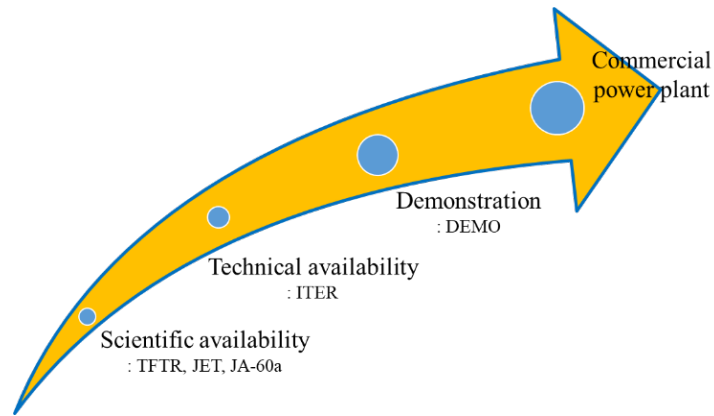


Figure 2.3 Fusion energy roadmap.

The roadmap of fusion development is required as shown in figure 2.3 in order to reach a commercial power plant based on the scientific possibilities. Table 2.1 shows the world's main nuclear testing equipment for scientific possibilities, which is the first step on the milestone (in table 2.1 is not including the contents about table 2.2).

The blanket is the component which will be located between the fusion plasma and vacuum vessel and provides the main thermal and nuclear shielding to the vessel and other components (in figure 2.4).

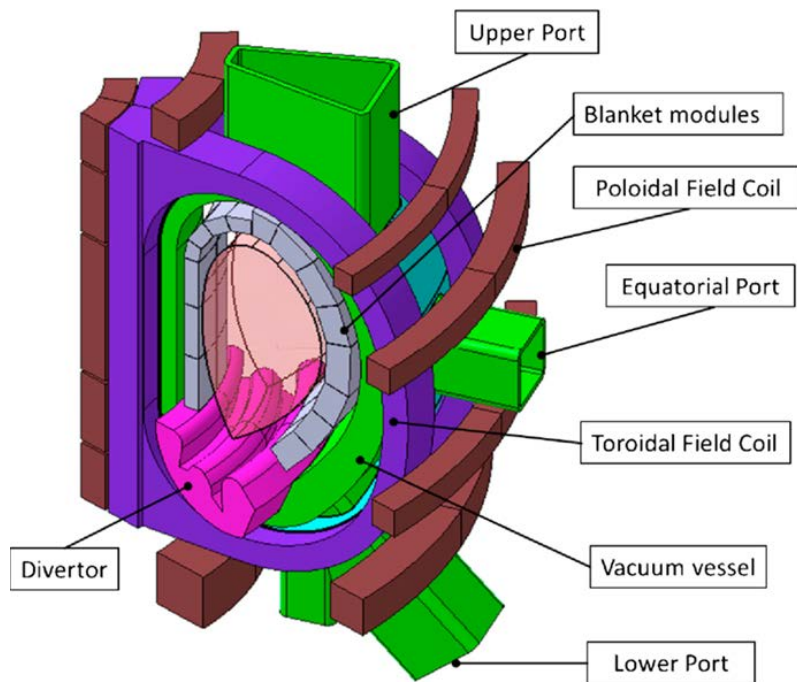


Figure 2.4 Schematic of fusion reactor and each components (this figure is marked based on the European DEMO [31]).

This component may correspond to the reactor core of the fission plant where neutron energy is converted into the heat which is removed by coolants. The blanket also works as tritium producer and thermal generator in the fusion reactor. To realize these goals, many different concepts were proposed. All of the demonstration (DEMO) concepts could be classified with regard to the breeding materials into two categories [25-29]: solid ceramic and liquid breeders with the options of self-cooled or separately cooled versions (a detail is shown in figure 2.6). These concepts also depend on development of structure materials and the design parameters, such as thermal exchange ratio, neutron flux and Tritium Breeding Ratio (TBR). The main functions of blanket are:

- 1) The generation of heat energy from neutron energy
- 2) The tritium breeding (recycle of tritium)
- 3) The shielding of neutron (i.e. protecting fusion system)

Fusion energy can offer an abundant source of energy for these processes and can be improved by the development of high performance blanket. In this phase, the high temperature blanket types are assessed and a high temperature blanket concept for hydrogen production is proposed, shown in Table 2.2 [30].

At present, Thousands of engineers and scientists have contributed to the design of the International Thermonuclear Experimental Reactor (ITER) since the idea for an international joint experiment in fusion was first launched in 1985 for verification of technical possibilities. The ITER Members “China, the European Union, India, Japan, Korea, Russia and the United States” are now engaged in a 35-year collaboration to build and operate the ITER experimental device, and together bring fusion to the point where a demonstration fusion reactor can be designed. The drawing of technical design for ITER is shown in Figure 2.5 [2].

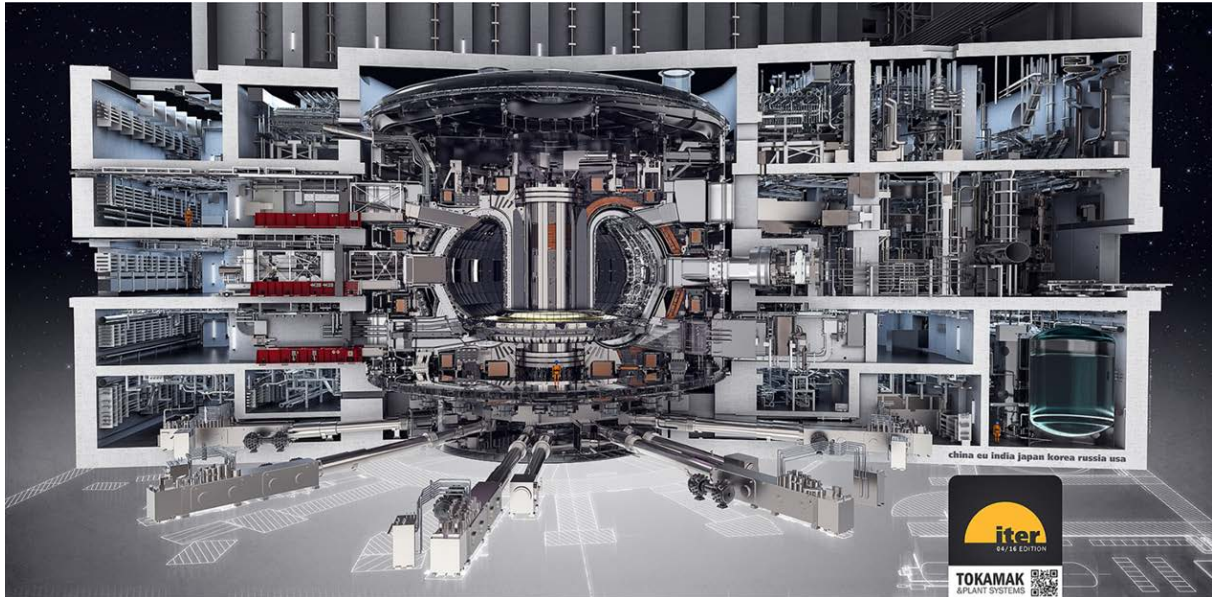


Figure 2.5 Drawing of the ITER tokamak and integrated plant systems [2].

ITER will be the first fusion device to produce net energy. ITER will be the first fusion device to maintain fusion for long periods of time. And ITER will be the first fusion device to test the integrated technologies, materials, and physics regimes necessary for the commercial production of fusion-based electricity [2]. The ITER has been performed [2] specifically to:

- 1) Product 500 MW of fusion power
- 2) Demonstration the integrated operation of technologies for a fusion power plant
- 3) Achievement a deuterium-tritium plasma in which the reaction is sustained through internal heating
- 4) Testing of tritium breeding
- 5) Demonstration the safety characteristics of a fusion device

The ITER project progress to aim the technical specification, which has to perform horizontally with the innovated design concept and R&D of materials. In addition to the high performance requirements of the fusion system, it is important to utilize 'low activation' materials in the first-wall/blanket system in order to achieve the ultimate safety and environmental advantages of fusion. The products of the deuterium + tritium ($D + T$) fusion reaction are helium, which is environmentally benign, and an energetic neutron, which is needed to react with lithium to breed tritium for the fuel cycle.

Distinguish	Device	Location	period	Major Radius (m)	Minor radius (m)
Magnetic confinement	Tokamak-15 (T-15)	Russia	1988-1995	2.43	0.7
	KAERI Tokamak-1 (KT-1)	South Korea	1985-1997		
	KSTAR	South Korea	2007-present	1.8	0.5
	Tokamak Fusion Test Reactor (TFTR)	USA	1982-1997		
	Joint European Torus (JET)	UK	1984-present		
	Japan Torus-60 (JT-60)	Japan	1985-2010	3.3	1
	JT-60 super, advanced (JT-60 SA)	Japan	expected 2020		
	JFT-2M	Japan	1983-2004	1.3	0.35
	TRIAM-1M	Japan	1987-2005	0.8	0.02
	JIPPT-II U	Japan	1983-1984	0.93	0.22
Inertial confinement	Shiva and Nova	USA			
	ETIGO	Japan			

Table 2.1 Fusion device in the world for development of fusion energy

Fusion reactor	ARIES-AT	TAURO	A-SSTR-E	A-HCPB	W/Li/He	EBOLVE	V/Li/He	V/Li	FFHR-2	A-DC	ARIES-ST	FDS-II	FDS-III
Fusion power (GW)	1.7	3	4	4.5	3.5	3.5	1.9	2.43	1	3.4	2.9	2.5	2.6
FW heat flux (MW/m ²)	0.26 (ave.)	0.5 (ave.)	1.0 (ave.)	0.6 (peak)	2.0 (peak)	2.0 (peak)	0.3	0.1	0.1	0.45 (ave.)	0.46 (ave.)	0.54 (ave.)	0.8 (ave.)
Neutron all loading (MW/m ²)	3.2 (ave)	2 (ave)	6 (ave)	2.76 (ave)	7 (peak)	10 (peak)	2.9 (ave)	2.5 (ave)	1.7	2.27 (ave)	4.1 (ave)	2.72 (ave)	4 (ave)
Structure material	SiC/SiC composites		W-alloy		V-alloy		RFAM						
Maximum allowed temperature	1000	1000	1100	1000	1400	1400	700	700	700	550	550	550	550
FW material, Kth (W/mk)	20	15	15	15	85 (at 1400K)	85 (at 1400K)	35	27 (at 700K)	35	33	33	33	33
Fuel form	L	L	S	S	L	L	L	L	L	L	L	L	L
Tritium breeder (neutron multiplier)	Pb-Li	Pb-Li	Li ₂ TiO ₂ (Be)	Li ₄ SiO ₄ (Be)	Li	Li	Li	Li	Flibe(Be)	Pb-Li	Pb-Li	Pb-Li	Pb-Li
Coolant	Pb-Li	Pb-Li	He	He	He	Li	He	Li	Flibe	He/Pb-Li	He/Pb-Li	He/Pb-Li	He/Pb-Li
Coolant Tin	654	650	600	350	800	~800	400	250	450	450 (Pb-Li)	550 (Pb-Li)	480 (Pb-Li)	400 (Pb-Li)
Coolant Tout	1100	850	900	700	1100	1200	650	650	700	700 (Pb-Li)	700 (Pb-Li)	700 (Pb-Li)	1000 (Pb-Li)

Table 2.2 High temperature blanket designs and key parameters [30].

2.1 Functional & structure materials for breeding blanket in fusion reactor

The challenge is to develop structural materials which maintain high performance during prolonged exposure to high thermal and radiation flux. In addition to their structural properties, they may need chemical compatibility with coolants and be relatively easy to manufacture. The thermo-mechanical properties must not be degraded significantly due to damage and activation by 14 MeV neutrons. Heat conductivity should be maintained as well as low swelling and void formation, despite high levels of helium and hydrogen production. Weldability after irradiation should also be considered in order to allow re-welding after the maintenance operation. They should also have low levels of nuclear self-heating after irradiation and low activation to ease both maintenance and recycling of material. In the sixties and seventies the high temperature advantage of refractory alloys (based on molybdenum, tungsten, and vanadium) gave impetus to their development for fusion applications. Their major drawback was their embrittlement after irradiation. Therefore, in the late seventies attention shifted to low activation alloys and the development of vanadium-alloys was emphasized. Research work was started on reduced activation austenitic steels where elements with high neutron induced activation (like nickel) were replaced by elements (such as manganese) with similar overall properties, but low activation. These steels fell into disfavor due to their poor phase stability and the complexity of fabrication. In the early nineties the study of low activation ferritic-martensitic steels started. The track record of conventional chromium steels exposed to high neutron fluxes in fast breeder reactors encouraged the investigation of ferritic/martensitic steels including oxide dispersion strengthened ferritic/martensitic steels. The present decade has seen attention broaden to high temperature SiC/SiC composites. Some attention has been devoted recently to titanium and chromium alloys but these are still at an early stage of development.

The functional material is very important in respect of the high efficiency of energy generation and management of fusion reactor. Typically, the functional materials is implied the tritium breeding materials and neutron multiplier. In case of some design such as HCCR is including neutron reflector. There can be used a lot of materials as functional materials. However, this study is mentioned tritium breeding material as a functional material. A detailed description of the tritium breeding material is presented in chapter 2.1.2.

A suitable breeding blanket technology will have to be proven to work reliable in a demonstration or prototype fusion reactor with satisfying performance and overall parameters and at the same time should show a clear route towards further improvements in the ongoing technological development. If

the systems applied to a demonstration or prototype fusion reactor would not allow the latter, a different blanket technology has to be brought to the market at a certain point, which most likely would require additional demonstration and prototype reactors. Table 2.3 is summarized the expected degree of application of each material to fusion reactor [36]. Where, the TSP is advanced reactor attractiveness parameter in view point of the ‘would it be attractive in the long term?’, and DAP is DEMO attractiveness parameter in view point of the ‘is a corresponding near term variant available and attractive for DEMO?’, and TSP is technological simplicity parameter in view point of the ‘are most technical issues solved today and is the system relatively simple (is the R&D demand tremendous)?’[36].

	TSP	DAP	AAP
Ceramic breeder concepts (steel structures)	High	High	Medium-low
Ceramic breeder concepts (SiC/SiC structures)	Low	Very low	High
Dual coolant concept (steel structures)	Medium (high for HCLL)	High	High
Self-cooled PbLi (siC/SiC structures)	Low	Very low	Very high
Flibe	Medium	Medium	Medium-low
Helium	Very low	Very low	Very high

Table 2.3 expected degree of fusion reactor when use variable structural & functional materials [36].

2.1.1 SiC_f/SiC composites

The structural materials of first wall and blanket in DT tokamak reactor suffer from:

- 1) High surface heat flux causes mechanical and electromagnetic loading and alternating thermal stresses;
- 2) High energy (14.1 MeV) fusion neutrons produce displaced atoms and helium, hydrogen, and solid transmutation products, leading to changes in bulk properties.

The blanket systems are large systems with combined thermal, hydraulic and mechanical loading, irradiation, compatibility etc. The requirements for fusion structural materials are:

- 1) The material could withstand high neutron wall loads under temperatures and coolant pressure conditions necessary to drive efficient thermodynamic cycles in a blanket;
- 2) The lifetime of structural material must be long enough to minimize the necessary replacements of near-plasma components;
- 3) The material should be of low activation in order to achieve the ultimate environmental attractiveness of fusion power.

Ceramics generally are compounds of metallic or non-metallic elements and other non-metals such as oxygen, nitrogen, carbon and boron. Compared to metals these compounds have higher melting temperatures, Young's moduli and hardness and lower densities, electrical and thermal conductivities. Engineering ceramics are used in thermal and structural applications requiring high temperature resistance, high hardness and chemical inertness. Applications that exploit the thermal structural properties of ceramic commonly include cutting tool inserts, wear resistant components, ballistic armor, heat exchanger, burner tubes, prosthetics, dental implants, heat engines components and thermal barrier coatings. The dominating characteristics of ceramics that limit these and other engineering applications are their lack of plastic behavior at room temperatures and their low tolerance to flaws, i.e. low fracture toughness, that lead to catastrophic failure. Ceramic matrix composites are known as the oldest composite materials; the Bible refers to this particular type of materials when it tells a story of the fabrication of bricks with and without straw. Actually, bricks made of muck and clay and fired by sunlight are also ceramic matrix composites. The pre-history of modern fibrous ceramic matrix composites (CMCs) had a start in the early 60s when the first attempt to increase fracture toughness of ceramic materials by introducing refractory metal wires in a ceramic matrix were carried out.

SiC materials of interest for nuclear structural applications are mostly continuous fiber-reinforced ceramic matrix composites, which consist of SiC fiber, SiC matrix, and the fiber-matrix interphase. Nuclear-grade composites consist specifically of fully crystalline and stoichiometric SiC fibers and matrices and use a carbon interphase. Such composites are available through the nanoinfiltration and transient eutectic-phase (NITE) processing routes.

All of the SiC/SiC composites properties that govern structural utility and life depend upon the constituent properties (fibers, matrix, and interfaces) as well as the fiber architecture. It is now well established that ceramic materials can be toughened appreciably by the addition of strong, continuous fiber reinforcements [3]. A major portion of the toughness is attributable to the work required to pull broken fibers out of the matrix against a frictional sliding resistance between the fiber and matrix [4, 5]. However, substantial pullout occurs only if the fibers can survive the onset of matrix cracking which occurs at a stress also dependent on many system properties [6]. Figure 2.6 shows the basic phenomena that give rise to inelastic strains are matrix cracks and fiber failures subject to interfaces that deboned and slide [7, 8].

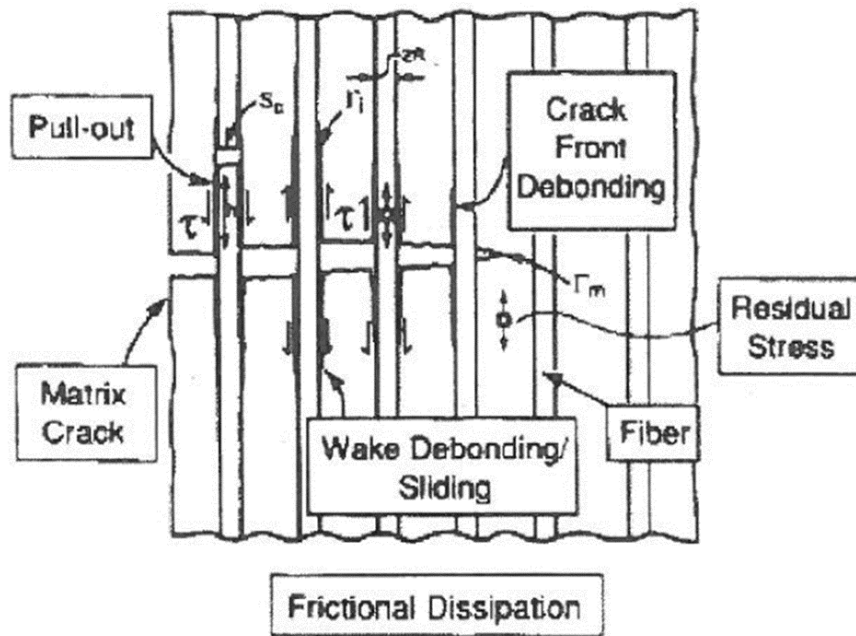


Figure 2.6 The fundamental crack propagation mechanism associated with the matrix and the interface.

The thermomechanical properties of coatings at fiber-matrix interfaces are critically important. A consistent characterization approach is necessary and the most commonly adopted hypothesis is that

there are two parameter, as shown in figure 2.7. One is associated with fracture and another with slip [9].

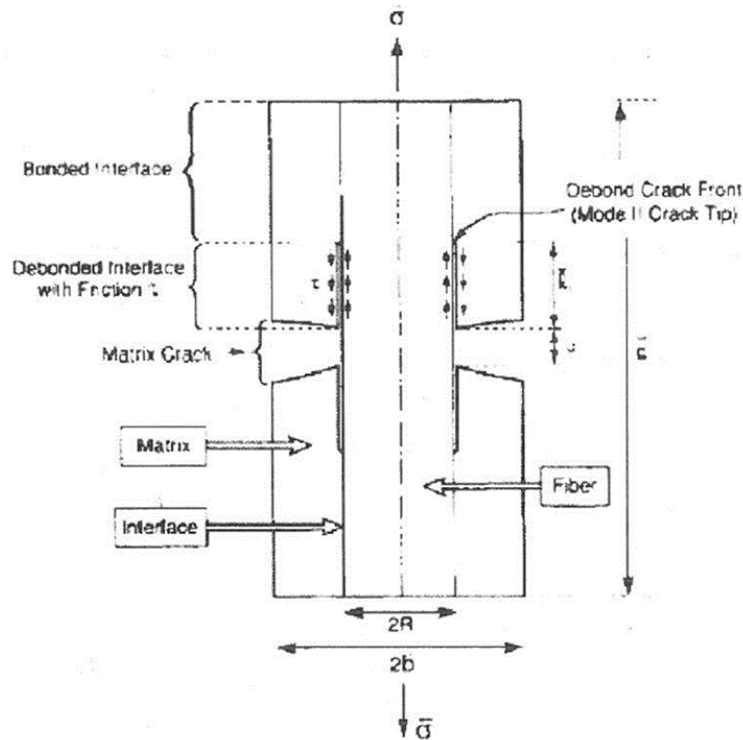


Figure 2.7 Schematic diagram indicating the sliding and debonding behavior envisaged in CMCs.

Fracture, or debonding, is considered to involve a debond energy (Γ_i). Slip is expected to occur with a shear resistance [10, 11]. Slip is expected to occur with a shear resistance (τ). Debonding must be a Mode II (shear) fracture phenomenon. In brittle systems, Mode II fracture typically occurs by the coalescence of micro-cracks within a material layer. In some case, this layer coincides with the coating itself, such that debonding involves a diffuse zone of micro-crack damage. In other case, the layer is very thin and the debond has the appearance of of a single crack. For both situations, it is believed that debond propagation can be represented by a Γ_i with an associated stress jump above and below the debond front. When a discrete debond crack exists, fractional sliding of the crack faces provides the shear resistance. Such sliding occurs in accordance with a friction law,

$$\tau = \tau_0 - \mu\sigma_{rr}$$

Where μ is the Coulomb friction coefficient, σ_{rr} is the compression normal to the interface, and τ_0 is a term associated with fiber roughness. When the debond process occurs by diffuse micro-cracking in the coating, it is again assumed that the interface has a constant shear resistance (τ_0).

For debonding and sliding to occur, rather than brittle cracking through the fiber, the debond energy (Γ_i) must not exceed an upper bound, relative to the fiber fracture energy (Γ_f). Calculations have suggested that the following inequality must be satisfied.

$$\Gamma_i \leq \left(\frac{1}{4}\right) \Gamma_f$$

Measurement of the τ and the Γ_i have been obtained by a variety of an approaches, as summarized in table 2.4. The most direct involves displacement measurement. These are conducted in two ways: (1) fiber push-through/push-in, by using a small-diameter and (2) tensile loading in the presence of matrix cracks. Indirect method for obtaining τ also exist. These include measurement of the saturation matrix crack spacing and the fiber pull out length.

Direct method	Indirect method
Single fiber push-in and push-out	Pull-out length
Single fiber and bundle pull-out	Saturation crack spacing
Bundle push-in	Hysteresis loop
Tensile evaluation of mini-composites(4 phases)	Unloading-reloading modulus

Table 2.4 summary for the evaluation approaches of interfacial properties.

In SiC/SiC composites with good composite properties, fiber pull-out is one of the evidences after fracture of specimen. These fracture surfaces measured by various methods provide valuable information. Regions with highly correlated fiber failures, with minimal pull-out, are indicative of manufacturing flaws. Such flaws often occur in regions where fiber coating problems existed. In zones where fiber failures are uncorrelated, the distribution of fiber pull-out lengths provides essential information. The pull-out lengths are related explicitly of the stochastics of fiber failure.

The basic realization is that on average, fibers do not fail on the plane of the matrix crack, even though the stress in the fibers has its maximum value at this site. This unusual phenomenon relies exclusively on statistics, where in the locations of fiber failure may be identified as a distribution function that depends on the shape parameter (m). Furthermore, the mean pull-out length (\bar{h}) has a connection with the characteristics length (ξ_c). Consequently, a functional dependence exists, dictated by the non-dimensional parameters, $\bar{h}\tau/RS_c$ and m ,

$$\bar{h}\tau/RS_c = \lambda(m)$$

There are two bounding solutions for the function (λ). Composite failure subject to multiples matrix cracking give the upper bound. Failure in the presence of a single crack gives the lower bound. Because of pull-out, a frictional pull-out resistance exists, which allows the material to sustain load, beyond the UTS. The associated ‘pull-out’ strength (S_p) is an important property of the composite. The S_p is given by

$$S_p = 2\tau f \bar{h}/R := 2f S_c \lambda(m)$$

Matrix cracking in SiC/SiC composites is strongly dependent on the microstructure of the composite and the fiber architecture. Matrix cracking stress (δ_{mc}) is one of important properties of SiC/SiC composites, because the fiber pull-out depends on the matrix crack as well as other system properties. Besides, the oxidative gas can be infiltrated though the matrix cracks and it may decrease the durability of SiC/SiC composites under high temperature and oxidative condition.

The development of damage in the form of matrix cracks within 1-D SiC/SiC composites subject to tensile loading has been traced by direct optical observations on specimens with carefully polished surfaces, and by acoustic emission detection, as well as by ultrasonic velocity measurements. Interrupted tests, in conjunction with sectioning and SEM observations, have also been used. Analysis of the matrix damage found in 1-D CMCs provides the basis upon which the behavior of 2-D and 3-D SiC/SiC composites may be addressed.

We consider that a ceramic matrix of modulus E_m uniaxial reinforced with a volume fraction (f) of cylindrical fibers of radius (γ), modulus E_f mean tensile strength σ_0 at reference length (L_0) and Weibull modulus m describing both the distribution of strengths about σ_0 and the scaling of strength with fiber length L . Under uniaxial tension along the fiber axis, the response of the composite is linear with modulus $E = fE_f + (1-f) E_m$ until a critical matrix-cracking load σ_{mc} is applied. At σ_{mc} small preexisting matrix cracks propagate across the sample. It is assumed that, rather than propagating through the fibers, the fiber-matrix interface propagating though fibers, the fiber-matrix interface debonds and sliding of the fibers relative to the matrix occurs with sliding resistance τ . Under these conditions, σ_{mc} has been calculates as

$$\sigma_{mc} = \left(\frac{q\tau\Gamma_m}{r} \frac{f^2 E_f E^2}{(1-f)E_m^2} \right)$$

Where, the Γ_m is the matrix fracture energy.

Linear elastic fracture mechanics (LEFM) is the basic theory of fracture, originated by Griffith and completed completed in its essential aspects by Irwin and Rice. LEFM is a highly simplified. Yet

sophisticated theory that deals with sharp crack in elastic bodies. LEFM is applicable to any material as long as certain conditions are met. These conditions are related to the basic ideal situation analyzed in LEFM in which all the material is elastic except in a small region at the crack tip. In fact, the stresses near the crack tip are so high that some kind of inelasticity must take place in the immediate neighborhood of the crack tip; however, if the size of the inelastic zone is small relative to linear the dimensions of the body (including the size of the crack itself), the disturbance introduced by this small inelastic region is also small and, in the limit, LEFM is verified exactly.

For certain cracked configurations subjected to external forces, it is possible to derive closed-form expressions for the stresses in the body, assuming isotropic linear elastic material behavior. If we define a polar coordinate axis with the origin at the crack tip. It can be shown that the stress field in any linear elastic cracked body is given by

$$\sigma_{ij} = \frac{k}{\sqrt{r}} f_{ij}(\theta) + \sum_{m=0}^{\infty} A_m r^{\frac{m}{2}} g_{ij}^{(m)}(\theta)$$

Where the σ_{ij} is the stress tensor, r and θ are as defined in figure 2.8, the k is a constant, and f_{ij} is a dimensionless function of θ . The higher order terms depend on geometry, but the solution for any given configuration contains a leading term that is proportional to $1/\sqrt{r}$, regardless of the configuration of the cracked body. It can also be shown that displacement near the crack tip varies with \sqrt{r} . The equation of σ_{ij} describes a stress singularity, since stress is asymptotic to $r = 0$.

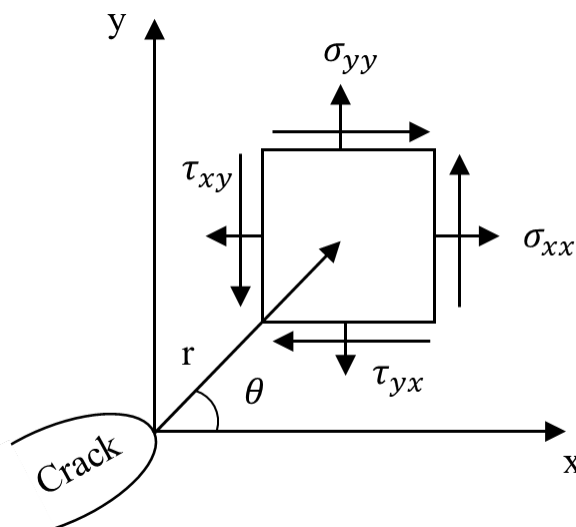


Figure 2.8 Definition of the coordinate axis ahead of crack tip

There are three types of loading that a crack can experience, as figure 2.9 illustrates. Mode I loading,

where the principal load is applied normal to the crack plane, tend to open the crack. Mode II corresponds to in-plane shear loading and tends to slide one crack face with respect to the other. Mode III refers to out-of-plane shear. A cracked body can be loaded in any one of these modes, or a combination of two or three modes.

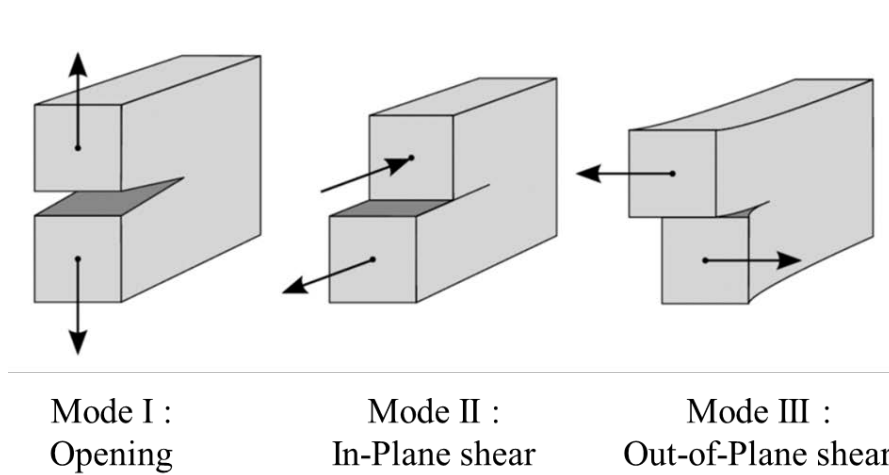


Figure 2.9 Three modes of loading that can be applied to the crack.

Each mode of loading produces the $1/\sqrt{r}$ singularity at the crack tip, but the proportionality constant (k) and f_{ij} depend on mode. At this point, it is convenient to replace k by the stress intensity factor (K), where $K = k\sqrt{2\pi}$. The stress intensity factor is usually given a subscript to denote the mode of loading: i.e. K_I , K_{II} , and K_{III} . Thus the stress fields ahead of a crack tip in an isotropic linear elastic material can be written as

$$\lim_{r \rightarrow 0} \sigma_{ij}^{(I)} = \frac{K_I}{\sqrt{2\pi r}} f_{ij}^{(I)}(\theta)$$

$$\lim_{r \rightarrow 0} \sigma_{ij}^{(II)} = \frac{K_{II}}{\sqrt{2\pi r}} f_{ij}^{(II)}(\theta)$$

$$\lim_{r \rightarrow 0} \sigma_{ij}^{(III)} = \frac{K_{III}}{\sqrt{2\pi r}} f_{ij}^{(III)}(\theta)$$

for Mode I, II, and III, respectively. In a mixed-mode problem (i.e. when more than one loading mode is present), the individual contributions to a given stress component are additive.

$$\sigma_{ij}^{(total)} = \sigma_{ij}^{(I)} + \sigma_{ij}^{(II)} + \sigma_{ij}^{(III)}$$

Above equations stems from the principle of linear super position.

SiC/SiC composites are attractive as structural materials in a fusion reactor system because of their favorable mechanical and low induced radioactivity properties under high-energy neutron irradiation. Due to their favorable mechanical properties at high temperatures and low activation, SiC/SiC composites are candidate structural materials for future fusion reactors. Several conceptual designs of fusion reactor including ITER utilizing a deuterium-tritium (D-T) fusion reaction have been proposed [12-16]. The blanket behind the armor facing the D-T plasma consists of structural material, breeding material that converts lithium to tritium, a neutron multiplier, and coolant that removes heat to generate the electrical output of the reactor. The breeder and coolant for each design are selected in consideration of their compatibility with structural materials. Thus far, the SiC/SiC composite is proposed as a candidate structural material with marten ferritic steel and vanadium alloy. In the case of the SiC/SiC composite, the maximum inlet temperature of the coolant is assumed to be around 1000 °C due to its heat resistivity as compared to that of metal alloys. The structural materials are assumed to be replaced after reactor operation of 10–20 MW•a/m² corresponding to 100–200 dpa irradiation [17]. However, these composites are relatively new materials with a limited data base; however, there is sufficient understanding of their performance to identify key issues in their application. These issues include: mechanical such as inter-laminar shear strength (Chapter 3) and oxidation behavior (Chapter 4).

Fracture resistance of SiC/SiC composites is dependent on the various parameters of test materials. Such as the strength and surface roughness of reinforcing fiber, bonding strength between fiber and matrix, the tensile and compressive strength and fracture resistance of matrix and so on. The graceful failure manner and high fracture resistance of SiC/SiC composites can be expected by the adoption of proper interphase and the high strength reinforcing fiber with low Weibull modulus. Usually SiC/SiC composites includes a little amount of micro and macro pores in its matrix and inter/intra fiber bundles. These pre-induced defects make the fracture behavior of SiC/SiC composites to be complex.

After matrix cracking, the force, which is applied on the test specimen, is mainly maintained by the reinforcing fiber. The failure of reinforcing fiber leads to a large amount of energy release and the propagation of macro crack. The propagation of macro crack is intermittently progressed, because of the random failure of reinforcing fibers and the combination with pre-induced defects. The fracture behavior of SiC/SiC composites is also strongly affected by the properties of fiber/matrix interface and the architecture of reinforcing fiber bundles, but only limited papers have been reported the correlation between these material properties and fracture resistance.

2.1.2 Tritium Breeding Materials

Based on the deuterium-tritium reaction, the main energy obtained in a fusion reactor is the neutron generated from the reaction. Therefore, it is necessary to convert the energy of neutrons into heat energy capable of generating power in order to the practical application of the fusion reactor. In the case of the TOKAMAK-type fusion reactor, the number of blanket modules that completely cover the inner walls of the vacuum vessel protect the steel structure and the superconducting toroidal field magnets from the heat and high-energy neutrons produced by the fusion reactions. The heat energy is recovered by transformed the kinetic energy when the neutrons are slowed in the blanket. At the same time, also it takes on the role of producing tritium using neutrons such as figure 2.10. And breeding blanket types in accordance with the breeder types are summarized in figure 2.11. As the fusion fuels, the deuterium can be extracted from seawater in virtually boundless quantities, but tritium is extremely rare in nature, which undergoes beta decay in a half-life of 12.3 years to become helium. Therefore, for the practical use of high-efficiency fusion energy, it is essential to develop a breeding blanket design concept that enables self-sufficiency of tritium in power plants. In this section, tritium breeding materials (i.e. functional materials) are described based on the breeding blanket design concept.

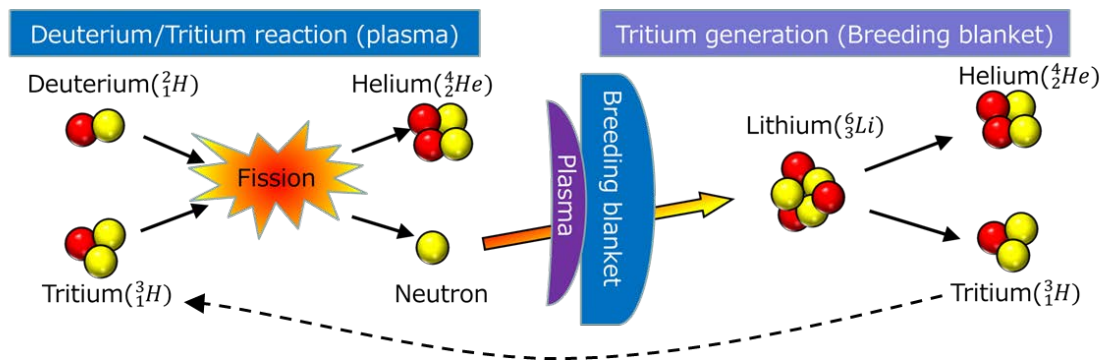


Figure 2.10 Breeding blanket design concept

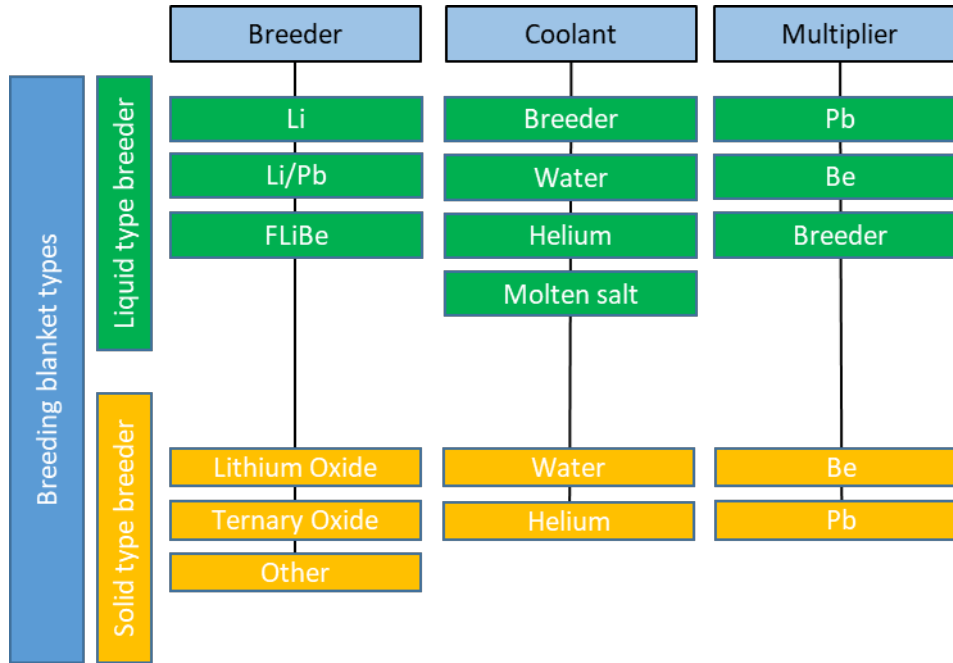


Figure 2.11 Breeding blanket types according to the breeder types.

Tritium can be obtained by both charged particle and neutron-induced nuclear reactions. The use of charged particle reactions based on the accelerator an accelerated beam proves to be uneconomic. The majority of the accelerator particles incident on the target dissipate their kinetic energy through inelastic collisions with the electrons in the target rather than inducing the desired nuclear reaction. The result is that the average energy required to produce a triton in this way is orders of magnitude greater than the energy that can be ultimately removed by burning the tritium thus produced in a fusion reactor [5]. Neutron-induced reactions can produce tritium with very high particle efficiency and convenience. The reactions are the following:



The reaction of (1) is a possible reaction caused by a slow neutron. It is an exothermic reaction and generate 4.8 MeV of energy. The second reaction is and endothermic reaction, which occurs only when neutrons move rapidly and absorbs 2.5 MeV of energy. The lithium exists 92.6% of ${}^7\text{Li}$ and 6.4% of ${}^6\text{Li}$ on the earth [4]. Based on the neutron-induced reaction, there are some candidates as tritium breeding material for the generation of tritium. The tritium breeding materials can be distinguished typically liquid or solid types.

The main liquid type material candidates are liquid lithium, the eutectic alloy 17Li-83Pb, FLIBE,

and a molten salt consisting of $(\text{LiF})_2\text{BeF}_2$. Where FLIBE and a molten salt although certainly not a metal; this material has been rejected because of its low breeding potential. Lithium-Lead-bismuth (Li-Pb-Bi) eutectic is another non-mainstream choice generally rejected because of the production of ^{210}Po from Bi under irradiation. The liquid metal breeders, as distinct from the solid breeder compounds, present the possibility of self-cooling, i.e. the breeding material can also be the heat transport fluid. Liquid metals are attractive because of the apparent simplicity of the blanket systems they offer and, indeed, in the early days of fusion when all attention was focused on plasma physics, it was simply assumed that the breeder blanket would be liquid lithium. However, in the past decades-long increasing emphasis has been placed on the technology and engineering of fusion reactors, with the result that serious concerns have emerged about liquid metal breeders. Table 2.5 lists these critical issues in which they are discussed in detail. The major issue concerns the safety problems inherent in using liquid metals and the danger of fire with these materials resulting in tritium release. The crux of this concern is largely judgmental in that arguments can be made from the liquid metal fast breeder reactor (LMFBR) experience that liquid metals could be safely used but on the other hand, there is strong pressure from the fusion community to avoid any perceived safety issue with fusion.

Safety	Lithium of ^{17}Li - ^{83}Pb fires with consequent tritium release; water cooling dangerous
Corrosion	Degradation of blanket structure by flowing liquid metals and resulting plugging and activity transport
MHD effects	Interaction of flowing liquid metals with reactor magnetic fields may lead to high pumping powers and poor heat transport
Tritium control	High solubility of tritium in lithium requires an effective large-scale extraction method; very low solubility in ^{17}Li - ^{83}Pb causes concerns about tritium permeation

Table 2.5 Critical issues of liquid metal breeders, which extract Ref [5].

In the viewpoint of the structure material, the corrosion and compatibility are important concerns.

Because it can be occurred the degradation of structure possible. The magnetohydrodynamics (MHD) problem refers to the difficulties of pumping liquid metals through the high magnetic fields characteristic of fusion reactor. Tritium is highly soluble in liquid lithium and thus there may be problem in removing it completely and reliably. In ^{17}Li - ^{83}Pb , tritium has very low solubility, and tritium permeation and possible escape are major concerns.

The search for alternatives to the liquid metals has lead in the last few years to the consideration of solid breeder materials. The major compounds considered are lithium oxide (Li_2O) and the ternary oxides: lithium aluminate (LiAlO_2), lithium silicate (Li_2SiO_3), lithium orthosilicate (Li_4SiO_4), lithium titanate (Li_2TiO_3), lithium zirconate (Li_2ZrO_3), and Li_8ZrO_6 (referring to table 2.7) [9, 10]. Other compounds such as the intermetallic alloys, Li_7Pb_2 and LiAl have been considered, but they suffer from high reactivity with water and air - precisely the problems one is trying to avoid by using solid breeders. The oxides are ceramics and being relatively inert, permit safe water cooling. Helium cooling is also possible but, of course, there can be no self-cooling. Helium is used as a coolant and is supplied at a static pressure of 8 MPa with an inlet temperature of 350°C and an outlet temperature up to 550°C depending on the operating conditions. These breeders are one of the most significant designs used in the DEMO reactors. In order to extract tritium from the breeder bed high energy neutrons obtained from the fusion reaction are made to strike the ceramic pebble bed made up of Li_2TiO_3 , Li_4SiO_4 , etc., which results in the formation of tritium around the pebble bed. The generated tritium atom in the lithium vacancy is bonded to the oxygen atoms surrounding the vacancy. The vacancy-tritium complex formation energies are in the range of 0.41-1.28 eV under oxygen rich condition [11]. Then by passing helium with 0.1-1% hydrogen as a purge gas tritium is extracted from the ceramic breeder.

As a key Li-ceramics material, Li_2TiO_3 has been considered as candidate for tritium breeder materials in fusion reactor, because of its reasonable lithium atom density, low activation, excellent chemical stability, good compatibility with structural materials and good tritium release characteristics at low temperature $200\sim 400^\circ\text{C}$ [32-35]. The properties (room temperature) of selected Li compounds as T breeder is shown table 2.6 [38].

Compound	Compound atomic density [at/Å ³]	Atomic density of Li [at/Å ³]	% Li atomic density	Compound density RT [kg/cm ³]	Melting point [°C]	Ref.
Non-ceramics						
Li_3N	0.0899	0.0674	75	1.3	813	[39]
LiF	0.1223	0.0612	50	2.64	848	[40]
Ceramics						

Li_2TiO_3	0.1129	0.0376	33.3	3.43	1533	[41]
Li_4TiO_4	0.0998	0.0444	44.5	2.57	>1000	[42]
Li_4SiO_4	0.1085	0.0482	44.4	2.4	1258	[43]
Li_8SiO_6	0.1106	0.059	53.3	2.2	830	[43]
$\text{Li}_6\text{Zr}_2\text{O}_7$	0.0957	0.0383	40	3.56	1267	[44]
Li_8ZrO_6	0.1109	0.0591	53.3	2.98	1336	[44]
Li_8PbO_6	0.1077	0.0575	53.4	4.28	>800	[45]
Li_4GeO_4	0.1031	0.0463	44.9	3.16	1298	[46]
Li_8GeO_6	0.1062	0.0567	53.4	2.64	n/a	[47]
Li_8CeO_6	0.1006	0.0537	53.3	3.25	n/a	[48]
Li_5AlO_4	0.1078	0.0539	50	2.25	1047	[49]
Li_6CoO_4	0.1113	0.0607	53.2	2.77	n/a	[50]
Li_8CoO_6	0.106	0.0565	53.3	2.47	n/a	[51]
Li_8SnO_6	0.114	0.0608	53.3	3.41	1050	[52]
Li_6ZnO_4	0.1116	0.0609	54.6	2.86	n/a	[53]
Li_2MnO_2	0.1053	0.042	39.9	3.9	n/a	[54]
Li_6MnO_4	0.1031	0.0562	54.5	2.5	n/a	[55]
Li_5FeO_4	0.1028	0.0514	50	2.64	n/a	[55]

Table 2.6 Properties (room temperature) of selected Li compounds as T breeders [38].

	Li₂O	LiAlO₂	Li₂ZrO₃	Li₄SiO₄	Li₂TiO₃
Melting Point (K)	1696	1883	1888	1523	1808
Density (g/cm³)	2.02	2.55	4.15	2.4	3.43
Li at. Density (g/cm³)	0.94	0.27	0.38	0.51	0.43
Thermal conductivity _773K_(W/mK)	4.7	2.4	0.75	2.4	1.8
Reactivity with water	large	Small	None	Small	None
Tritium retention time _713K_(h)	8.0	50	1.1	7.0	2.0
Li Vaporization (In additional +x% H₂)	600 °C	900 °C	800 °C	700 °C	800 °C
Long period use (2 years)	Instability (Li vaporization)	Stability	Instability (crack)	Instability (Li vaporization)	Instability (Reduction of Ti)
Tritium release	400 °C	400 °C	400 °C	350 °C	300 °C
Optimum operating Temp.	400-600 °C	400-900 °C	400-800 °C	350-700 °C	300-800 °C
Tritium breeding ratio (TBR)	High	Lower	Middle	Middle	Middle

Table 2.7 Candidates of solid breeder and characterize.

The tritium breeding ratio (TBR) is generated tritium per neutron. The Li_2TiO_3 breeder has to satisfy the required properties for high TBR. Parametric or general assessment studies usually depending on one- or two-dimensional transport code calculations of the neutron flux. As design becomes better defined, more realistic geometrical modeling is required, it is particularly important to model the effects of ports and duct penetrations through the blanket, especially for blankets with marginal breeding potential. Considering TBR from the view-point of the Li_2TiO_3 breeder, the required properties are typically small diameter of 1mm, small grain size, homogeneous microstructure, and good compatibility with structure materials.

The tritium inventory of an operating solid breeder blanket may be its single most important performance parameter and is essentially intrinsic to a specific material under specific conditions. The tritium inventory is thought to be partitioned into several distinct phenomena; solubility, bulk diffusion, irradiation effects and gas diffusion within the pores. While selection of an inventory limit - be it 10 wppm or 1% - is controversial, candidate materials exhibiting low inventory are clearly more desirable. The tritium inventory causes an extra burden on breeding ratios for solid breeder designs. The tritium inventory within a candidate breeder material is predicted to possess a strong dependence on temperature and an uncertain dependence on burn up [37].

As mentioned, the Li_2TiO_3 compound has strong points as a tritium breeding material, but several conditions for TBR must be satisfied or evaluated in order to increase the efficiency. It is necessary to evaluate the operating temperature of the Li_2TiO_3 pebble bed based on the sintering behavior and creep phenomenon of the pebble bed, also the manufacturing method has to improve to obtain suitable shaping with size and uniform microstructure. In addition, it is a necessary step to evaluate the integrity of each material from the compatibility test between Li_2TiO_3 tritium breeding material and structural material.

References

- [1] T. J. Mackin, K. E. Perry, J. S. Epstein, C. Cady and A. G. Evans, Strain fields and damage around notches in ceramic-matrix composites, *Journal of American Ceramic Society*, 79, 1 (1996) 65-73
- [2] W. P. Keith, K. T. Kedward, Notched strength of ceramic-matrix composites, *Composites Science and Technology*, 57 (1997) 631-635
- [3] A. G. Evans and D.B. Marshall, The mechanical behavior of ceramic-matrix composites, *Acta Metall.* 37 (1989) 2567-2583
- [4] M. Sutcu, Weibull statistics applied to fiber failure in ceramic composites and work of fracture, *Acta Metall.*, 37 (1989) 651-661
- [5] M. D. Thouless and A. G. Evans, Effects of pullout on the mechanical properties of ceramic-matrix composites, *Acta Metall.*, 36 (1988) 517-522
- [6] D. B. Marshall, B. N. Cox and A. G. Evans, The mechanics of matrix cracking in brittle-matrix composites, *Acta Metall.*, 33 (1985) 2013-2021 Shanti V. Nair and Karl Jakus, High temperature mechanical behavior of ceramic composites, Butterworth-Heinemann (1995)
- [7] William A. Curtin, Theory of mechanical properties of ceramic-matrix composites, *Journal of American Ceramic Society*, 74 (1991) 2837-2845
- [8] John W. Hutchinson and Henrik M. Jensen, Models of fiber debonding and pullout in brittle composites with friction, *Mechanics of Materials*, 9 (1990) 139-163
- [9] Emmanuel Vagaggini, Jean-Marc Domergue, and Anthony G. Evans, Relationships between hysteresis measurements and the constituent properties of ceramic matrix composites: I, Theory, *Journal of American Ceramic Society*, 78 (1995) 2709-2720
- [10] Jean-Marc Domergue, Emmanuel Vagaggini and Anthony G. Evans, Relationships between hysteresis measurements and the constituent properties of ceramic matrix composites: II, experimental studies on unidirectional materials, *Journal of American Ceramic Society*, 78 (1987) 542-548
- [11] D. B. Marshall and W.C. Olibver, Measurement of Interfacial Mechanical properties in fiber-reinforced ceramic matrix composites, *Journal of American Ceramic society*, 70 (1987) 542-548
- [12] Seki Y, Kikuchi M, Ando T, Ohara Y, Nishio S, Seki M, Takizuka T, Tani K, Ozeki T, Koizumi K, Matsuda Y, Azumi M, Oikawa A, Madarame H, Mizoguchi T, Iida F, Ozawa Y, Mori S, Yamazaki S, Kobayashi T, Hirata S, Adachi J, Ikeda B, Suzuki Y, Ueda N, Kageyama T, Yamada M, Asahara M, Konishi K, Yokogawa N, Shinya K, Ozaki A, Takase H, Kobayashi S., The steady state Tokamak reactor. In: *Proceedings of 13th international conference on plasma physics and controlled fusion research*, IAEA 13 (1990) 473-485
- [13] Giancarli L, Ferrari M, Fuetterer MA, Malang S., Candidate blanket concepts for a European fusion power plant study. *Fusion Eng Des* 49-50 (2000) 445-456
- [14] Giancarli L, Golfier H, Nishio S, Raffray R, Wong C, Yamada R., Progress in blanket designs using SiCf/SiC composites. *Fusion Eng Des* 61-62 (2002) 307-318
- [15] Abdou A, Bromberg L, Brown T, Chan VC, Chu MC, Dahigren F, El-Guebaly L, Heitzenroeder P, Hendrson D, St. John HE, Kessel CE, Lao LL, Longhurst GR, Malang S, Mau TK, Merrill BJ, Miller RL, Mogahed E, Moore RL, Petrie T, Petti DA, Polizer P, Raffray, AR, Steiner D, Sviatoslavsky I, Synder P, Syaebler GM, Turnbull AD, Tillack MS, Wagner

- LM, Wang X, West P, Wilson P., The ARIES-AT advanced tokamak, advanced technology fusion power plant. *Fusion Eng Des* (2006)
- [16] Nishio S, Tobita K, Ushigusa K, Konishi S, Reactor Design Team, Conceptual design of Tokamak high power reactor (A-SSTR2). *J Plasma Fusion Res* 78 (2002) 1218–1230
- [17] Raffray AR, Akiba M, Chuyanov V, Giancarli L, Malang S, Breeding blanket concepts for fusion and materials requirements. *J Nucl Mater* 307-311:21 (2002) 3080:3–23
- [18] Nishio S, Tobita K, Ushigusa K, Konishi S, Reactor Design Team, Conceptual design of Tokamak high power reactor (A-SSTR2). *J Plasma Fusion Res* 78 (2002)1218–1230.
- [19] Raffray AR, Akiba M, Chuyanov V, Giancarli L, Malang S., Breeding blanket concepts for fusion and materials requirements. *J Nucl Mater* 307-311 (2002) 21–30.
- [20] ITER – the way to new energy <https://www.iter.org/>
- [21] Konishi T, Enoeda M., The current status of the world ITER test blanket module program. *J Plasma Res* 90 (2014) 332–337.
- [22] Conn RW, Holdren JP, Sharafat S, Steiner D, Ehst DA, Hogan WJ, Krakowski RA, Miller RL, Najmabadi F, Schultz KR., Economic, safety and environmental prospects of fusion reactors. *Nucl Fusion* 30 (1990) 1919–1934.
- [23] Seki Y, Tabara T, Aoki I, Ueda S, Nishio S, Kurihara R Impact of low activation materials on fusion reactor design. *J Nucl Mater* 258-263 (1998) 1791–1797.
- [24] Noda T, Fujita M (1996) Effect of neutron spectra on the transmutation of first wall materials. *J Nucl Mater* 233-237:1491–1495
- [25] T. Muroga, T. Tanaka, A. Sagara, Blanket neutronics of Li/vanadium-alloy and Flibe/vanadium-alloy systems for FFHR, *Fusion Engineering and Design*, 81 (2006) 1203–1209.
- [26] L.V. Boccaccini, L. Giancarli, G. Janeschitz, S. Hermsmeyer, Y. Poitevin, A. Cardella, E. Diegele, Materials and design of the European DEMO blankets, *Journal of Nuclear Materials*, 329 (2004) 148–155.
- [27] M. Enoeda, M. Akiba, S. Tanaka, A. Shimizu, A. Hasegawa, S. Konishi, A. Kimura, A. Kohyama, A. Sagara, T. Muroga, Overview of design and R&D of test blankets in Japan, *Fusion Engineering and Design*, 81 (2006) 415–424.
- [28] F. Najmabadi, A. Team, Overview of ARIES-RS tokamak fusion power plant, *Fusion Engineering and Design*, 41 (1998) 365–370.
- [29] K. Ehrlich, E.E. Bloom, T. Kondo, International strategy for fusion materials development, *Journal of Nuclear Materials*, 283 (2000) 79–88.
- [30] H. Chen, Y. Wu, S. Konishi, J. Hayward, A high temperature blanket concept for hydrogen production, *Fusion Engineering and Design*, 83 (2008) 903–911.
- [31] U.Fischer, C.Bachmann, J.-C.Jaboulay, F.Moro, I.Palermo, P.Pereslavitsev, R.Villari, Neutron performance issues of the breeding blanket options for the European DEMO fusion power plant, *Fusion Engineering and Design*, 109-111 (2016) 1458-1463
- [32] Kazuki Omoto, Takuya Hashimoto, Kazuya Sasaki, Takayuki Terai, Tsuyoshi Hoshino, Masatomo Yashima, Structural analysis of Li₂TiO₃ by synchrotron X-ray diffraction at high temperature, *Journal of Nuclear Materials* 417 (2011) 692-695.
- [33] J.P. Kopasz, J.M. Miller, C.E. Johnson, Tritium release from lithium titanate, a low-activation

tritium breeding material, *Journal of Nuclear Materials* 212-215 (1994) 927-931.

- [34] D. Mandal, M.R.K. Sheno, S.K. Ghosh, Synthesis & fabrication of lithium-titanate pebbles for ITER breeding blanket by solid state reaction & spheroidization, *Fusion Engineering and Design*, 85 (2010) 819-823.
- [35] K. Ochiai, T. Hoshino, Examination of tritium release properties of advanced tritium breeder by DT neutron, *Ceramic breeder blanket interactions (CBBI-17)*, 2013
- [36] T. Ihli, T.K. Basu, L.M. Giancarli, S. Konishi, S. Malang, F. Najmabadi, S. Nishiog, A.R. Raffray, C.V.S. Rao, A. Sagara, Y. Wu, Review of blanket designs for advanced fusion reactors, *Fusion Engineering and Design*, 83 (2008) 912-919.
- [37] G. W. Hollenberg, C. E. Johnson, M. Abdou, Tritium breeding materials, master degree thesis in University of California at Lows Angeles, (2001)
- [38] F.A. Hernández, P. Pereslavl'tsev, First principles review of options for tritium breeder and neutron multiplier materials for breeding blankets in fusion reactors, *Fusion Engineering and Design* 137 (2018) 243-256
- [39] J. Sangster, et al., The Li-N (lithium-nitrogen) system, *J. Phase Equilibria Diffus.* 13 (1992) 291–296.
- [40] T.B. Douglas, et al., Lithium fluoride: heat content from 0 to 900 °C, the melting point and heat of fusion, *J. Am. Chem. Soc.* 76 (19) (1954) 4826.
- [41] S. Saitoa, et al., Density dependence on thermal properties of Li₂TiO₃ pellets, *J. Nucl. Mater.* 253 (1-3) (1998) 213-18.
- [42] T. Hoshino, et al., New synthesis method of advanced lithium titanate with Li₄TiO₄ additives for ITEM-TBM, *Fusion Eng. Des.* 84 (2-6) (2009) 956–959.
- [43] S. Claus, et al., Phase equilibria in the Li₄SiO₄-Li₂SiO₃ region of the pseudo binary Li₂O-SiO₂ system, *J. Nucl. Mater.* 230 (1) (1996) 8–11.
- [44] G.P. Wyers, et al., Phase relations in the system Li₂O-ZrO₂, *J. Nucl. Mater.* 168 (1989) 24–30.
- [45] T. Hayashi, et al., Tritium release behavior from neutron irradiated Li₈PbO₆, *J. Nucl. Mater.* 170 (1990) 60–65.
- [46] P.P. Budnikov, et al., A study of the phase diagram GeO₂-Li₂O, *Proc. USSR Acad. Sci.* 99 (1954) 761–763.
- [47] R. Hofmann, et al., Ein neues Oxogermanat: Li₈GeO₆ = Li₈O₂[GeO₄], *Zeitschrift für anorganische und allgemeine Chemie* 555 (1987) 118–128.
- [48] P. Kroeschell, et al., Neue Vertreter der Li₈SnO₆-Familie: Li₈IrO₆, Li₈PtO₆ and Li₈CeO₆, *Zeitschrift für anorganische allgemeine Chemie* 536 (1986) 81–91.
- [49] Y. Ikeda, et al., Thermal stability of lithium aluminates by high temperature mass spectrometry, *J. Nucl. Sci. Technol.* 17 (8) (1980) 650–653.
- [50] S. Narukawaa, et al., Anti-fluorite type Li₆CoO₄, Li₅FeO₄, and Li₆MnO₄ as the cathode for lithium secondary batteries, *Solid State Ion.* 122 (1-4) (1999) 59–64.
- [51] M. Jansen, et al., Zur Kenntnis von Li₈CoO₆, *Zeitschrift für anorganische allgemeine Chemie* 898 (1973) 54–62.
- [52] R. Hoppe, et al., Die Kristallstruktur von Li₈SnO₆, *Zeitschrift für anorganische allgemeine Chemie* 488 (1977) 181–188.

- [53] H. Untenecker, et al., Ein neues Oxozincat: $\text{Li}_6[\text{ZnO}_4]$, Zeitschrift für anorganische allgemeine Chemie 551 (1987) 147–150.
- [54] H. Hofmann, et al., 2013 Werkstoffe in der Elektrotechnik Ed Hanser. L. Liang, et al., Synthesis and characterization of novel cathode material Li_5FeO_4 for Li-ion batteries, Int. J. Electrochem. Sci. 8 (2013) 6393–6398.
- [55] S. Narukawaa, et al., Anti-fluorite type Li_6CoO_4 , Li_5FeO_4 , and Li_6MnO_4 as the cathode for lithium secondary batteries, Solid State Ion. 122 (1-4) (1999) 59–64.
- [56] D.L. Smith, M.C. Billone, S. Majumdar, R.F. Mattas, D.-K. Sze, Material integration issues for high performance fusion power systems, Journal of Nuclear Materials 258-263 (1998) 65-73.
- [57] <https://www.iter.org/proj/inafewlines> in 2020
- [58] S Atzeni, J Meyer-Ter-Vehn, The physics of inertial fusion: Beam plasma interaction, Hydrodynamics, Hot dense matter, CLARENDON PRESS-OXFORD, (2004)
- [59] Gerry McCracken, Peter Stott, Fusion 2nd edition: The energy of the universe, Academic Press, 2005
- [60] DP. Jackson R.A. Verrall P.M. Garvey W.N. Selander R.L. Tapping WJ. Holtslander B.M. Townes J.S. Geiger I.J. Hastings T.C. Leung O.S. Tatone A.D. Lane J.N. Miller E.C. Carlick, A review of fusion breeder blanket technology, Canadian Fusion Fuels Technology Project (CFFTP), 1985
- [61] E Khodarev, Liquid metal fast breeder reactor, IAEA Bulletin (1978)
- [62] J. W. Bennett, K.E. Horton, Materials requirements for liquid metal fast breeder reactors, Metall Mater Trans, 8 (1978) 143-149
- [63] Staffan Alexander Qvist, Safety and core design of large liquid-metal cooled fast breeder reactors, (2013)
- [64] Kaiming Feng, 2nd workshop on MFE development strategy in China, 2012
- [65] Y. Shi, T. Lu, T. Gao, X. Xiang, Q. Zhang, X. Yu, Y. Gong, M. Yang, Density functional study of lithium vacancy in Li_4SiO_4 : Trapping of tritium and helium, Journal of Nuclear Materials (2015) 519-526

3. Mechanical properties of NITE-SiC/SiC composites with different fiber architecture

3.1 Introduction

A silicon carbide (SiC) is a candidate ceramics material for fusion system in future because of its lightweight, high strength at high temperature, microstructural stability at elevated temperature and irradiation environment, reduced radio-activation property and low decay heat [1-4]. The SiC as ceramics is inherently brittle because of its covalent bonding which makes materials low fracture toughness. Only the way to enhance the fracture toughness of ceramics materials is the composite. In the case of SiC, a SiC fiber-reinforced SiC matrix (SiC/SiC) composite is considered to be able to use for structural components because of their enough toughness [5]. The SiC/SiC composites are expected to have both good properties of SiC and high fracture toughness, while the characters have orientation due to the architecture of reinforcements. The ceramic composites are hard and difficult to be bent or to be stretched by mechanical methods. Thus, ceramic composites are usually sintered by “near-net shaping” which is a shaping way to sinter the products having very closed shape to that of the final product. In case of metals which are homogeneous solid materials, their results of tensile or fracture toughness tests using plate-shaped specimens are able to apply to the design of tube or cylinder shaped products. Much of the early work on fracture in composites involved investigations of the applicability of linear elastic fracture mechanics, which had been originally developed for the analysis of through-thickness cracks in homogeneous, isotropic metals. The origin of fracture mechanics can be traced back to the seminal work of Griffith [13-14], who explained the discrepancy between the measured and predicted strength of glass by considering the stability of a small crack. However, ceramic composites with complicated shapes have own properties depending on their processing methods, shapes and the architecture of reinforcements, etc [6]. There are many kinds of processing method for SiC/SiC composites, such as polymer impregnation and pyrolysis (PIP), chemical vapor infiltration (CVI) and reaction sintering / melt infiltration (RS/MI). Moreover, Nano-Infiltration and Transient Eutectic phase (NITE) process is one of promising methods to provide a dense and stoichiometric SiC matrix composite. In the processing of NITE SiC/SiC composite, the architecture of reinforcements is determined at the step of their preform fabrication. Under the consideration of product requirements (such as shape, size, mechanical properties and so on), a proper architecture among cross-ply (CP), woven prepreg (WP) and filament winding (FW), should be selected. Additionally, the randomly

arranged short fiber (SF) architecture is preferred for the high productivity of practical components with large sizes and complicated shapes, shorter process time and lower cost [12]. Also, In order to improve the mechanical properties of SiC/SiC composite materials, there is a hybrid (HB) fiber reinforced architecture in which the structures of CP and SF are mixed. Thus, the establishment of material database including mechanical properties is essential for this purpose. Several in-plane mechanical properties of NITE-SiC/SiC composite have been already evaluated, but some data, like inter-laminar mechanical properties related to fiber reinforcing architectures, are still not enough. This insufficient database leads to problems in application to the practical environment of NITE-SiC/SiC composites. Present research focuses on the structure of fiber reinforcing and discusses their effects on the tensile and shear strength. The objects of this study are to obtain the inter-laminar mechanical properties of NITE-SiC/SiC composites for the establishment of their mechanical property database and to obtain an understanding on the correlation between inter-laminar mechanical properties and fiber reinforcing architecture for the further improvement of NITE process.

3.2 Experimental

3.2.1 Materials

Highly crystalline stoichiometric SiC fiber (Hi-Nicalon Type-S, NGS Advanced Fiber Co., Ltd., Japan) was employed as reinforcements. Pyrolytic carbon monolayer (thickness: ~500nm) was formed on the surface of SiC fiber as F/M (fiber/matrix) interphase by a conventional chemical vapor deposition (CVD) method. In order to investigate the effects of fiber reinforcing architecture on the tensile strength and inter-laminar shear strength of NITE-SiC/SiC composites, specimens of various type with different fiber reinforcing architectures, SF, CP, WP, and HB were prepared by NITE process. Figure 3.1 shows the schematic illustrations of both fiber reinforcing architectures. In this study, cut prepreg sheet (fiber length: 5mm) has been used for the intermediate materials for SF architecture. CP architecture were prepared from the alternately stacked uni-directional (UD) prepreg sheets in the direction of 0° and 90°. WP specimens were made by 2D prepreg fabrics which were plainly woven with narrow prepreg ribbons with 3 mm width. The HB architecture is combined both of CP (8 wt%) and SF (2 wt%). This means that short fibers are inserted between the UD prepregsheets. Where, the prepreg sheet is an

intermediate material of uni-directionally aligned continuous SiC fiber bundles impregnating with SiC powder and a small amount of oxide additives. The details of NITE process were described at elsewhere [7-8]. The fiber volume fraction of CP and WP specimens were about ~45%, ~59.4%, respectively. The density of specimens was measured by Archimedes' method. The average densities of CP and WP specimens were 2.84g/cm³ and 2.93 g/cm³.

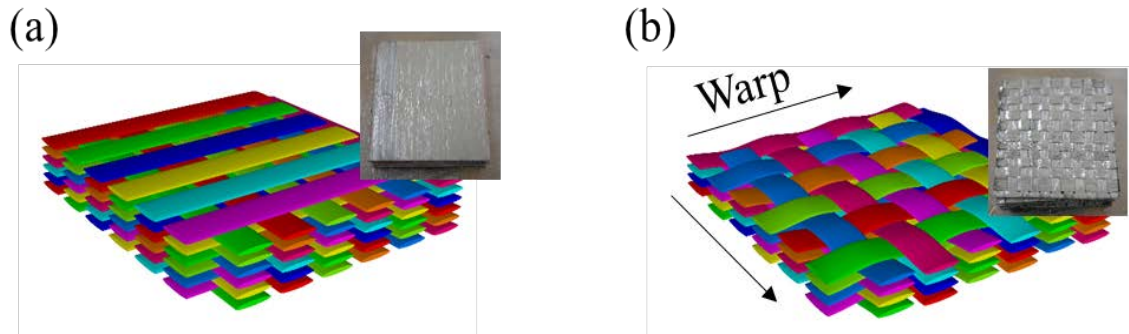


Figure 3.1 The schematic illustration of (a) Cross-ply (CP), (b) Woven-prepregsheet (WP).

3.2.2 Testing method

The tensile tests were conducted at room temperature in ambient air atmosphere. The bar type specimens with dimensions of 4mmW×40mmL×1.5mmT were machined. Aluminum tabs were bonded on the both ends of each specimen for gripping and protecting specimens from the gripping damage. The crosshead speed was 0.5mm/min. The tensile strain was measured by a pair of strain gauges (FLK-6, Tokyo Sokki Kenkyujo Co., Ltd., Japan) with 6 mm gage length bonded on both surfaces of the specimen.

The inter-laminar shear strength (ILSS) of NITE-SiC/SiC composites were evaluated by Double Notch Shear (DNS) test [9-11]. Figure 3.2 shows a schematic illustration of the DNS test and the geometry of specimen used in this study. Straight notches with round tip (R=0.25mm) were applied on both sides of the specimen by a precision cutting machine using a diamond blade. DNS tests were performed using a universal testing machine (AG-50kNG, Shimadzu Corp., Japan) at room temperature in the ambient air atmosphere. The crosshead speed was 0.5mm/min. After the tests, the fracture surfaces were observed by a field emission SEM (JSM-6700F, JEOL Ltd., Japan).

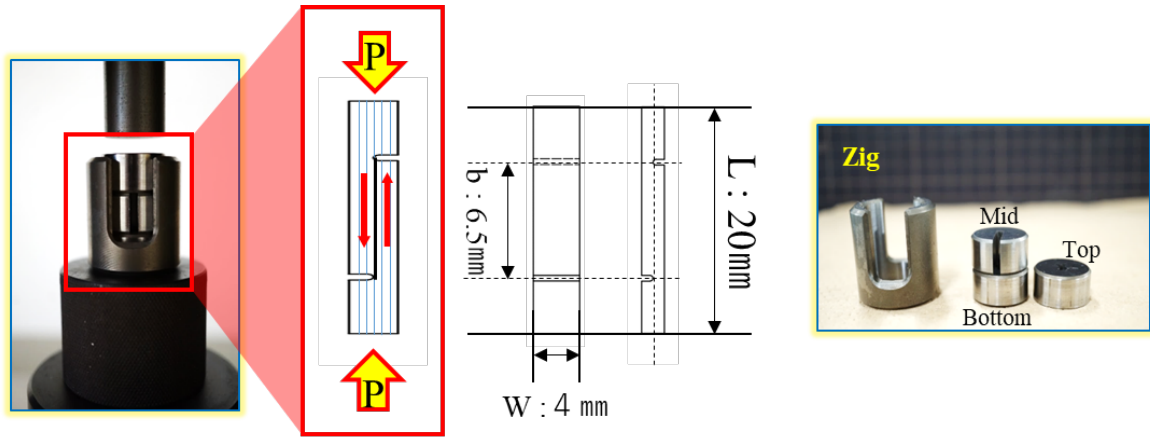


Figure 3.2 Schematic illustration of the DNS test and the geometry of specimen

3.3 Results & Discussion

3.3.1 Mechanical properties depending on the architecture

Figure 3.3 shows tensile test results of CP and WP specimens. The tensile strength of both type specimens was almost similar, but their elastic modulus was significantly different. Table 3.1 summarizes elastic modulus, proportional limit stress (PLS) and ultimate tensile stress (UTS). Average values of PLS of CP and WP specimens were 92 MPa and 105 MPa, respectively. And, the tensile strengths of CP and WP specimens were 191 MPa and 192 MPa, respectively. These values are not significantly different, but the elastic modulus is significantly affected by the fiber reinforcing structures. The elastic modulus of CP specimens was ranged from 97 GPa to 117 GPa, while these of WP specimens

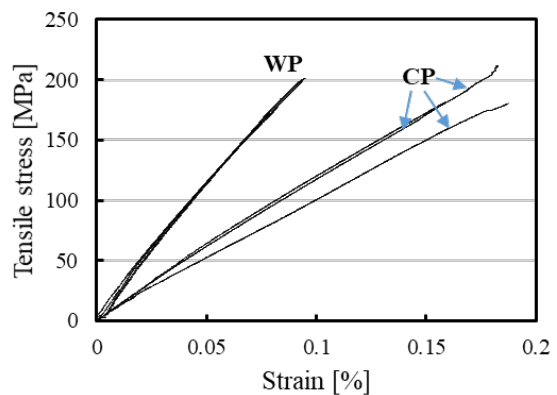


Figure 3.3 Stress-Strain curves of tensile test for CP and WP specimens.

were ranged from 220 GPa to 234 GPa. FE-SEM images of fractured specimens were shown in figure 3.4.

Specimen ID	E_c (GPa)	PLS (MPa)	UTS (MPa)
CP-1	114	114	181
CP-2	97	89	180
CP-3	117	72	211
WP-1	220	119	198
WP-2	234	99	201
WP-3	231	98	176

Table 3.1 Elastic modulus, proportional limit stress and tensile strength of CP and WP specimens in tensile test

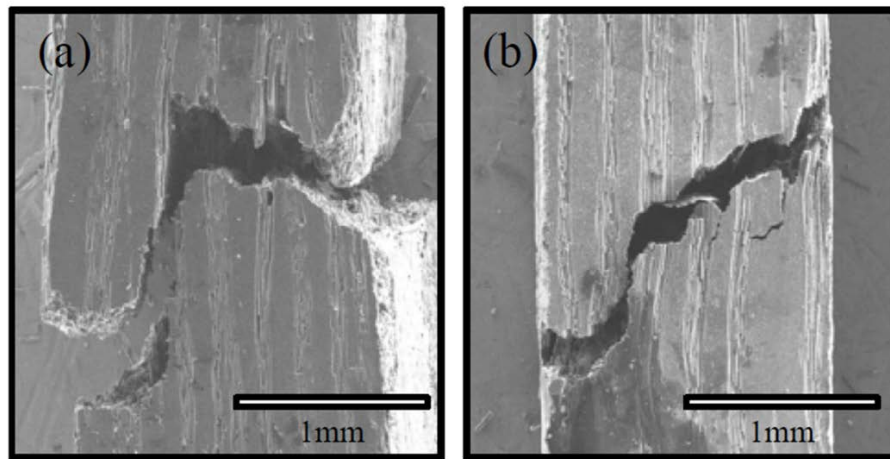


Figure 3.4 Typical failure images of (a) CP and (b) WP specimens after tensile test.

Fibers aligned to longitudinal direction are clearly visible on the side of each specimen, but fibers aligned to transverse direction and matrix are difficult to be distinguished. Both images are very similar. But the fiber bundles of longitudinal and transverse directions on the CP specimens were stacked flatly, and those on the WP specimens were locked together, as shown at Figure 3.1. The cracks on both specimens seemed to be branched and deflected complicatedly. Moreover, the interface of the fiber bundles was delaminated. Some pulled out fibers are observed from the fracture surface, especially on

the CP specimen, as shown in figure 3.4. Fibers aligned to longitudinal direction are clearly visible on the side of each specimen, but fibers aligned to transverse direction and matrix are difficult to be distinguished. However, the fiber bundles of longitudinal and transverse directions on the CP specimen were stacked flatly, and those on the WP specimens were locked together. The cracks on both specimens seemed to be branched and deflected complicatedly. Moreover, the interface of the fiber bundles was delaminated. Some pulled out fibers are observed from the fracture surface, especially on the CP specimen, as shown in figure 3.4.

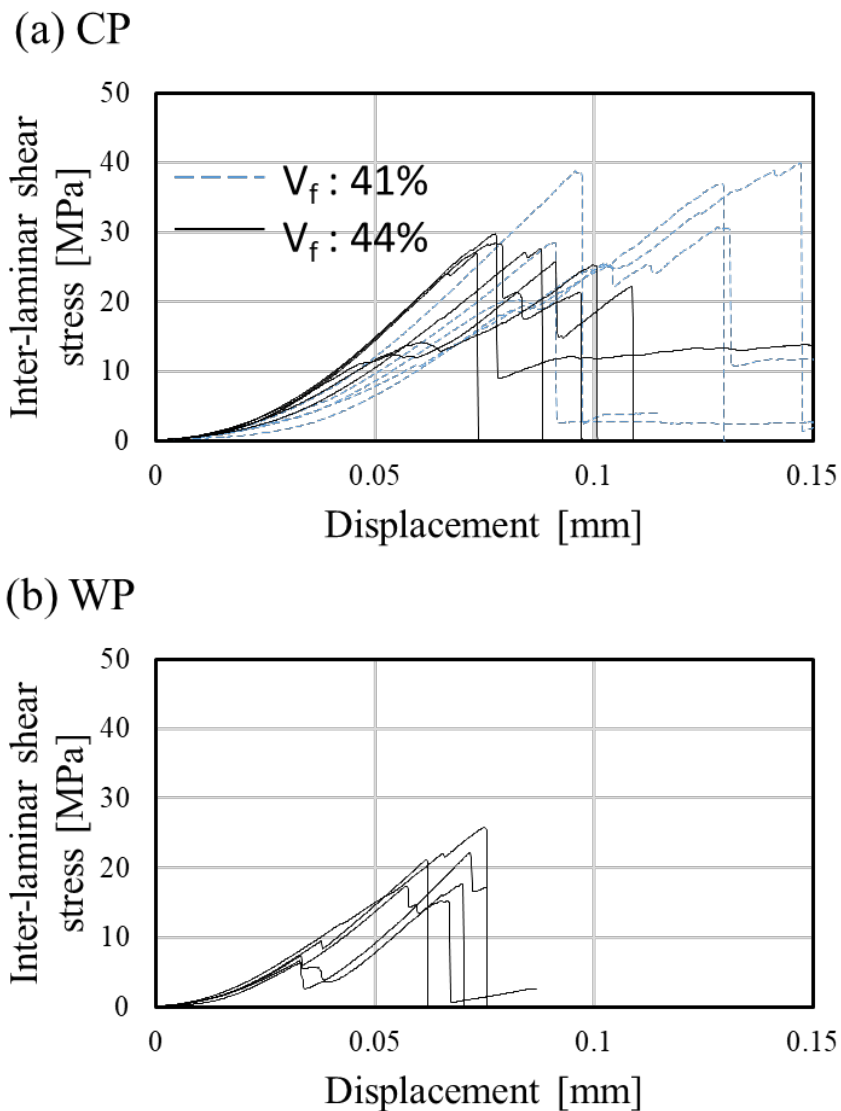


Figure 3.5 ILSS-Displacement curve of DNS test for (a) CP and (b) WP

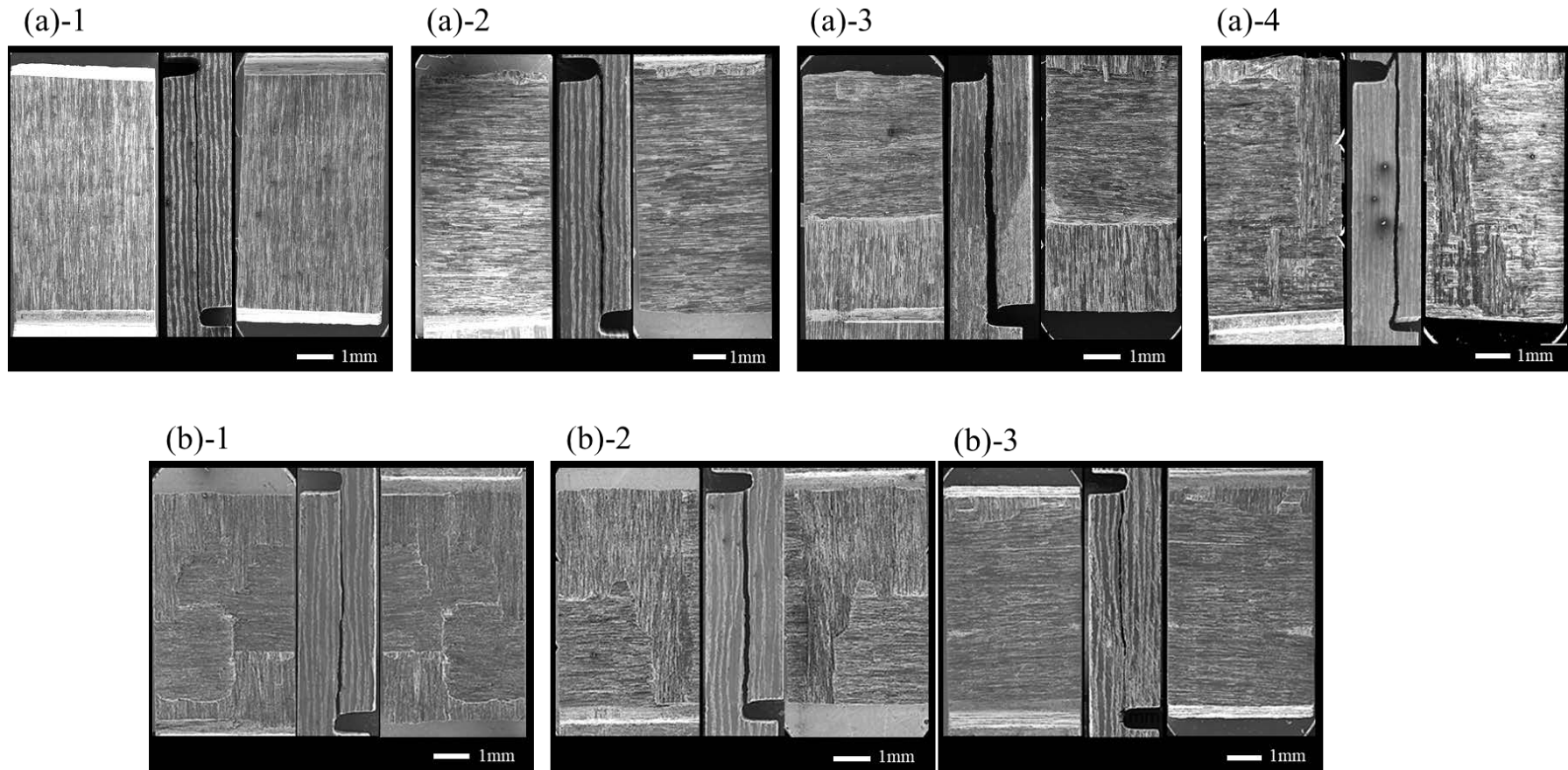


Figure 3.6 The typical fracture surface and side views of (a) CP and (b) WP.

Figure 3.5 shows the inter-laminar shear stress-displacement curves of CP and WP specimens. In spite of the specimens machined from the same sintered body according to the reinforced architecture, inter-laminar shear strength were scattered. The inter-laminar shear strength of ranges for CP and WP were 25~30MPa and 17~25MPa, respectively. In the case of inter-laminar shear stress-displacement of WP, specimens with Woven fiber reinforced architecture tend to occur events at 5 to 10MPa. The typical fracture surface and side views of DNS test specimens corresponding to figure 3.5 are shown in figure 3.6. The fracture surface of CP seemed to be fibers of longitudinal and transverse directions or both of the directions, respectively. One of CP specimens on figure 3.6 had a mixed surface, 1/3 was fibers of the longitudinal direction and the rest of the fracture surface was those of transverse direction. The fracture surface can be predicting patchwork of longitudinal and transverse direction fibers. On the other hand, WP specimens have both longitudinal and transverse direction fibers included on the fracture surface of all specimens.

The figure 3.7 is shown inter-laminar shear strength according to fiber direction. The 0° is mean that the load direction is parallel with fiber direction and the 90° is perpendicular between load direction and fiber direction. 0° of inter-laminar shear strength was 11MPa. Be other side, the 90° was 19MPa it is better than 0°.

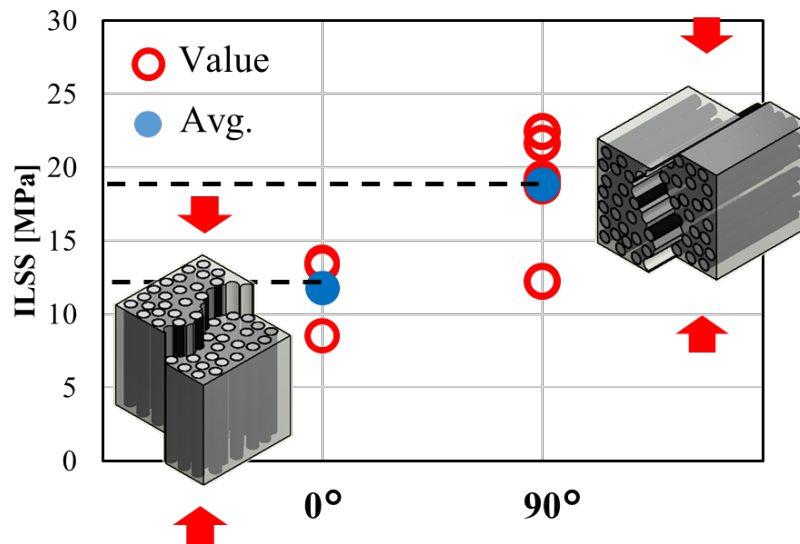


Figure 3.7 Inter-laminar shear strength according to fiber direction. 0° (load direction \parallel fiber direction), 90° (load direction \perp fiber direction)

The larger scattered data of CP specimens were suggested to be caused by size effects of the specimens because of the less number of obstacles on CP specimens than that on WP specimens. If we enla

As the size of CP specimens, the slope and strength are considered to be closed to larger values. And the quasi-elongation of specimens will be smaller. For the larger products, the CP structure may be better from the view of convenience of fabrication method and ensuring the toughness of the composites. But for the smaller products, especially for thin products, the WP structure will be necessary to ensure the obstacles against the deformation and crack propagations to enhance strength. The large products made by WP structure may tend to be strong and brittle because of the same reason.

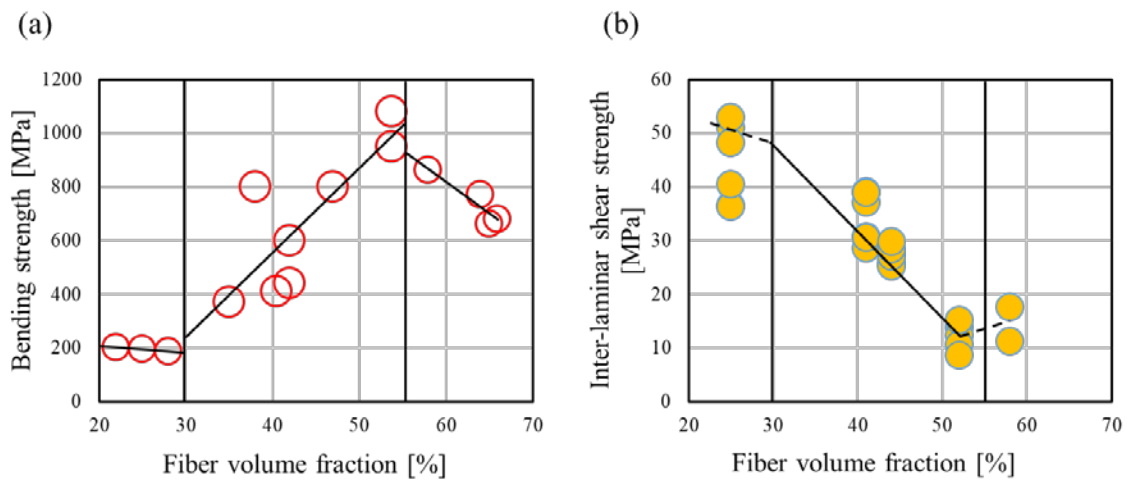


Figure 3.7 Mechanical strength of the NITE-SiC/SiC composites with CP architecture in order to the various fiber volume fraction. (a) Bending strength, (b) inter-laminar shear strength.

Figure 3.7 is presented mechanical strength such as bending and inter-laminar shear strength of the NITE-SiC/SiC composites with CP architecture in order to the various fiber volume fraction. The bending strength was expressed using data from the material strength laboratory for Muroran Institute of Technology in figure 3.7 (a). And the inter-laminar shear strength was combined with reference data and data from this study. The bending strength is increased with increase the fiber volume fraction, while the decreasing of strength is presented at above V_f 55%. On the other hand, the inter-laminar shear strength is decreased with increasing the fiber volume fraction, and it is increased at above 55%. The bending strength included complex stress such as tensile, compression, shear stress is proportional to the fiber volume fraction, but the inter-laminar shear strength is inversely proportional. Therefore, it is necessary to satisfy that the required conditions in the practical environment and design, it in consideration of the fiber volume fraction as shown in figure 3.7 when applied the NITE-SiC/SiC composite material.

3.3.2 Shear elastic modulus depending on the architecture

There is an insufficient number of the test specimen and large scattering of experimental results. Thus, this discussion will focus on the points as follows. For the first point, the elastic modulus of CP specimens was apparently smaller than that of WP specimens despite the similar value of tensile strength. Because both CP and WP specimens have an almost same volume fraction of fibers (V_f), their elastic modulus needed to be similar from the viewpoint of the law of mixture. The second point was that the elastic modulus of CP specimens were scattered largely. In order to explain these points, it is needed to consider on the strength of the interface between fiber bundle and inter-bundle matrix, precisely. There are inter-laminar share strength and inter-laminar detachment strength in the strength of the interface, figure 3.4 indicates that the inter-laminar share strength seemed to be more effective for the tensile test.

Although DNS test results in this research are also scattered, it is useful to understand the tensile test results. The shear strength, τ , obtained from DNS test was calculated by following formula;

$$\tau = \frac{F}{wl} \quad (1)$$

Where, F is load, w is the width of the specimens and l is the distance between notches. Inter-laminar share strength values were scattered, but their maximum values of CP and WP specimens were the almost same.

Then, we focus the slope of the DNS test results corresponding to “elastic” behavior of specimens. A displacement by a loaded force, F, is shown as (Total displacement) = (Displacement by specimen deformation) + (Displacement by deformation of jig). The slope of load-displacement of the jig used in this research was evaluated at first. And the effect of jig was removed from each data of DNS test results. The slope which is define as a, of load-displacement curve for each specimen is shown in table 3.2. The unit of ‘a’ is N/mm. And we assumed a deformation factor, f, with a following formula;

$$f = \frac{at}{wl} \quad (2)$$

Where, t is the thickness of DNS specimens. All data are listed in table 3.2. The deformation factor f is corresponding to be shear modulus G, but the displacement by specimen was not perfectly reflected the shear deformation of each specimen, thus, we handled the factor f to discuss the trend of shear deformation behavior of specimens.

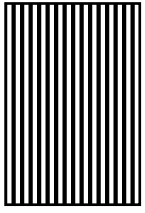
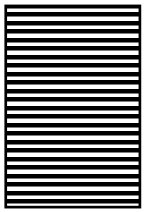
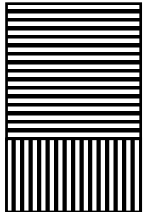
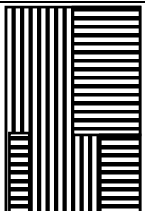
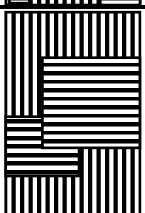
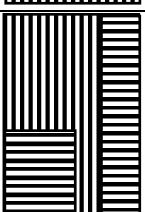
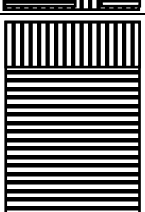
		Slope (<i>a</i>)	Thickness (<i>t</i>)	Width (<i>w</i>)	Length (<i>l</i>)	<i>F</i>	Schematic of fracture surface
		N/mm	Mm	Mm	Mm	GPa	
CP	(a)-1	27,170	2.00	3.95	6.48	2.1	
	(a)-2	16,116	1.98	3.99	6.98	1.1	
	(a)-3	20,638	2.00	3.97	7.26	1.4	
	(a)-4	67,476	1.99	4.00	7.70	4.3	
WP	(b)-1	16,799	1.99	4.03	6.42	1.3	
	(b)-2	36,298	2.00	4.00	6.03	3.0	
	(b)-3	21,653	2.00	3.96	6.60	1.7	

Table 3.2. Comparison of shear modulus in stress-displacement curve in DNS test.

Schematic images of fracture surface in figure 3.6 are also shown in Table 3.2. Either of fibers of longitudinal or transverse directions were seen on the fracture surface of (a)-1 and (a)-2 in figure 3.6. The crack is considered to propagate on a plane without any obstacles. Although a fracture surface is not equal to be the deformation region, it seems to be understandable that the existence of such weak plane reduces the elastic modulus. All WP specimens were included both longitudinal and transverse fiber surface. This means that cracks in WP specimens propagated on multiple planes during the specimen failure, the WP specimens are suggested to have more dense obstacles than the CP specimens. It is needed to note the fiber structure near notch at the upper and lower ends of the fracture surface, as shown at Table 3.2. The notches on (a)-4 and (b)-2 faced both longitudinal and transverse direction fibers. The shear stress-displacement curves of these specimens had large slope as shown in figure 3.5. Both curves went straight up to the shear strength and dropped soon after arriving at the top of the curve. The toughness of the both specimens was smaller than that of the other specimens. These data suggest that such cross points may behave as strong obstacles for both deformation and crack propagation.

The larger scattered data of CP specimens were suggested to be caused by size effects of specimens because of the less number of obstacles on CP specimens than that on WP specimens. If we enlarge the size of CP specimens, the slope and strength are considered to be larger, and the quasi-elongation will be smaller. For the larger products, the CP structure may be better from the view of convenience of fabrication method and ensuring the toughness of the composites. But for the smaller products, especially for thin products, the WP structure will be necessary to ensure the obstacles against the deformation and crack propagations to enhance strength. The large products made by WP may tend to be too strong and too brittle because of the same reason.

3.4 Summary

Tensile and shear properties of NITE-SiC/SiC composites having two different types of reinforcement architecture, CP and WP structure, were investigated. The tensile strength was almost same but the elastic modulus of WP specimens was larger than that of CP specimen in spite of same fiber volume fractions. In the case of DNS test, the maximum shear strength of both CP and WP specimens were almost same, but the elastic and toughness factors, especially of CP specimens, were scattered. From the comparison of fracture surface and load-displacement curve analysis of DNS test,

The cross points of longitudinal or transvers direction fibers was suggested to behave as obstacles for both deformation and crack propagation, and the density of such point on WP specimens seemed to be more than on CP specimens. The scattering of the data on CP specimens is suggested by the size effects caused by the sparser obstacles than the WP specimens.

Additionally, the bending strength and interlayer shear strength of the NITE-SiC/SiC composites with the CP fiber reinforcing structure were proposed according to the fiber volume fraction. This proposal is implied that the consideration of the fiber volume fraction of the composites as well as the fiber reinforcing structure in application of materials.

References

- [1] R. Naslain, Design, Preparation and properties of non-oxide CMCs for application in engines and nuclear reactors: an overview, *Compos. Sci. Technol.*, 64 (2004) 155-170.
- [2] A. Kohyama, H. Kishimoto, SiC/SiC composite materials for nuclear application, *Nucl. Saf. Simul.*, 4 (2013) 72-79.
- [3] Y. Katoh, K. Ozawa, C. Shih, T. Nozawa, R.J. Shnavski, A. Hasegawa, L.L. Snead, Continuous SiC fiber, CVI SiC matrix composites for nuclear applications: Properties and irradiation effects, *J. Nucl. Mater.*, 448 (2014) 448-476.
- [4] T. Hinoki, Y. Katoh, L.L. Snead, H.C. Jung, K. Ozawa, H. Katsui, Z.H. Zhong, S. Kondo, Y.H. Park, C. Shih, C.M. Parish, R.A. Meisner, A. Hasegawa, Silicon carbide and Silicon carbide composites for fusion reactor application, *Mater. T. JIM*, 54(2013)472-476.
- [5] T. Hinoki, E. Lara-Curzio, L.L. Snead, Mechanical properties of high purity SiC fiber reinforced CVI-SiC matrix composites, *Fusion Sci. Technol.*, 44 (2003) 211.
- [6] T. Nozawa, K. Ozawa, Y.B. Choi, A. Kohyama, H. Tanigawa, Determination and prediction of axial/off-axial mechanical properties of SiC/SiC composites, *Fusion Eng. Des.*, 87 (5-6) (2012) 803-807.
- [7] A. Kohyama, S.M. Dong, Y. Katoh, Development of SiC/SiC composites by Nano-Infiltration and Transient Eutectoid (NITE) process, *Ceram. Eng. Sci. Proc.*, 23 (2002) 311-318.
- [8] A. Kohyama, J.S. Park, H.C. Jung, Advanced SiC fibers and SiC/SiC composites toward industrialization, *J. Nucl. Mater.*, 417 (1-3), (2011), 340-343
- [9] P. Dadras, J.S. McDowell, Analytical and experimental evaluation of double notch shear specimens of orthotropic materials, *Exp. Mech.*, 30 (1990), 184-189
- [10] Ünal Ö, Bansal N, In-plane and interlaminar shear strength of a unidirectional Hi-Nicalon fiber reinforced celsian matrix composites, *Ceram. Int.*, 28 (2002) 527-540
- [11] C. Shih, Y. Katoh, K. Ozawa, L. Snead, Interlaminar shear strength and trans-thickness tensile strength of CVI and NITE SiC/SiC composites, *Fusion Reactor Materials Program, DOE/ER-0313/52*, 52 (2012), 59-75.
- [12] Joon-Soo Park, Hiroshi Nishimura, Daisuke Hayasaka, Ju-Hyeon Yu, Hirotatsu Kishimoto, Akira Kohyama, Fabrication of short SiC fiber reinforced SiC matrix composites with high fiber volume fraction, *Fusion Eng. Des.*, 109-111 (2016) 1174-1178
- [13] Nawaz, G. M. (ed.), *Delamination in advanced composites*, Technomic Publishing Co., Lancaster, PA (1991).
- [14] Griffith, A. A., The phenomena of rupture and flow in solids, *Philosophical Transactions of the Royal Society*, 221A (1920) 163-198.

4. Oxidation behavior of NITE-SiC/SiC composites

4.1 Introduction

Silicon carbide fiber reinforced silicon carbide matrix (SiC/SiC) composites were considered as a promising candidate for the blanket/ divertor components of the fusion energy plant, the core components of fission reactor and the target components of high energy accelerator, due to their lots of attractiveness including superior heat resistance and the inherent low activation/low decay heat [1–3]. Especially, SiC/SiC composites, which were fabricated by nano-infiltration and transient eutectic-phase (NITE) process, represented a dense microstructure with high crystallinity compared with that of SiC/SiC composites fabricated by polymer impregnation and pyrolysis (PIP) or chemical vapor infiltration (CVI) method. The NITE process could provide superior thermo-mechanical properties under a severe environment such as high temperature and neutron bombardment [4–7]. In general, SiC/SiC composites were consisted of SiC fiber, SiC matrix, and interfacial coating layer between SiC fiber and matrix (F/M interface). Both carbon (C) single coating and C/SiC multi-layered coating can be selected as F/M interphase for a nuclear grade of SiC/SiC composites [8–10]. Especially, the carbon interphase provides excellent heat resistance under non-oxidative environment and proper mechanical properties such as elastic modulus, friction, and bonding strength. Although potential applications of SiC/SiC composites for fusion reactor and high energy accelerator is applied under very high vacuum environment ($\sim 10^{-5}$ Pa), it is required to consider their oxidation resistance for the prediction of accident tolerance at the loss of vacuum accident (LOVA) as well as the adulation of proper lifespan at long-term normal operation. The service temperature for SiC/SiC composites could be expected as the range of 600–1000 °C in the fusion reactor [3]. It is not necessary to consider the oxidation behavior at the temperature higher than 1000 °C. Because the fusion reaction is not able to maintain at a poor vacuum condition, the temperature will be decreased below 1000 °C. However, the conventional researches in the application field of aerospace mainly focused on the oxidation test at the temperature higher than 1000 °C, because SiC components were expected to apply for the hottest section of the gas turbine engine. It was well known that the oxidation behavior of SiC materials strongly depended on the temperature and oxygen partial pressure [11,12]. At the high oxidation temperature (> 1000 °C) in the air, the gap between fiber and matrix formed by the oxidation of PyC is rapidly fulfilled by the protective film (SiO_2) accompanying the suppression of further PyC oxidation [8,10]. Although the passive oxidation forming the protective SiO_2 film is still a main oxidation mechanism of SiC at the

medium temperature range ($< 1000\text{ }^{\circ}\text{C}$) and the high oxygen partial pressure, there is a possibility that SiO_2 film cannot protect the interphase of PyC due to its slow growth. In the present study, the oxidation resistance of NITE-SiC/SiC composites with/without CVD-SiC outer coating was investigated in conjunction with the detailed analysis of their microstructures. Especially, the effects of oxidation temperature and oxygen contents on the oxidation resistance of NITE-SiC/SiC composites were examined to understand their oxidation mechanism at a lower temperature. The feasibility of CVD-SiC outer coating as an environmental coating for NITE-SiC/SiC composites were also evaluated.

4.2 Experimental

4.2.1 Materials

NITE-SiC/SiC composites with/without CVD-SiC outer coating were prepared for the oxidation test. SiC/SiC composites have the fabric architecture with $0^{\circ}/90^{\circ}$ cross-ply ($0^{\circ}/90^{\circ}$ XP) of a near-stoichiometric SiC fiber (Hi-Nicalon Type-S, NGS advanced fiber co., Ltd., Japan). The interphase of PyC with the thickness of about 300–500 nm was formed on the SiC fiber surface, using a conventional chemical vapor deposition (CVD) method. Prior to the hot pressing, the preform of SiC fabrics were prepared by the lay-up of unidirectional (UD) prepreg sheets, which consisted of fibers and precursors for the formation of SiC matrix. The oxide powder of Al_2O_3 and Y_2O_3 were added as sintering additives for the consolidation of SiC matrix. The total amount of oxide additives was fixed as about 10 wt%. The preform of layered prepreps was densified at the sintering temperature of $1820\text{ }^{\circ}\text{C}$ and the applied pressure of 20 MPa under an inert gas atmosphere, using a uniaxial hot press device. The density of NITE-SiC/SiC composites measured by the Archimedes' principle is about 3.0 g/cm^3 . The densities of SiC fiber and PyC are assumed 3.1 g/cm^3 and 2.0 g/cm^3 , respectively. The volume or weight fraction of SiC fiber, PyC interphase and SiC matrix in this composite system can be calculated approximately, based on the weight ratio of SiC fiber and PyC interphase and the total amount of coated SiC fiber for the fabrication of the preform. The roughly estimated volume (weight) fraction of SiC fiber, PyC interphase and SiC matrix are 53 vol % (55 wt%), 7 vol% (4.6 wt%) and 40 vol% (40.4 wt%), respectively. The dimension of specimens for the oxidation test was $10(\text{w}) \times 10(\text{l}) \times 2(\text{t})\text{ mm}^3$. The surface of oxidation test specimen was mechanically grinded without the mirror polishing. In order to protect the interphase of PyC inside NITE-SiC/SiC composites from oxidation, the CVD-SiC outer

coating on the surface was performed using a formation method of environmental barrier coating. For the formation of CVD-SiC outer coating on the whole surface, the coupon of specimen with small holes of $\phi 2\text{mm}$ hanged with a carbon yarn in the CVD chamber. These coupon was coated twice. The thickness of CVD-SiC outer coating was measured as about $150\ \mu\text{m}$. As a reference material, the nuclear grade fine-grained isotropic graphite specimens (IG-430U, Toyo Tanso Co., Ltd.) was also prepared with the same procedure. The appearances of IG-430U and NITE-SiC/SiC with/ without CVD-SiC outer coating were shown in figure 4.1.

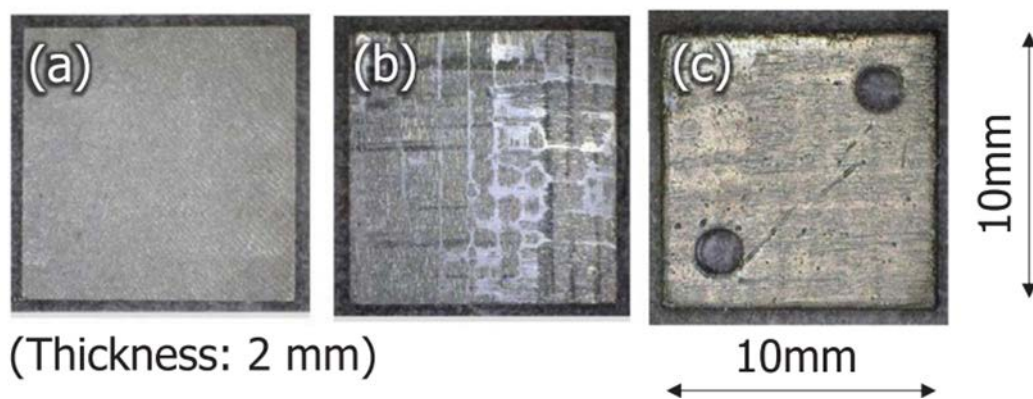


Figure 4.1 Appearances of oxidation test specimens: (a) IG-430U, (b) NITE-SiC/SiC composites, and (c) NITE-SiC/SiC composites with CVD-SiC outer coating.

4.2.2 Oxidation test

The oxidation tests for NITE-SiC/SiC composites were carried out using an infrared gold image furnace (Advance Riko, Inc., Japan). The conceptual illustration of the heating zone in the infrared gold image furnace was shown in figure 4.2. The total pressure and the flow rate of environmental gas was 1 atm and 200 ml/min, respectively. The environmental gases were supplied through the nozzle located at the top of the specimen. Two kinds of environmental gases were utilized to investigate the effects of the oxygen content. The one is an air gas containing the oxygen of about 21% (O_2 21%). The other is a nitrogen gas including a small amount of oxygen (O_2 1%). The specimen was placed on the semicircular quartz stand, which stood on the center of quartz specimen holder. The edges of specimen were partially contacted with the semicircular quartz stand, thus nearly entire surface of specimen was exposed to the

environmental gas. The concentration of moisture inside the air were ignored in this test. In order to investigate the effect of temperature oxidation history on the weight change of NITE-SiC/SiC composites, the test specimen were heat-treated at various conditions of temperature range (400–1000 °C) and its holding time (1 min – 10 h). As shown in figure 4.3, two kinds of heating patterns such as simple monotonic heating and cyclic heating with different holding times were utilized for the oxidation test of NITE-SiC/SiC composites.

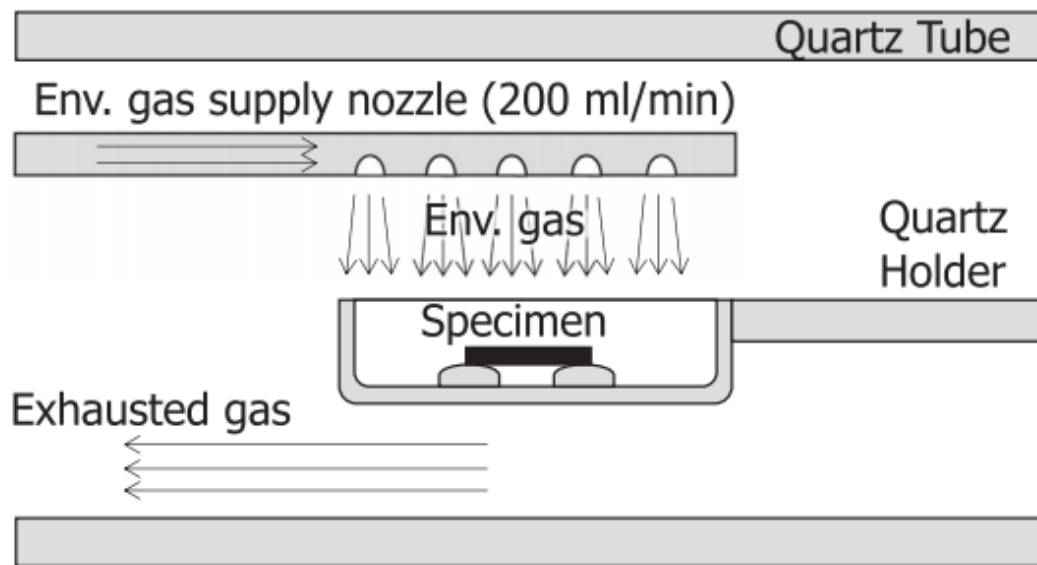


Figure 4.2 Conceptual illustration of the heating zone in the infrared gold image furnace.

The specimens were heated up to the test temperature within 1 min. The environmental gas was continuously supplied during the heating/cooling step and the holding step. Because of the continuous supply of environmental gas and the fast response of infrared gold image furnace, the specimen was rapidly cooled down to room temperature within about 5 min. The weight of specimen subjected to the oxidation test was measured, using a high accuracy electronic balance. The oxidation test conditions of NITE-SiC/SiC composites were summarized in Table 4.1. In general, it is difficult to detect the weight and appearance changes of NITE-SiC/SiC composites heat-treated at the condition of “short holding time - low temperature”. Moreover, the weight change of graphite specimens for the heat-treated condition of “long holding time - high temperature” is also difficult to measure, due to the occurrence of full oxidation on the entire surface.

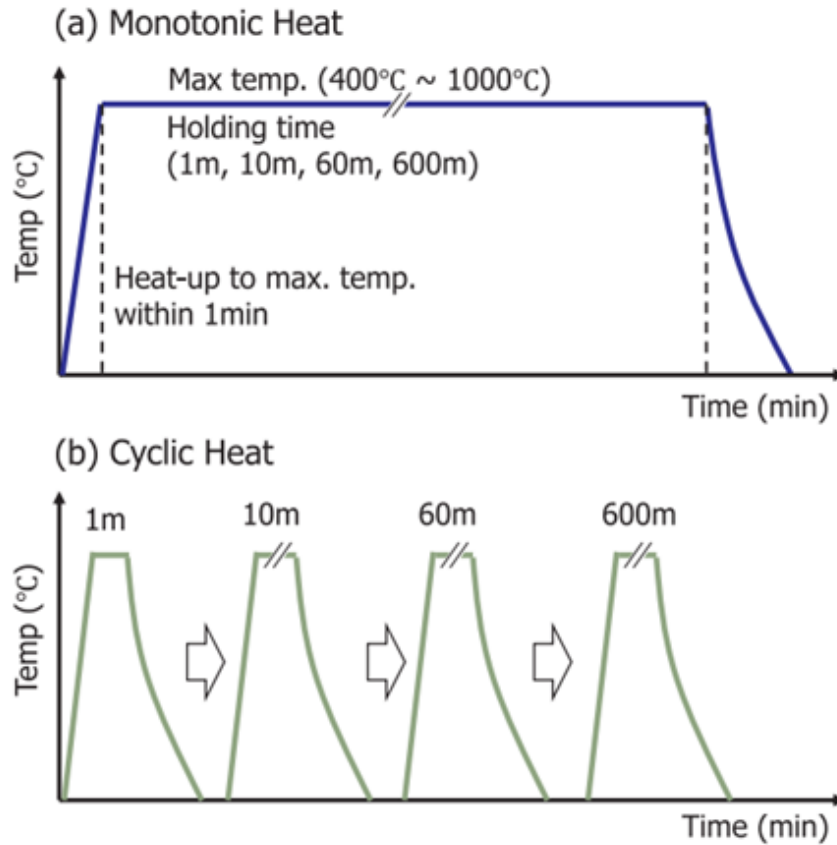


Figure 4.3 Heating patterns utilized for the oxidation test.

Thus, the test condition like “short holding time - low temperature” or “long holding time-high temperature” was omitted in this study. The weight change speed of test specimen is determined from the amount of weight change divided by the nominal surface exposure and the holding time. In this study, the change of specimen surface exposed from the oxidation test was also ignored. Since the weight change of NITE-SiC/SiC composites is only affected by the loss of PyC interphase, the amount of PyC interphase remained in the specimen after the oxidation test is measured to estimate the oxidation behavior. After the oxidation test, the specimens were machined with a precision diamond saw. The test specimen for the observation was carefully polished with a diamond slurry containing an average particle size of about 3 μm .

	O ₂ = 21%				O ₂ = 1%					
	Temp. [°C]	Time [min] () is accumulated time at the cyclic heating pattern				Temp. [°C]	Time [min] () is accumulated time at the cyclic heating pattern			
		1 (1)	10 (11)	60 (71)	600 (671)		1 (1)	10 (11)	60 (71)	600 (671)
Graphite (IG-430U)	400				C					
	600				C					
	800	M	M	M	C	M	M	M	C	
	1000				C					
NITE-SiC/SiC	400				M	M				
	600				M	M	M			
	800				M	M			M	
	1000				M	M				
NITE-SiC/SiC with CVD-SiC outer coating	400									
	600									
	800				C				C	
	1000				C					

• **M** means Monotonic heating pattern
 • **C** means Cyclic heating pattern

Table 4.1 Oxidation test conditions of graphite, NITE-SiC/SiC composites, and NITE-SiC/SiC composites with CVD-SiC/SiC outer coating

4.3 Results & Discussion

4.3.1 Oxidation rate of carbon in atmosphere

Figure 4.4 shows the relation between weight change speed and holding time for the oxidation of isotropic graphite specimen (IG-430U). The cross section of graphite specimen tested at the oxidation temperature of 800 °C under the air (O₂ 21%) and N₂ gas containing O₂ 1% was also shown in figure 4.5. The symbol of open diamonds in figure 4.5 represents the oxidation test results of IG-430 graphite reported by Fujita et. al. [13].

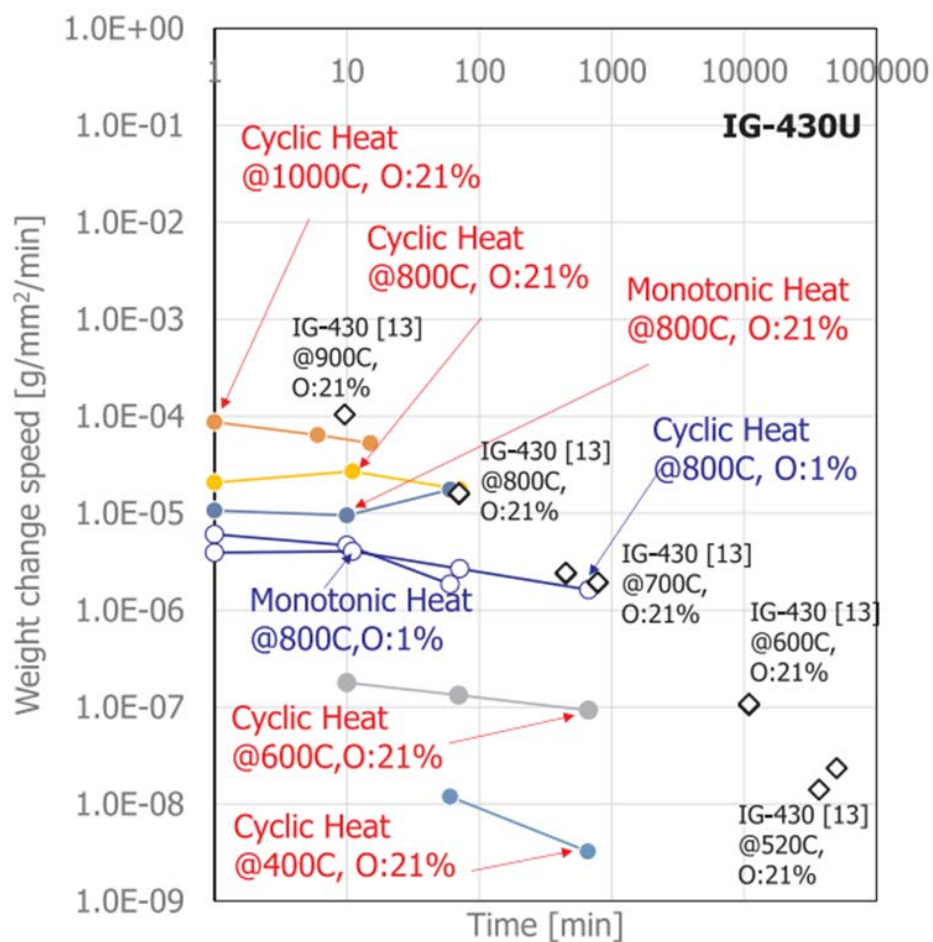


Figure 4.4 Relation between weight change speed and holding time for the oxidation of isotropic graphite specimen (IG-430U)

It was used as reference data in order to verify the reliability of oxidation test. The reference data were obtained from the oxidation test under the similar test condition the (air flow = 200 ml/min), using a specimen with the shape of cylindrical column. It was found that these data represented a good agreement with the results for IG-430U graphite. The difference of weight loss for cyclic and monotonic heating pattern was also small. Especially, the weight loss amount of IG-430U graphite was too small to measure at the test temperature lower than 600 °C. However, such an amount of weight loss drastically increased with increasing the test temperature. The IG-430U graphite represented the weight change speed up to about 8.7×10^{-5} g/mm² /min at the test temperature of 1000 °C under the air atmosphere. It was found that the weight change speed of IG-430U graphite slightly decreased or maintained with increasing of holding time.

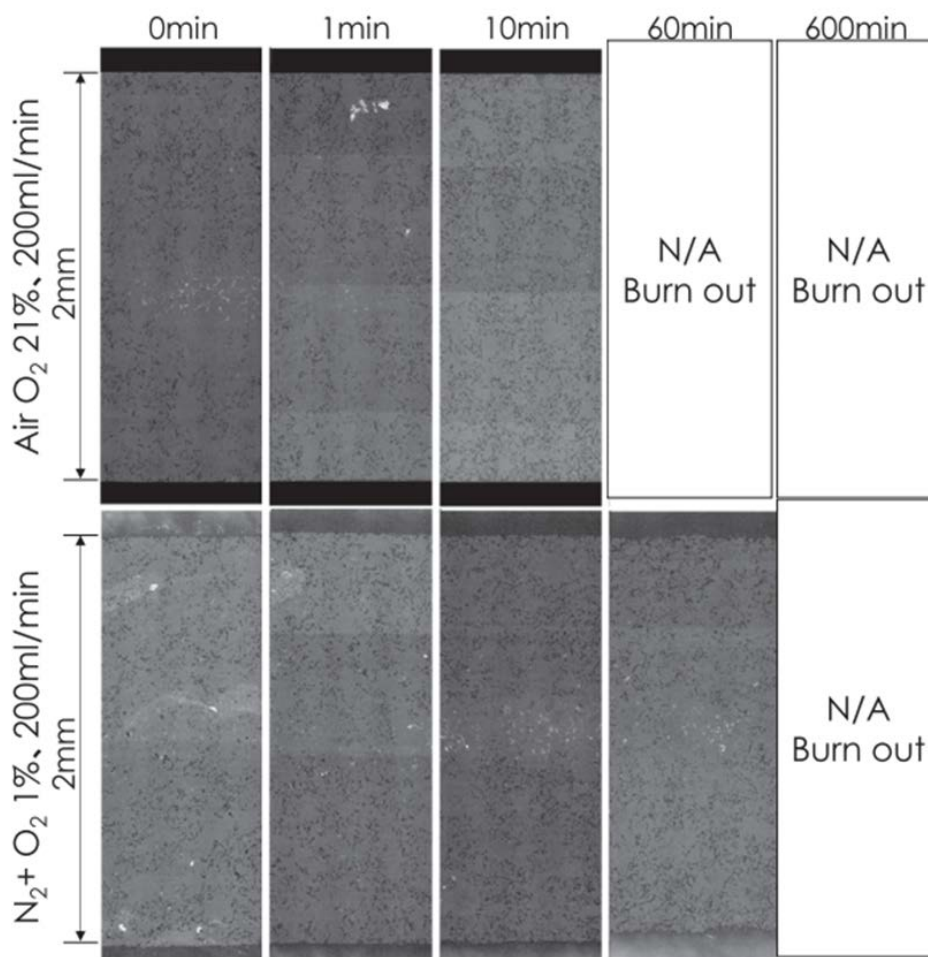


Figure 4.5 Cross section of graphite specimen tested at the oxidation temperature of 800 °C under the air (O₂ 21%) and N₂ gas containing O₂ 1%

As shown in figure 4.5, the thickness of IG-430U graphite and its surface exposure area continuously decreased during the oxidation test. This phenomena can be regarded as one of reasons for the small decrease of weight change speed. In the case of the oxidation test at 800 °C, the weight change speed of IG-430U graphite suffered from the conditions of O₂ 21% and O₂ 1% were $1.7\text{--}2.7 \times 10^{-5}$ g/mm²/min and $1.6\text{--}4.0 \times 10^{-6}$ g/mm²/min, respectively. This means that the decrease of oxygen content leads to the activation of weight change of speed for IG-430U graphite. It seems that the oxidation of carbon in the high O₂ environment is greatly affected by the diffusion mechanism and the boundary-layer formed near at the exposed surface [14].

4.3.2 Oxidation of NITE-SiC/SiC composite with/without CVD-SiC outer coating

Figure 4.6 shows the relation between weight change speed and holding time in the oxidation of NITE-SiC/SiC composites. It is found that the effects of oxidation temperature and oxygen content on the weight change speed of NITE-SiC/SiC composites are negligible. However, the weight change speed of NITE-SiC/SiC composites strongly depended on the holding time at the oxidation environment. The NITE-SiC/SiC composites possessed a weight change speed of 3.6×10^{-5} g/mm²/min at the holding time of 1 min under the oxidation temperature 800 °C and the oxygen content of 21% (O₂ 21%). Such a weight change speed drastically decreased with increasing the holding time of oxidation. Both volume fraction and weight fraction of PyC interphase inside NITE-SiC/SiC composites were estimated as about 7.0 vol% and about 4.6 wt%, respectively. The weight change of NITE-SiC/SiC composites was mainly dominated by the loss of PyC interphase, since the formation speed for the protective film of SiO₂ (< 20 nm/h) on the surface of SiC and Hi-Nicalon Type-S SiC fiber was very slow at the low oxidation temperature [15,16]. From these results, the remained amount of PyC interphase inside these composites after the oxidation treatment can be estimated.

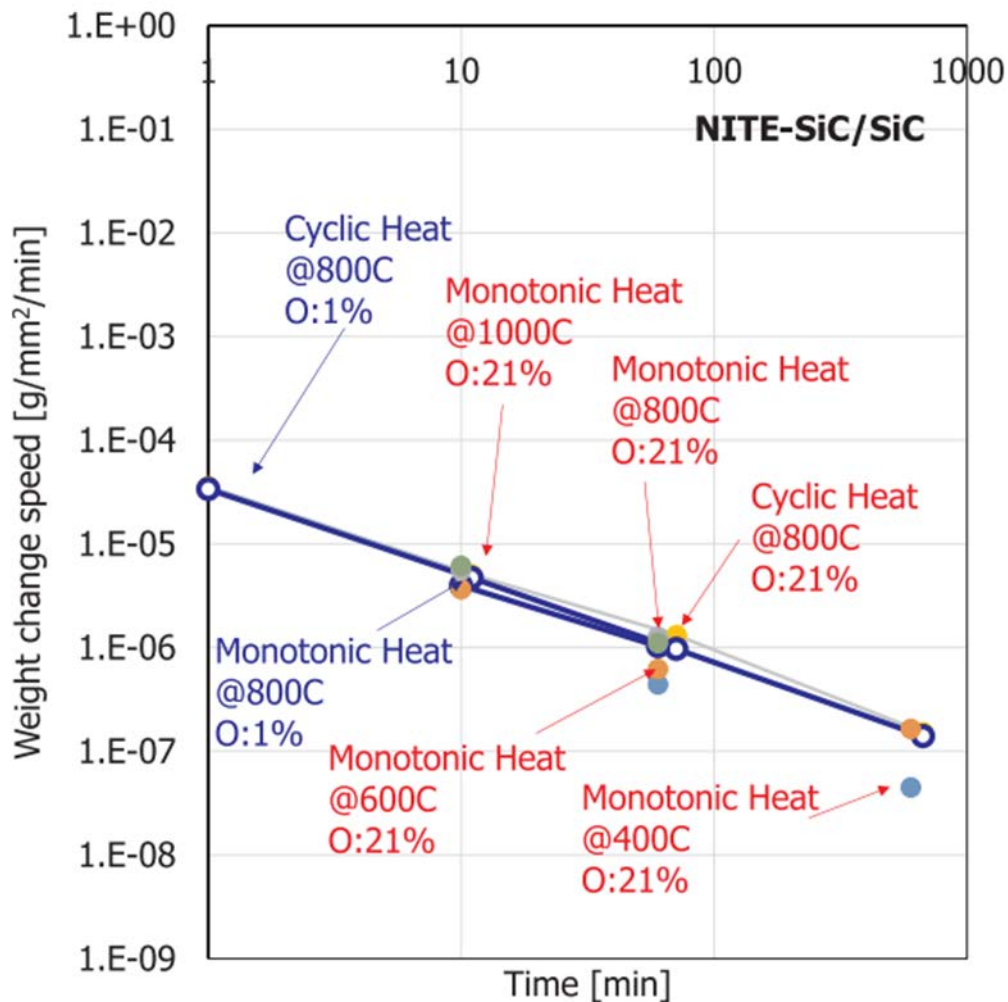


Figure 4.6 Relation between weight changing speed and holding time in the oxidation of NITE-SiC/SiC composites.

Figure 4.7 showed the relation between weight change speed and the amount of remained carbon in the oxidation of NITE-SiC/SiC composites. The oxidation behavior of NITE-SiC/SiC composites relatively displayed a large scattering at the monotonic heating pattern, due to the initial difference in the amount of fiber and PyC interphase inside each specimen. On the contrary, it could be clearly found from a cyclic heating pattern for the oxidation test that the weight change speed of NITE-SiC/SiC composites had a strong relation to the remained amount of carbon inside test specimen. However, it is difficult to explain from the results for the simple loss of PyC interphase, because the weight change speed of carbon (IG-430U) is almost constant or slightly decreases with increasing the holding time of oxidation as mentioned in figure 4.4 and figure 4.5.

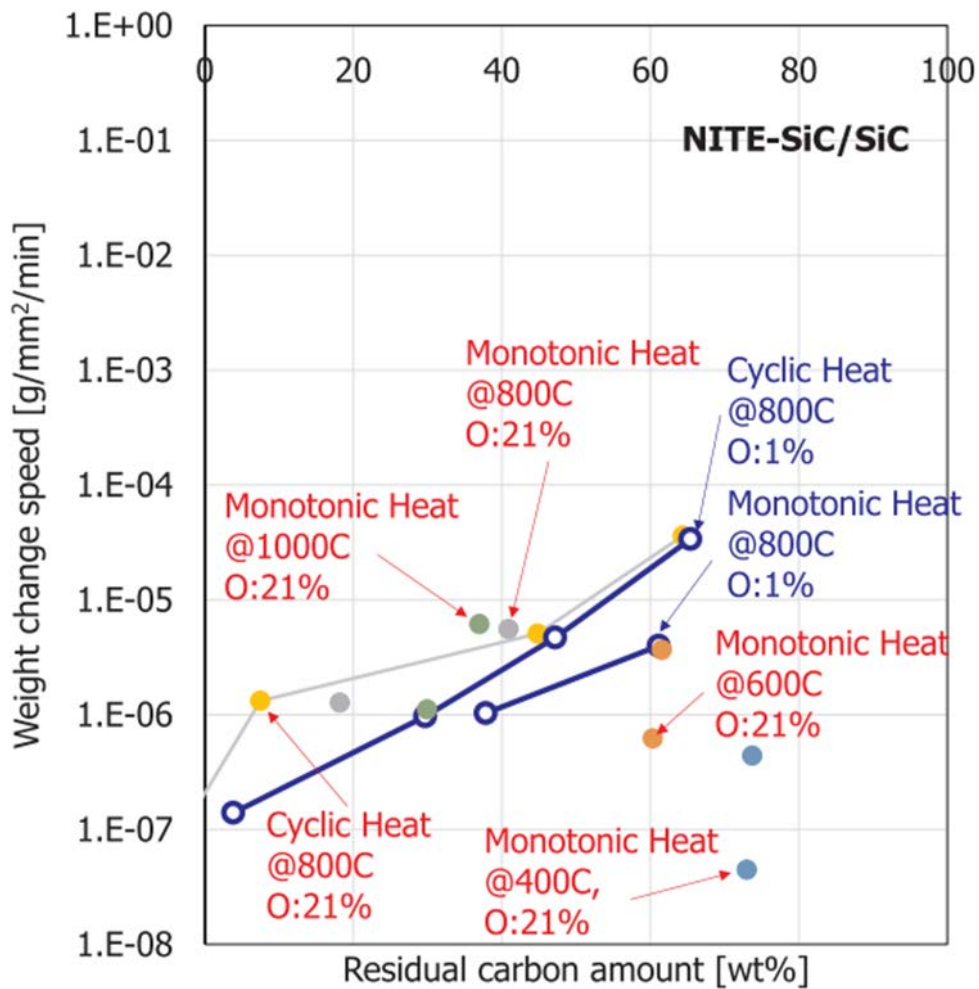


Figure 4.7 Relation between weight change speed and the amount of remained carbon in the oxidation of NITE-SiC/SiC composites

Figure 4.8 shows the cross section of NITE-SiC/SiC composites exposed at the oxidation environment. The microstructure of fiber bundle inside NITE-SiC/SiC composites after the oxidation test was also shown in figure 4.9. The oxidation test of NITE-SiC/SiC composites was carried out at the temperature of 800 °C under the N₂ gas atmosphere containing the oxygen of 1% (O₂ 1%) and the holding time of 671 min, using a cyclic heating pattern. It is well known that Si-based material such as Si, SiC and Si₃N₄ obviously created the oxide film (SiO₂) on the surface in the oxidation environment of high temperature and high oxygen. However, as already mentioned in figure 4.6, the growth rate of the oxide film on monolithic SiC and Hi-Nicalon Type-S SiC fiber was less than 20 nm/h at the lower oxidation temperature (< 1000 °C) [15,16]. In this study, the thickness change of NITE-SiC/SiC composites subjected to the formation of oxide film was very hard to find from the observation results of FE-SEM. It was found from figure 4.9 (a) that the interphase of PyC also disappeared after the

oxidation test of NITE-SiC/SiC composites. However, a part of PyC interphase still existed inside some fiber bundles, as shown in figure 4.7 and figure 4.9 (b). Such an amount of PyC interphase after the oxidation test was estimated as almost 40 wt%. The results of conventional researches already showed that the monolithic NITE-SiC and NITE-SiC/SiC composites possessed the superior gas tightness at the gas permeability test of H₂ and He environments [17,18]. NITE-SiC/SiC composites used in this study have a fiber architecture of 0°/90° XP, in which UD prepreg sheets alternatively stacks. These fiber bundle were obviously separated from the inter-bundle SiC matrix. It means that it is difficult to infiltrate the environmental gas into the stacking direction of fiber prepreg. As shown in figure 4.9 (a), a gap of about 300 nm only exists between fiber and matrix. This fine gap can be considered as one of the main reasons for the difficult of environmental gas infiltration into NITE-SiC/SiC composites.

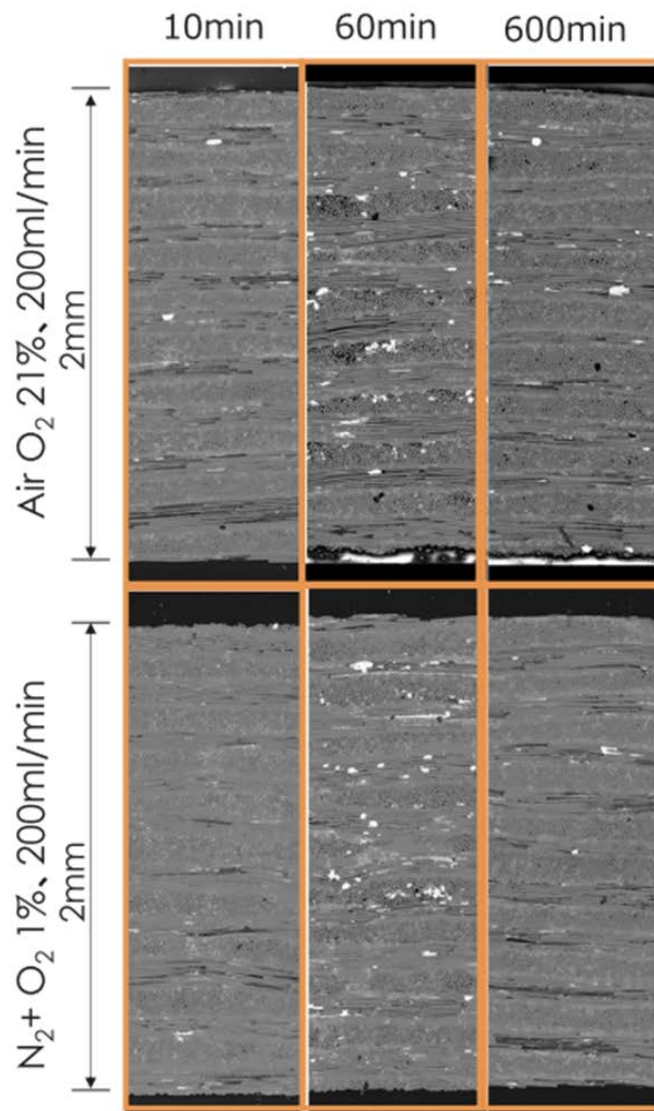


Figure 4.8 Cross section of NITE-SiC/SiC composites exposed at the oxidation environment.

Figure 4.10 shows the relation between weight change speed and holding time for the oxidation of NITE-SiC/SiC composites with CVD-SiC outer coating. The microstructure of intra-fiber bundle region for the cross section of NITE-SiC/SiC composites suffered from the oxidation test was also shown in figure 4.11. The oxidation of NITE-SiC/SiC composites were performed at the temperature of 800 °C under the air atmosphere containing the oxygen content of 21% (O₂ 21%). It was obviously found that the CVD-SiC outer coating could provide a superior oxidation resistance for NITE-SiC/SiC composites.

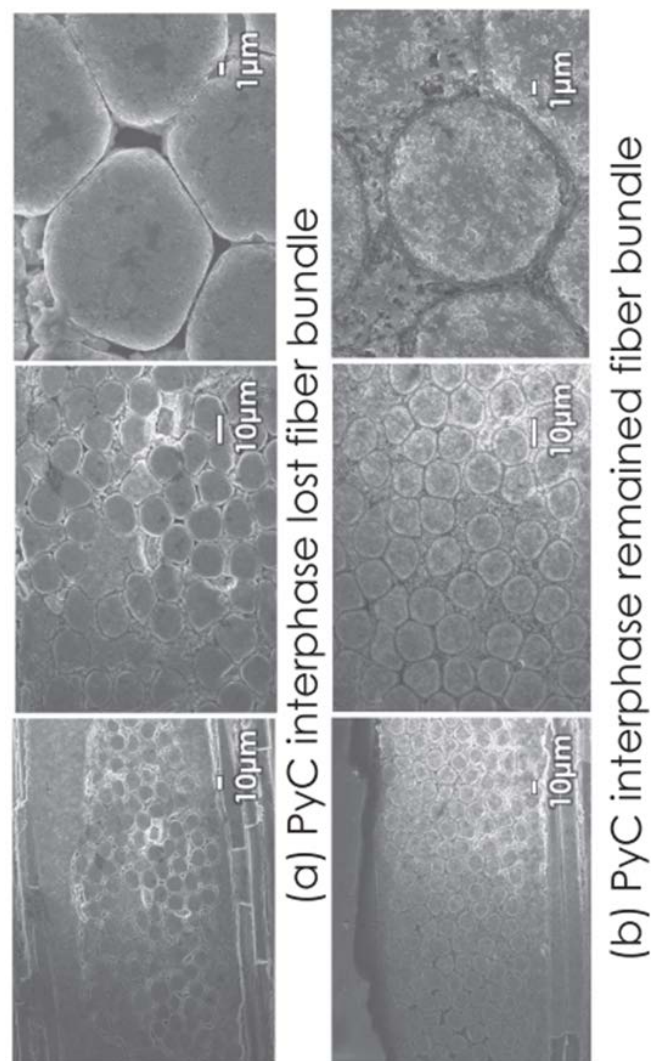


Figure 4.9 Microstructure of fiber bundle inside NITE-SiC/SiC composites after the oxidation test.

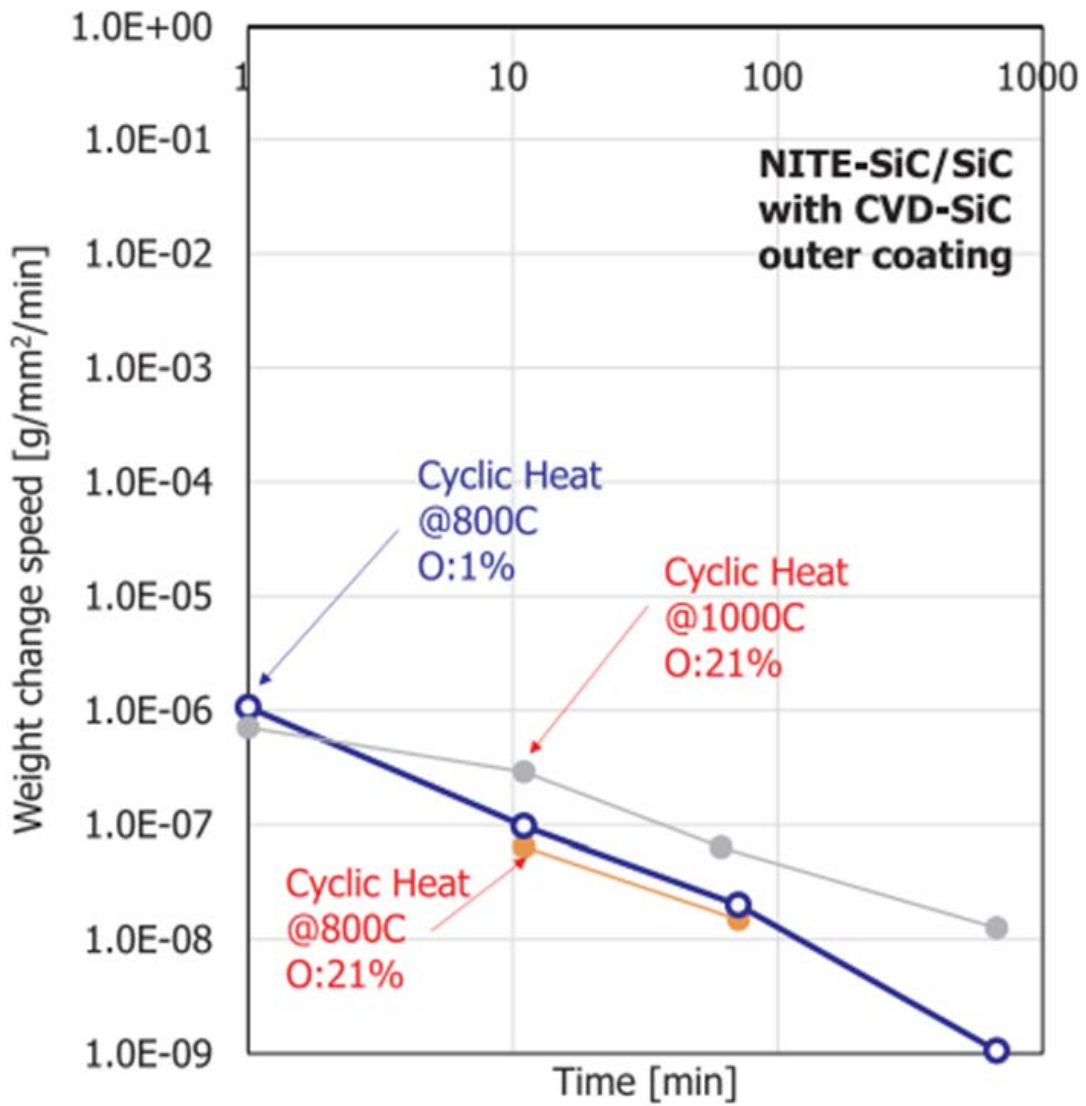


Figure 4.10 Relation between weight change speed and holding time in the oxidation NITE-SiC/SiC composites with CVD-SiC outer coating.

As shown in figure 4.11, a sound PyC interphase was obviously observed at the intra fiber bundle region inside NITE-SiC/SiC composites after the oxidation test. It was hard to find any evidence for the loss of PyC interphase resulted from the oxidation. In addition, NITE-SiC/SiC composites were not almost affected by the oxidation temperature and the oxygen content, due to the existence of CVD-SiC outer coating. However, it seems that there is some relation between weight change speed and oxidation holding time, even though the amount of weight change is very small up to the measurement limit of an electronic balance used in this study.

4.4 Summary

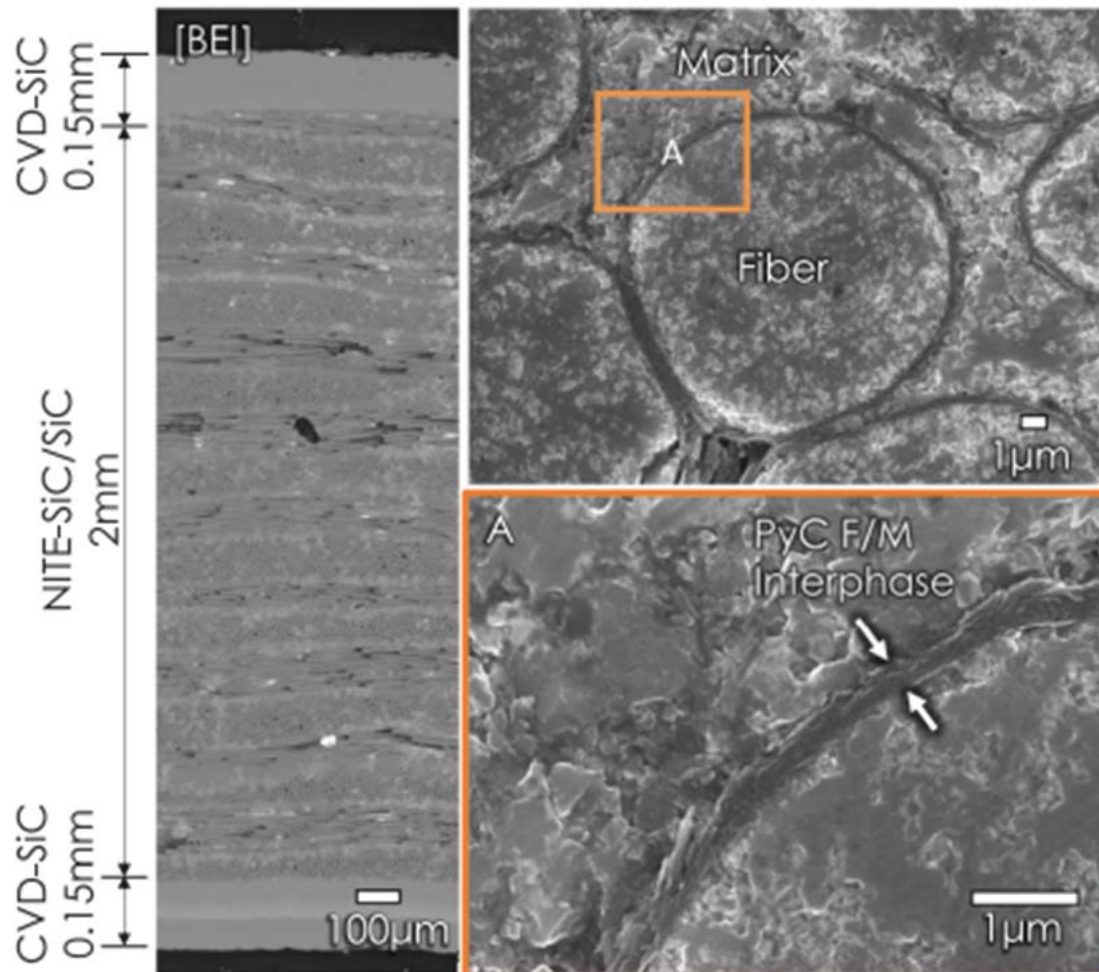


Figure 4.11 Microstructure of intra-fiber bundle region for the cross section of NITE-SiC/SiC composites with CVD-SiC outer coating suffered from the oxidation test at 800 °C in air (O_2 21%).

The oxidation resistance of NITE-SiC/SiC composites with/without CVD-SiC outer coating were evaluated under various oxidative conditions. The relation between weight change speed and holding time for the oxidation of isotropic graphite specimen (IG-430U) was examined at the oxidation atmosphere. The graphite materials (IG-430U) were easily burned out in an oxidation environment. The weight change speed of graphite materials was constant of slightly decreased with the increase of oxidation holding time. On the contrary, NITE-SiC/SiC composites represented an extremely low amount of weight loss without any change of shape and size, even if these materials exposed at the

severe oxidation environment under the forced flow of oxidative gas. The weight change speed of NITE-SiC/SiC composites clearly decreased with increasing the oxidation holding time, because the supply of oxidative gas and the extraction of combustion gas is not permitted from the direction of specimen thickness but is permitted only from the direction of specimen side. It was also confirmed that the CVD-SiC outer coating could be regarded as an effective environmental barrier for the oxidation proof resistance of NITE-SiC/SiC composites.

References

- [1] G.R. Hopkins, Silicon carbide and graphite materials for fusion reactors, in: Proc IAEA Symp. on Plasma Physics and Controlled Nuclear Fusion Research, Tokyo, Japan, IAEA-CN-33/s3-3, IAEA, Vienna, 1974, p. 2.
- [2] S.J. Zinkle, N.M. Ghoniem, Operating temperature windows for fusion reactor structural materials, *Fusion Eng. Des.* 51–52 (2000) 55–71.
- [3] T. Nishitani, H. Tanigawa, T. Nozawa, S. Jitsukawa, M. Nakamichi, T. Hoshino, T. Yamanishi, N. Baluc, A. Möslang, R. Lindou, S. Tosti, E.R. Hodgson, S. Clement Lorenzo, A. Kohyama, A. Kimura, T. Shikama, K. Hayashi, M. Araki, Recent progress in blanket materials development in the broader approach, *J. Nucl. Mater.* 417 (2011) 1331–1335.
- [4] A. Kohyama, S.M. Dong, Y. Katoh, Development of SiC/SiC composites by nanoinfiltration and transient eutectic (NITE) process, *Ceram. Eng. Sci. Proc.* (2000) 311–318.
- [5] S.M. Dong, Y. Katoh, A. Kohyama, Processing optimization and mechanical evaluation of hot pressed 2D Tyranno-SA/SiC composites, *J. Eur. Ceram. Soc.* 21 (2003) 1223–1231.
- [6] K. Shimoda, J.S. Park, T. Hinoki, A. Kohyama, Microstructural optimization of hightemperature SiC/SiC composites by NITE process, *J. Nucl. Mater.* 386–388 (2009) 634–638.
- [7] A. Kohama, J.S. Park, H.C. Jung, Advanced SiC fibers and SiC/SiC composites toward industrialization, *J. Nucl. Mater.* 417 (2011) 340–343.
- [8] R.R. Naslain, R.J.-F. Paillet, J.L. Lamon, Single- and multilayered interphases in SiC/SiC composites exposed to severe environmental conditions: an overview, *Int.J. Appl. Ceram. Technol.* 7 (2010) 263–275.
- [9] W. Yang, A. Kohyama, T. Noda, Y. Katoh, T. Hinoki, H. Araki, J. Yu, Interfacial characterization of CVI-SiC/SiC composites, *J. Nucl. Mater.* 307–311 (2002) 1088–1092.
- [10] Y. Chai, X. Zhou, H. Zhang, Effect of oxidation treatment on KD-II SiC fiber-reinforced SiC composites, *Ceram. Int.* 43 (2017) 9934–9940.
- [11] J.E. Antill, J.B. Warburton, Active to passive transition in the oxidation of SiC, *Corros. Sci.* 11 (1971) 337–342.
- [12] T. Narushima, T. Goto, T. Hirai, Y. Iguchi, High-temperature oxidation of silicon carbide and silicon nitride, *Mater. Trans.* 38 (1997) 821–835.
- [13] I. Fujita, M. Eto, H. Ohsaki, T. Shibata, J. Sumita, T. Konishi, M. Yamaji, E. Kunimoto, Evaluation of oxidation characteristics of fine-grained graphite (IG-110 and IG-430) for very high temperature reactor – changes in density distribution and compressive strength caused by air-oxidation, *IAEA-Res.* (2013) .
- [14] A. Theodosiou, A.N. Jones, B.J. Marsden, Thermal oxidation of nuclear graphite: a large scale waste treatment option, *PLoS One* 12 (2017) e0182860.
- [15] Y. Hijikata, S. Yagi, H. Yaguchi, S. Yoshida, Chapter. 7. Thermal oxidation mechanism of silicon carbide, physics and technology of silicon carbide devices, *IntechOpen* (2012) 181–205 (ISBN: 978-953-51-0917-4).
- [16] H. Serizawa, C.A. Lewinsohn, G.E. youngblood, R.H. Jones, D.E. Johnston, A. Kohyama, Evaluation of advanced SiC fibers for reinforcement of CMC, in: *Proceeding of 12th International Conference on Composite Materials (ICCM-12)*, Paris, July 5, 1999, paper 378.

- [17] T. Hino, E. Hayashishita, Y. Yamauchi, M. Hashiba, Y. Hirohata, A. Kohyama, Helium gas permeability of SiC/SiC composites used for in-vessel components of nuclear fusion reactor, *Fusion Eng. Des.* 73 (2005) 51–56.
- [18] D. Hayasaka, J.S. Park, H. Kishimoto, A. Kohyama, Gas leak tightness of SiC/SiC composites at elevated temperature, *Fusion Eng. Des.* 109–111 (2016) 1498–1501.

5. Improvement of Slurry Droplet Wetting method for Li_2TiO_3 Pebbles

5.1 Introduction

The nuclear fusion reactor is required a large amount of tritium as fuel. Because of enormous energy is generated by nuclear fusion between deuterium and tritium (the detail was presented in the 1. Introduction). However, the half-time of tritium is 12.3 years, which is not abundant in nature [1]. For that reason, the tritium has to be produced at a satisfactory tritium breeding ratio by utilizing a nuclear reaction of neutron and tritium breeder materials including lithium (Li). A lot of researchers have reported fabrication methods pebble-type Li_2TiO_3 tritium breeding materials. Several methods for fabrication of Li_2TiO_3 pebbles are being developed, which are direct/indirect wet method, sol-gel method, extrusion-spheronisation-sintering method, freeze drying method and so on [6-12].

At present, the slurry droplet wetting method has developed for Li_2TiO_3 pebbles in National Fusion Research Institute (NFRI) in Korea. Preliminary, the slurry droplet wetting method for the Li_4SiO_4 pebble has been developed [13].

General principles of falling drop method are: the principle of the method involves timing the fall of a drop of body fluid of known size, through a definite distance in a mixture non-miscible with the fluid. This mixture should have a low viscosity and a specific gravity somewhat below that of the fluid to be tested. It consists of two substances, one heavier and one lighter than the range of fluids to be tested, so that by adjusting the proportions, the specific gravity of the mixture can be adapted to the expected conditions [5]. The droplets producing devices used mostly are tubes containing sharp tips (such as nozzle) at one end where droplet are produced and wide mouth on the other side where the liquids are filled.[3] in these dropping devices, the produced droplets at the nozzle continue falling freely under the influence of gravity into gelation or coagulation bath. As gravity is the only driving force to generate the droplet from nozzle, these devices produce big droplet of the size of few millimeters, which is usually bigger than the nozzle diameter. In the conventional dropping method ds the shape and size of the particles are dependent on the thermophysical properties of the solution such as surface tension, density and dynamic viscosity and on process parameters such as nozzle geometry and gravitational force [4].

Engineering production of slurry droplet wetting method for Li_2TiO_3 tritium breeding materials from the Li_2TiO_3 slurry had already been developed from laboratory experiments to industrial scale. The equipment optimized industrial scale are shown at figure 5.1 [2]. However, the slurry droplet wetting method should be improved considering packing factor for TBR. In this study, the slurry droplet wetting method were improved focusing to the improving the shaping and homogeneous microstructure of Li_2TiO_3 pebbles.

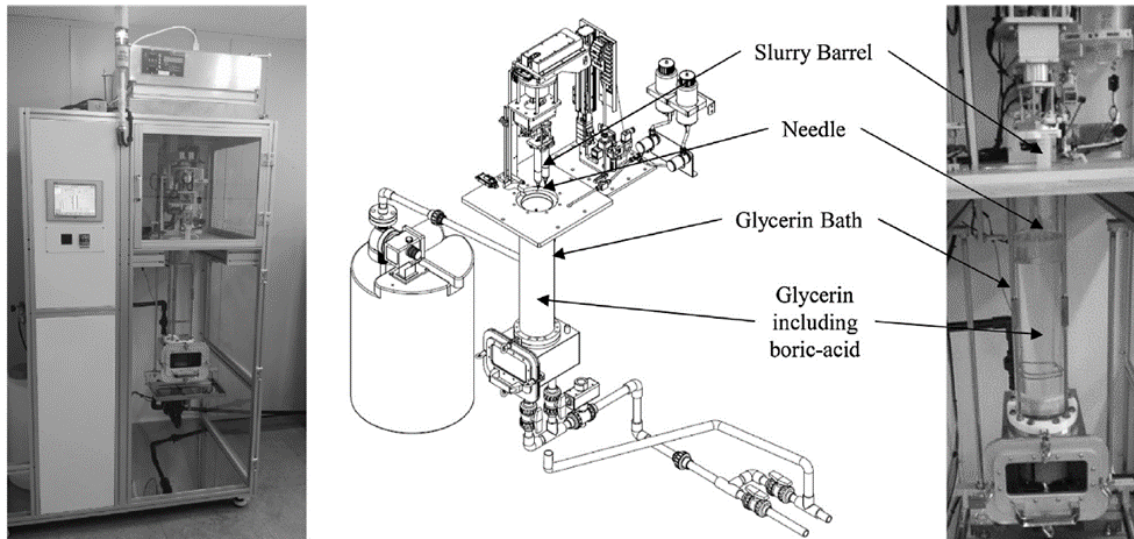


Figure 5.1 Automatic dispensing system and its schematic

5.2 Experimental

In this study, the all of experimental are used mock-up equipment such as figure 5.2. The mock-up equipment are fabricated based on the slurry droplet wetting method by TBM team of Korea institute of fusion energy.

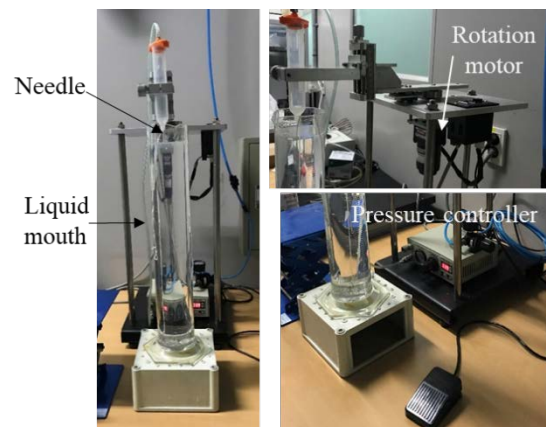


Figure 5.2 Mock-up equipment

5.2.1 Initial Material & Mixing Condition

Normally, the Li_2TiO_3 powder was synthesized by solid-state reaction process. Concretely, the fabrication methods are classified by the kind of initial material ($\text{Li}_2\text{CO}_3 + \text{TiO}_2$ or $\text{Li}_2\text{O} + \text{TiO}_2$). However, the Li_2TiO_3 powders were prepared as commercial high purity Li_2TiO_3 powder (Japan Pure Chemical Co. Ltd., Japan) for accessibility, which is presented in figure 5.3. The XRD pattern of Li_2TiO_3 powder were represented in figure 5.4. The pattern was matched as Li_2TiO_3 from the JCPDS No. 01-077-8280. The commercial powder were mixed with Polyvinyl Alcohol (PVA) from the Sigma-Aldrich Inc. For the refining particles, the commercial powder with PVA were wet ball-milled for 20h. Distilled water and zirconia balls were used as the solvent and ball media. The purity of glycerin and boric acid is 99% and 99.5%, respectively, which were prepared by Daejung Chemicals & Mats Co., Ltd. The boric acid was used as hardening agent of the PVA.

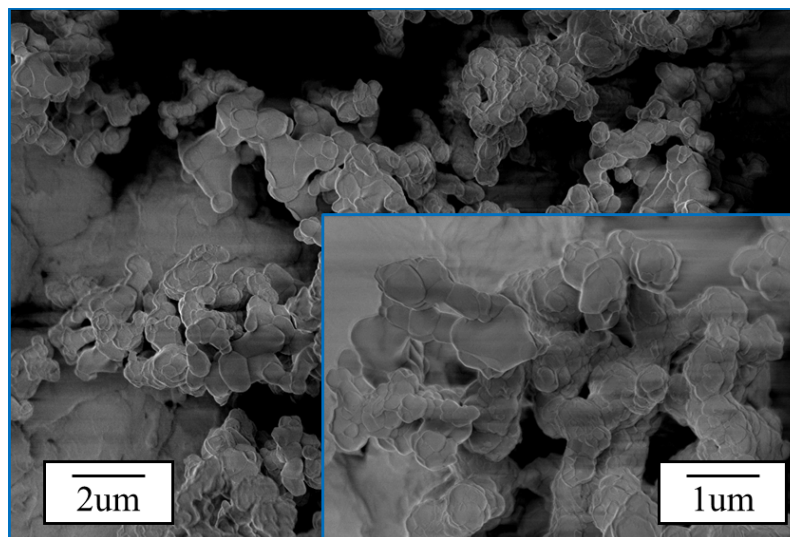


Figure 5.3 Morphology of Li_2TiO_3 powder from the Kojundo

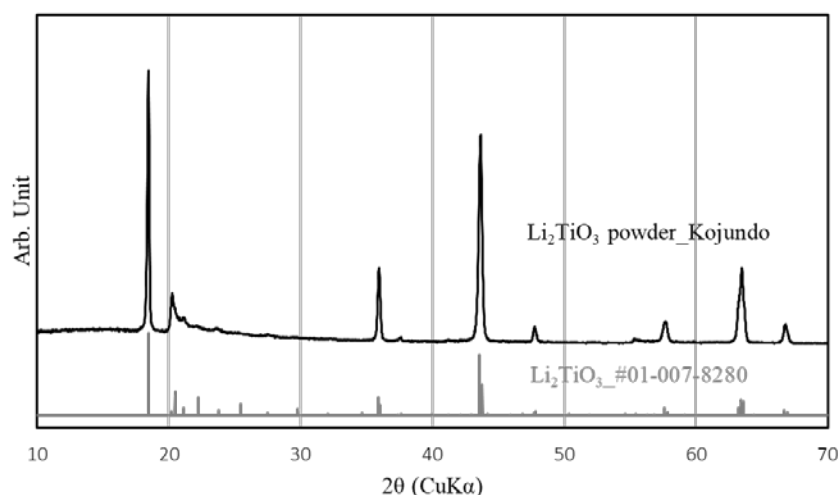


Figure 5.4 The pattern of Li_2TiO_3 powder from the Japan pure chemical.

5.2.2 Dynamic Interactions between Slurry and Glycerin with Boric acid

Polymer foams have been widely used in many fields because they have good properties such as lightweight and process a high specific surface area, good specific strength, and excellent thermal insulation, heat preservation, and sound absorption [14].

Shaping step among the slurry droplet wetting process which can be formed via covalent cross-linking between PVA inner slurry and Boric acid. Boric acid accepts a hydroxide OH^- from water and glycerin according to the following reaction [15]:



The ionized borate molecule acts in a condensation reaction of PVA molecules as shown in figure 5.5, which is a chemical cross-linking mechanism between PVA and Boric acid. Indeed, the boric acid plays a role as a hardening agent of the PVA. The boric acid were mixed with glycerin. Because of the distilled water existed in the slurry as well as H_2O generated from the cross-linking reaction, which have to remove for shaping with hardening. The glycerin can be absorbed the water at same time can be mixed with boric acid. Therefore, the glycerin and boric acid were prepared as wide mouth.

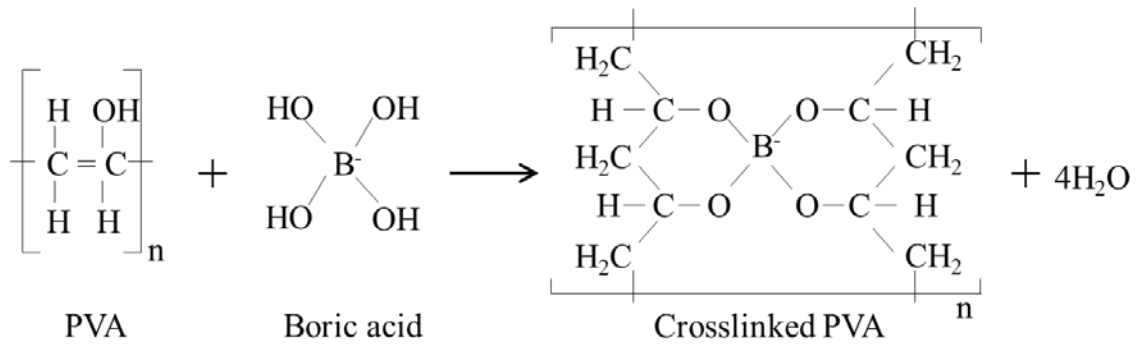


Figure 5.5 Didiol model cross-linkage with mechanism between PVA and Boric acid

The amount of PVA in the slurry or boric acid in the glycerin can effect the shaping of pebble. The Yi-hyun Park et al. were suggested suitable amount of PVA in the slurry when the ratio of glycerin and boric acid is 95 wt% and 5 wt% [15]. The unbalance ratio of PVA or boric acid lead to occur defectives such as wrinkle on the surface. It is expected the gradient reaction velocity between PVA and boric acid.

5.2.3 Surface Tension

Much of the ability to produce advanced materials relies on a well-developed understanding of surface tension. Surface tension is an important factor in the fabrication method to obtain a spherical pebble. Dynamic and static measurement methods were applied to obtain the surface tension value of the slurry, but the reliability of the value was very low due to the hardening and adhesion of PVA in the slurry. Therefore, the surface tension of the slurry was expressed as slurry mixing ratio. The surface tension of the liquid bath according to the surface tension of the slurry is also important. In the fabrication method, the liquid bath was replaced with a mixture of glycerin (95 wt%) and boric acid (5 wt%). The mixing ratio of the slurry applied in this experiment is shown in Table 5.1. In the previous paper [15], wrinkles was observed on the surface of the fabricated pebble according to the concentration of PVA in the slurry. The ratio of PVA was controlled at narrow rage (4~5%) at the slurry mixing ratio, and the ratio of H₂O and powder was controlled only. Where the PVA is used powder type from sigma Aldrich.

The needle size and injection pressure was 27 G and 0.2 MPa, respectively.

	Powder (wt%)	H2O (wt%)	PVA (wt%)
S-1	50	45	5
S-2	44.5	50.5	5
S-3	44	51	5
S-4	43.3	51.7	5
S-5	40	55	5

Table 5.1 Slurry mixing ratio

5.2.4 Penetration of Slurry into the Glycerin with Boric acid

In this study, boric acid was adopted as a hardening agency for the organic additive (PVA). Boric acid can be combined with glycerin. In the process to obtain spherical pebbles, it is an important parameter that the permeability of the slurry and liquid bath (glycerin and boric acid) as well as the surface tension. If it is not easy to penetrate into the liquid bath, a mixed slurry with an optimum mixing ratio is difficult to induce a spherical shape due to an increase in the contact angle with elapsed time.

For the decreasing the contact angle between slurry and liquid bath, the mixing ratio of glycerin and boric acid was controlled. The mixing ratio of boric acid/glycerin was controlled weight percentage and it is presented in Table 5.2.

	Boric acid	Glycerin
B(5) / G(95)	5 wt%	95 wt%
B(4) / G(96)	4 wt%	96 wt%
B(3) / G(97)	3 wt%	97 wt%
B(2) / G(98)	2 wt%	98 wt%
B(1) / G(99)	1 wt%	99 wt%
B(0) / G(100)	0 wt%	100 wt%

Table 5.2 Mixing ratio of boric acid and glycerin

A direct injection method and addition of acceleration-layer were devised to promote the penetration of the slurry with the optimum surface tension into the liquid bath. A schematic diagram of the adopted method is shown in figure 5.6.

The acceleration-layer exists between the liquid bath and the slurry, the LiOH solution and acetone were adopted as layers respectively. LiOH solution is distinguished into pH 8 and pH 14 with controlled pH. LiOH solution is composed with glycerin, H₂O, LiOH powder. Where the pH of the liquid bath and the slurry are 2 and 14, respectively. The direct injection method is a method of injecting the slurry directly into the bath by penetrating the needle into the liquid bath. At this time, injection pressure and a rotary turbine were used to control the injected amount of slurry.

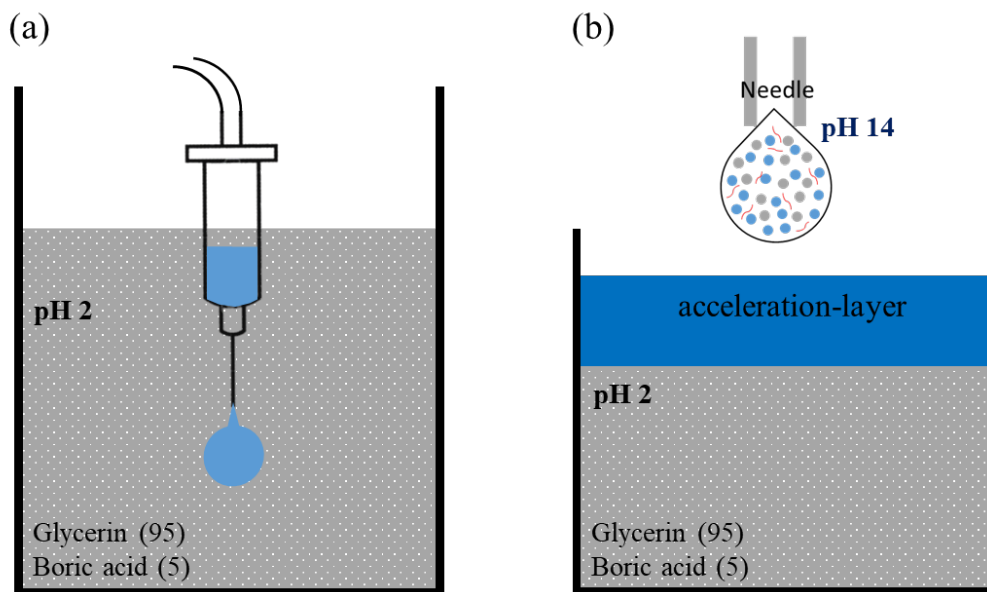


Figure 5.6 A schematic diagram of direct injection method (a) and acceleration-layer (b).

5.2.5 Optimization of heat-treatment conditions

Generally, the sintering properties can be improved by appropriately controlled the sintering parameters during the sintering process. The thermal cycle can be controlled simply among the sintering parameters, it means controlling the sintering temperature and heating rate.

A typical temperature cycle through control of the sintering temperature and the heating rate is shown in figure 5.7 [12].

Firstly, fast sintering method is a sintering method that has a much faster heating ratio than the conventional sintering method, which can be applied when the activation energy (E_d) of densification is greater than the activation energy (E_g) of grain growth. When E_d is higher than E_g , the densification/particle growth ratio is lower at lower temperatures and higher at higher temperatures.

Therefore, it is heated at a high speed to minimize grain growth, and sintering is performed at a high temperature than the sintering temperature to increase the densification rate when the powder-type material is heated. However fast sintering method needs to consider that problems such as non-uniform thermal distribution in the materials, removal of organic binders, and adsorbed ions occur during the sintering process due to a high heating ratio. Therefore it is necessary for some supplement activities such as the heating ratio, pyrolysis, and pre-treatment of the powder-types materials. In addition, this method is generally a method to obtain a fine-microstructure but it is observed a heterogeneous microstructure according to the temperature gradient between the inner and surface of the sintering materials.

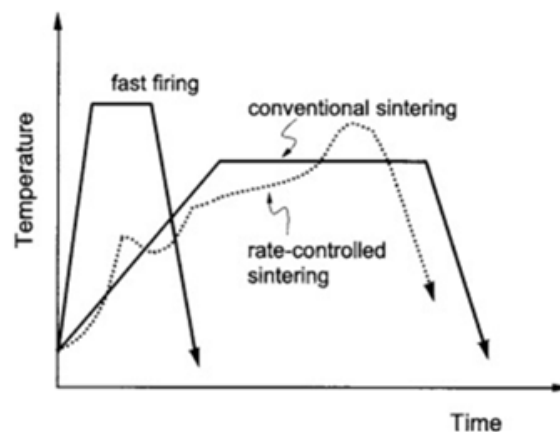


Figure 5.7 Schematic showing the thermal cycles of conventional sintering, fast firing and rate-controlled sintering.

Secondly, rate-controlled sintering method has a pattern for the densification of the materials by controlled heating ratio and temperature. These patterns determine the densification, volatility, and adsorption gas of the material with time and temperature through preliminary experiments and it depends on the materials. However, this method leads to grain growth compared with the general sintering method.

As in the above method, sintering has a lot of influence on the sintered material by temperature, heating rate, time and atmosphere among variables. In the case of Li_2TiO_3 breeder, microwave sintering and conventional sintering are typical methods to satisfy the function as fusion fuel. Typically sintering methods can be distinguished by the heating method the materials. The microwave sintering method is directly heating the materials using a microwave of 916MHz or 2.45GHz generated from electric magnetic [13]. Microwave sintering can be sintered low temperature compare with the conventional sintering method. It is possible with a sintering time of a few minutes, which is connected saving the cost and energy. Also it can be possible quickly volume heating causes the interaction between microwaves and fine particles inner materials. As a feature, it has excellent properties for densification of sintered bodies. Microwave sintering is accelerated sintering process because the densification of sintered bodies strongly depended on ion diffusion. However, it has to consider that the ion diffusion ions promoted the grain growth. It is also reported that a microstructure can be obtained densificated and homogeneous microstructure, but it has been confirmed that the deviation of grain size is increased from a certain temperature. On the other hand, the conventional sintering method is heating indirectly (such as radiation, convection, conduction) through a heating zone depending on the type of furnace.

To date, a lot of studies has been done on the Li_2TiO_3 breeder materials towards enhancing characteristics. The breeder materials are recommended to have homogeneous microstructure with small grain size [14]. The homogeneous microstructure is a fundamental property in the main function of tritium breeding materials, it directly affects breeding. In general, the microstructure of the sintered body can be strongly affected by the sintering parameters. Therefore, the sintering parameters are generally determined to achieve a homogeneous microstructure. In addition, the understanding of sintering behavior is important. In this experimental, the effects of sintering conditions on the microstructure of sintered Li_2TiO_3 pebbles were investigated.

The Li_2TiO_3 nano-powder with high purity was fabricated by the solid-state reaction between the lithium oxide (Li_2O) and titanium dioxide (TiO_2) where purities of Li_2O and anatase- TiO_2 were 99% and 99.9%, respectively. The starting materials were mixed by wet ball-milling process using isopropyl alcohol as solvent during 3h. mixed powders were dried at 60 °C in vacuum oven more than 6h. after than dried powders were heat treated in air atmosphere at 700°C for 12h. The XRD pattern of synthesized powder were shown in figure 5.8.

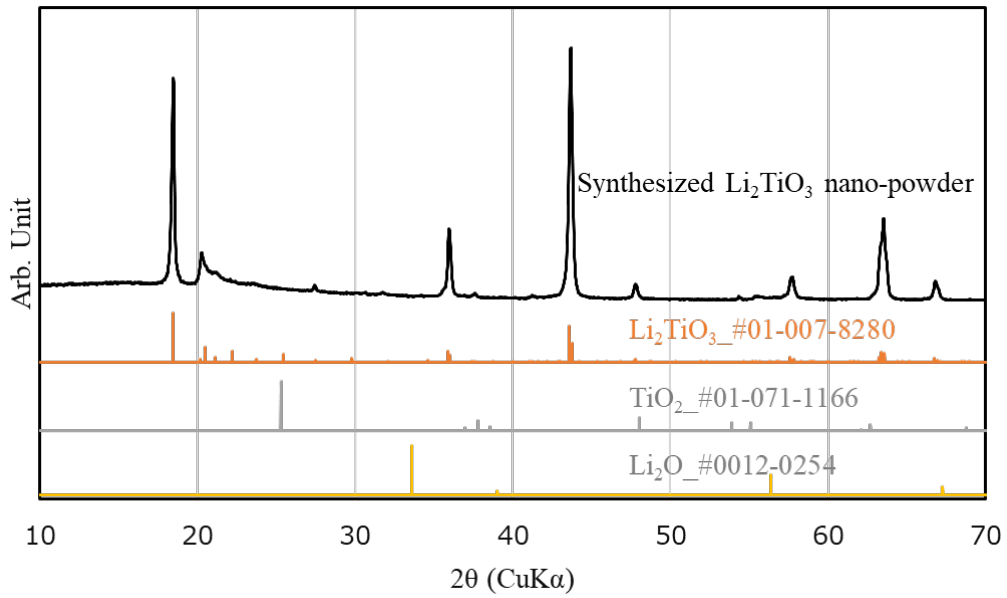


Figure 5.8 XRD pattern of synthesized Li_2TiO_3 nano-powder

The particle size of synthesized Li_2TiO_3 powder was approximately 150nm [6]. The morphology of synthesized Li_2TiO_3 nano-powder is presented in figure 5.9. The Li_2TiO_3 pebbles were fabricated by the slurry droplet wetting method [7]. The synthesized Li_2TiO_3 nano-powders were mixed with polyvinyl alcohol (PVA) and distilled water by ball milling process in 20h, a homogeneous slurry was achieved. And then, the Li_2TiO_3 slurry was dropped into the glycerin including boric acid by a syringe needle, and green spheres bodies were formed by dehydration and cross-linking reaction such as figure 5.4. Then the green bodies were dried at room temperature in air.

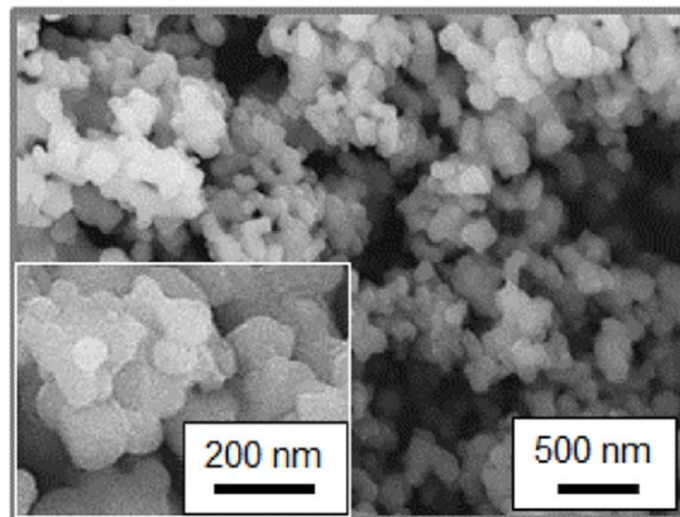
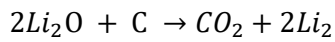
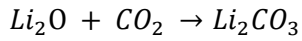


Figure 5.9 Morphology of synthesized Li_2TiO_3 nano-powder

In the fabrication process, the shaping of pebble is achieved hardening reaction between PVA in the slurry and Boric acid including glycerin. The fabricated Li_2TiO_3 green bodies were to be containing relatively a large amount carbon from the hardening reaction. Carbon can be affect the composition of Li_2TiO_3 pebble in the sintering process. Because of Carbon lead to change the molar ratio such as reaction:



The second phase (Li_4TiO_4) can be generate from the alteration of molar ratio in the $\text{Li}_2\text{O}-\text{TiO}_2$ system. The phase diagram of the $\text{Li}_2\text{O}-\text{TiO}_2$ system is shown in figure 5.10 [3-4].

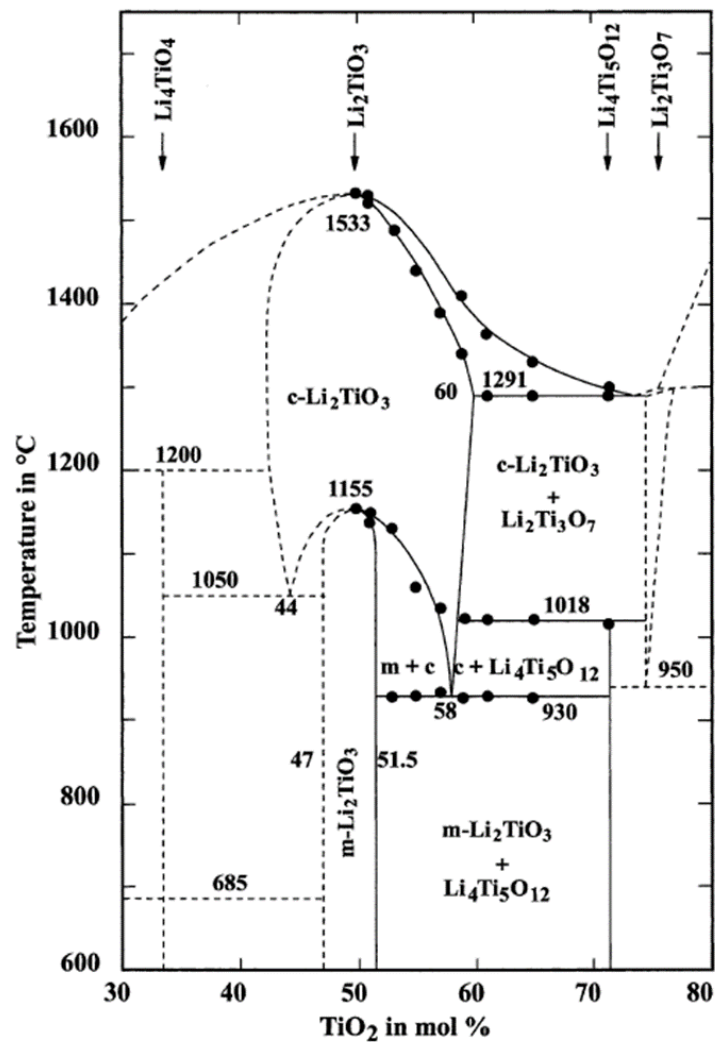


Figure 5.10 Phase diagram of the $\text{Li}_2\text{O}-\text{TiO}_2$ system [3-5]

The various heating time in the pyrolysis step were performed for removal the carbon. Where heating temperature were fixed at 600 °C because of the oxidation reaction of carbon begins at the 400 °C [6] and the lithium is very susceptible to the volatility from 200 °C in the air atmosphere. Indeed, fixed heating temperature is considered the acceleration oxidation of carbon with prevention for volatilization of lithium. The various heating temperature is marked in Table 5.3. Residual carbon in the pebbles were measured by Carbon/Surfer (C/S) analysis (ELTRA CS-2000). C/S analysis was performed the four times per sample for the increasing reliability. The deviation and relative standard deviation (RSD) of measured value were less than 0.0009 and 1.7 %, respectively. After pyrolysis step, the specimens was sintered at 900 °C for 1h in Air or He + 1% H_2 atmosphere.

Specimen ID	Temperature (°C)	Time (h)
P_5	600	5
P_10	600	10
P_20	600	20
P_50	600	50

Table 5.3 Pyrolysis conditions fixed at 600 °C

5.3 Results & Discussion

5.3.1 Effects of surface tension on the shaping of Li_2TiO_3 pebbles

As mentioned in the experimental section, the surface tension of the slurry was expressed as the slurry mixing ratio. The experiment was performed repeatedly and empirically. The morphology of the green pebble with different mixing ratios and the microstructure after sintering are represented.

Figure 5.11 is shown the morphology of green pebbles with different slurry mixing ratios. Where

the surface tension of the slurry is lower as the water content decreasing. In the case of a lower water ratio (a) it has a shape like a note (crochet). A decrease in surface tension means increasing the amount of powder in the slurry, which leads to an increase in the viscosity of the slurry. The (e) is expected to have the highest coefficient of surface tension, which is contorted sphere shaping. It is expected that the space occupied by water in the slurry is distorted by the dehydration reaction from the glycerin. The keys for the optimal shape are (b), (c), and (d). The (b) and (c) are shown the tear shape. The (d) is shown the spherical shape. Each condition has a difference in the proportion of H₂O within 1%. The shape clearly is observed a difference despite the narrow percentage range. In addition, the grooves due to the bubbles were observed on the surface of the green pebble despite using a defoaming machine.

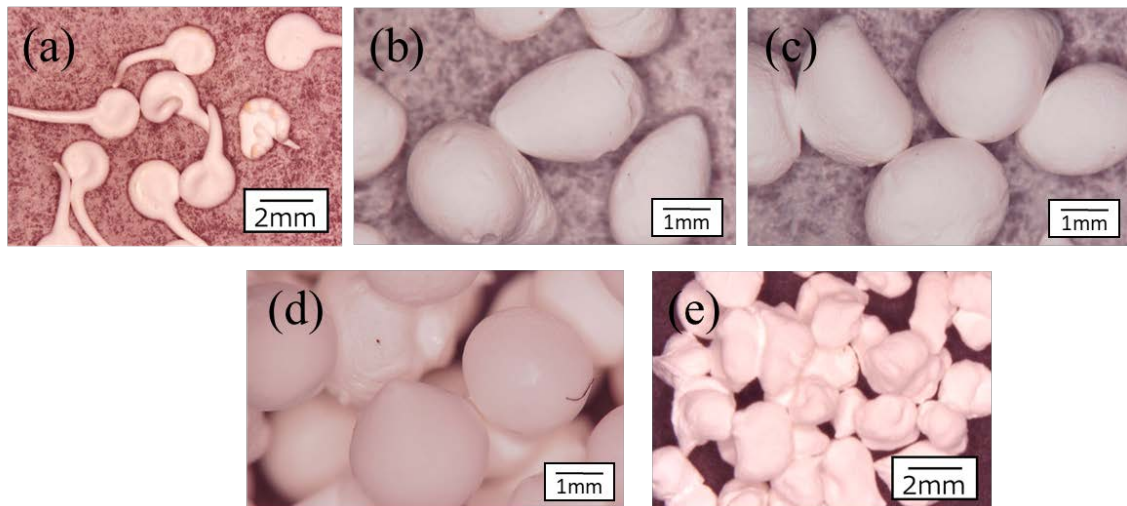


Figure 5.11 Morphology of green pebbles with different slurry mixing ratio. (a) S-1, (b) S-2, (c) S-3, (d) S-4, (e) S-5.

Figure 5.12 is represented the fracture surface of sintered pebbles with mixing ratio S-4 and S-5. In the case of S-4 (a), it showed a spherical shape, but a relatively dense shell was observed on the surface in the microstructure of the sintered pebble. It shows a homogeneous microstructure in the core region.

In S-5 (b), huge bubbles were formed in the microstructure with the shell. H₂O in the green pebble remains and forms pores through a curing reaction starting from the surface. The formed pores shrink during the sintering process, it will be huge bubbles.

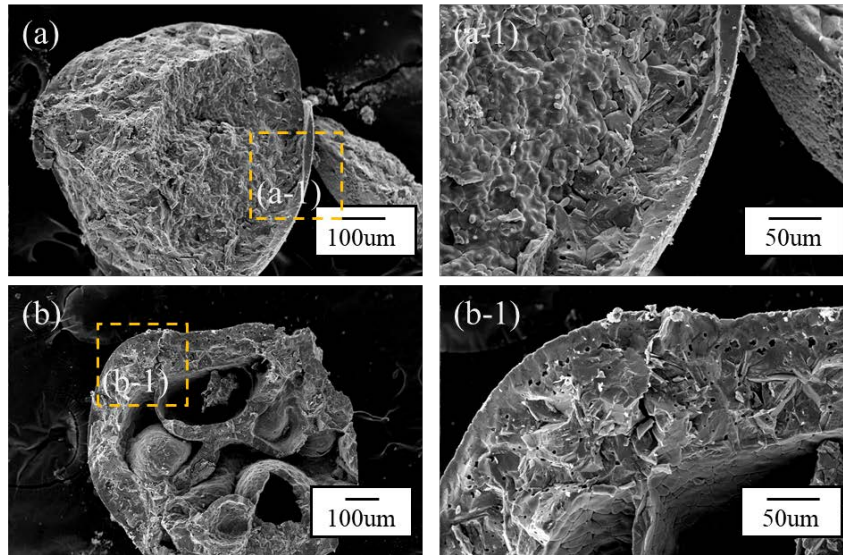


Figure 5.12 Morphology of sintered pebbles with different slurry mixing ratio. (a) S-4, (b) S-5.

5.3.2 Pebbles shaping with different conditions of liquid bath or injection method

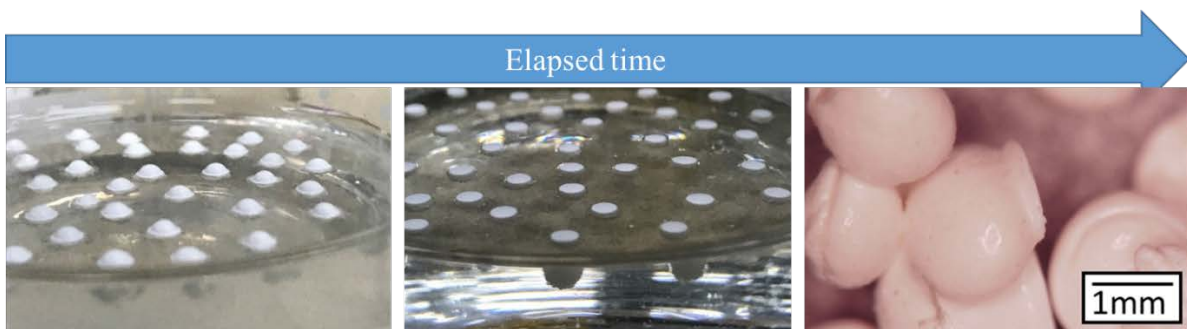


Figure 5.13 The process of forming pebbles dropped into the liquid bath (G(95)B(5)).

The slurry was dropped into a liquid bath with different mixing ratios of glycerin and boric acid. The penetration rate of the slurry was very slow in all of the conditions. In the case of only including pure glycerin, the dropped slurry increased the contact angle between the glycerin and the slurry with elapsed time, it could penetrate into the shape of a disk or a cylinder. Figure 5.13 is represented the pebble formation process of the slurry dropped on the liquid bath (G(95)B(5)). The slurry dropped under the

condition of G(95)B(5) was initially able to penetrate into a spherical shape, but it was not clearly spherical shape. The rate of penetration into the liquid bath was low, and the last part of the penetration was hardened in the air. In order to accelerate the penetration rate, there are an accelerator, a slurry injection method, and a method of increasing the specific gravity of the slurry. Currently, it is difficult to increase the specific gravity of the slurry when considering the initial raw materials. Therefore, a method of injection of the slurry, and a method of adopting an accelerator was devised.

Figure 5.14 is shown the morphology of sintered pebbles fabricated by the direct injection method (figure 5.6). The slurry mixing ratio was applied optimum mixing ratio (5.3.1). The shape of pebble is not a clear spherical shape. Pebbles fabricated by the direct injection method are mostly spherical with the tails. It was formed by the blades of the rotating turbine to control the amount of slurry injected from the needle. A problem of needle clogging was found due to the hardening of PVA because of the amount was controlled by interval injection along with the rotating turbine. This phenomenon will come as a big problem in the mass production of Pebble. In the case of the microstructure, the distribution of pores and grain size were in good condition, but a shell was found on the surface of the pebble. Directly injection method is not suitable for removing the shell.

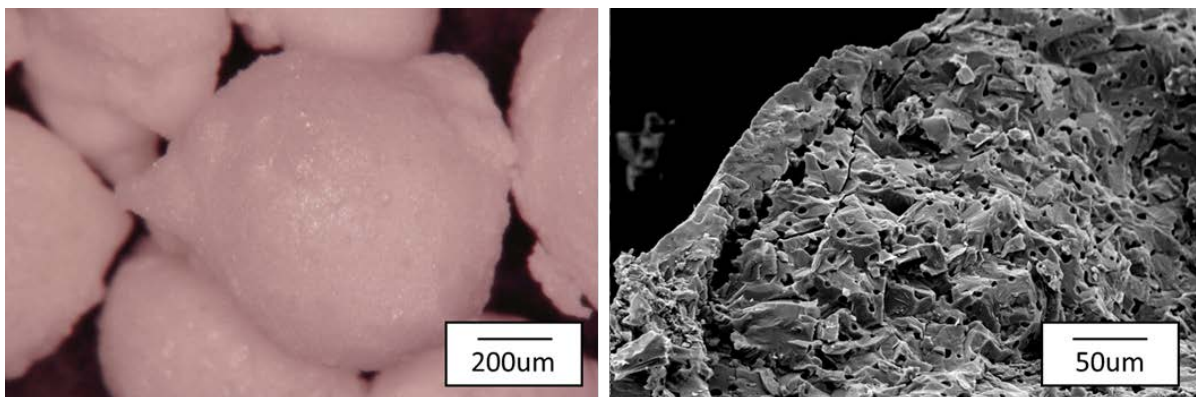


Figure 5.14 Morphology of sintered pebbles fabricated by directly injection method.

5.3.3 Penetration of slurry into the glycerin with boric acid

From the results such as 5.3.2, the acetone layer is adopted for acceleration for penetration of slurry into the glycerin with boric acid compound. The acetone layer is made on the glycerin and boric acid

compound such as figure 5.15. The specific of acetone is light better than glycerin and boric acid compound. And the surface tension is lower better than slurry. Therefore, the adoption of acetone layer can be accelerate the penetration of slurry into the glycerin and boric acid compound, which also can be confirmed in figure 5.15. Furthermore, it can be increase the production rate of slurry droplet wetting method.

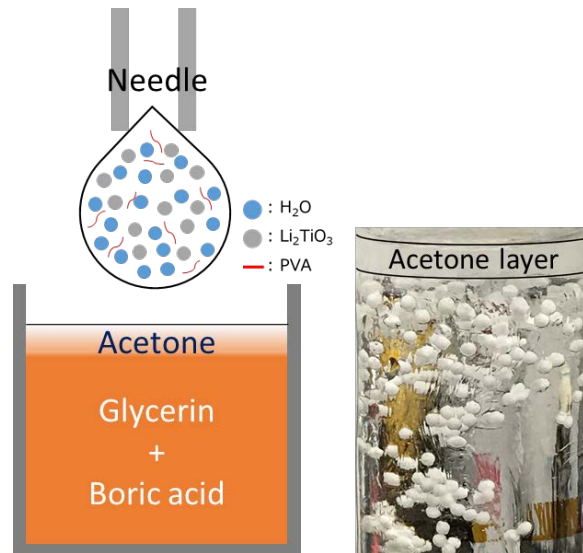


Figure 5.15 the schematic of acetone layer on the glycerin and boric acid compound.

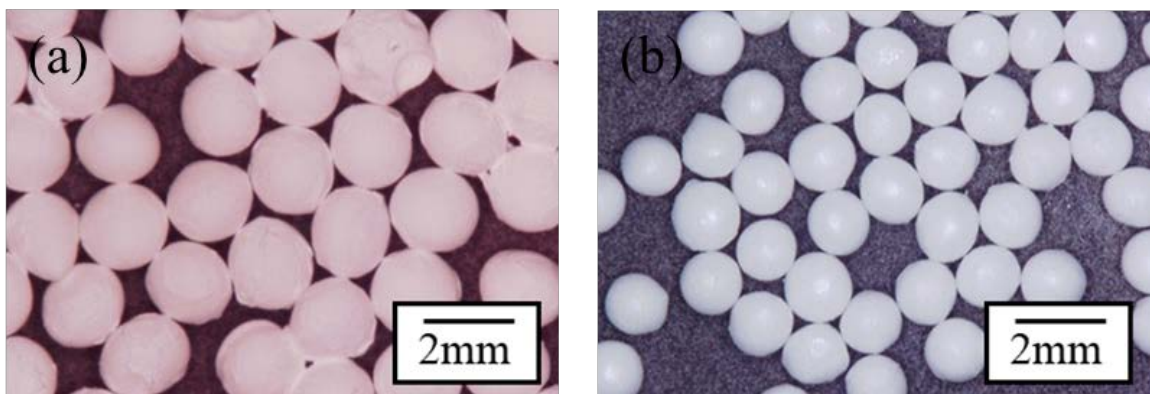


Figure 5.16 the shaping of fabricated pebble with acetone layer. (a) green pebble, (b) sintered body.

The morphology of fabricated Li_2TiO_3 pebbles with acetone layer are shown in figure 5.16. The sintered pebbles were sintered on $900\text{ }^\circ\text{C}$ for 1h in air. The shaping of green pebble are present generally sphere. After sintering process, the shaping of pebbles is better than green pebbles. It is assumed the shrinkage of the green pebble during the sintering process.

However, the shell is confirmed on the surface of sintered pebbles. Figure 5.17 shows the morphology of sintered Li_2TiO_3 pebbles at various sintering conditions. A shell structure with the irregular thickness from 30 up to 80 μm was observed from the surface of pebbles, which is indicated by the dashed line in the cross-section. The shell structure has a dense microstructure compared with core area. It can increase the tritium release time of the Li_2TiO_3 pebbles by disturbing the release behavior of the bred tritium in the pebble. At the same time, it can be a major source of dust from crack propagation on the surface of the pebbles. The generated dust from the propagation of crack would be disturbing the transportation pathways of tritium and sweep-gas within the solid breeding blanket, which is noted as the cause of the decrease of tritium breeding ratio.

Unfortunately, the shell was not removed through the sintering conditions such as temperature, heating rate, and atmosphere. Figure 5.18 shows glancing-incidence X-ray diffraction (GIXRD) patterns of sintered pebbles at different incidence angles. The absorption of electromagnetic waves is limited the penetration of the beam within the material [10]. In this result, α was set at 0.5° , 1° and 2° to analysis the phase of shell structure [11]. The penetration depth ($z(\alpha)$) is given by

$$z(\alpha) = \lambda / \left(4\pi(2)^{-\frac{1}{2}} \left\{ [(\alpha^2 - 2\delta)^2 + 4\beta^2]^{\frac{1}{2}} - (\alpha^2 - 2\delta) \right\}^{\frac{1}{2}} \right)$$

Where α , β , δ , and λ are incidence angle, absorption factor, dispersion factor and beam wave length, respectively. In this case, the wave length is 0.15406 nm because beam source was CuK α . The absorption factor and dispersion factor of Li_2TiO_3 is 6.04E-7 and 4.34E-6, respectively. The calculated penetration depth according to incidence angles are listed in table 5.4. The GIXRD patterns obtained by different α showed smaller intensity as approaching to the critical angle but it is matched with the Li_2TiO_3 phase. Indeed, the shell structure is identified as the Li_2TiO_3 phase.

The formation of the shell structure is presumed to originate from the non-homogeneous microstructure in the green pebble. Figure 5.19 is shown the cross-section of the Li_2TiO_3 green pebble. Despite the adoption of ball-milling processing for 20 hours to obtain a homogeneous slurry, a shell region was observed at the surface of green pebbles. The Li_2TiO_3 slurry with PVA and water is dropped into the glycerin bath including boric acid through the needle to obtain a spherical shape. The hardening reaction occurs between PVA and boric acid when the Li_2TiO_3 slurry descends to the bottom of the bath. At this process, the hardening reaction at surface of green pebble is relatively fast. Hence, the green pebble has a gradient hardening rate. Namely, the formation of a shell structure in the sintered Li_2TiO_3 pebbles is supervened before the sintering process. It is expected that the one of the reasons why these pebbles have a shell. At the same time, it is implied the improvement of fabrication method.

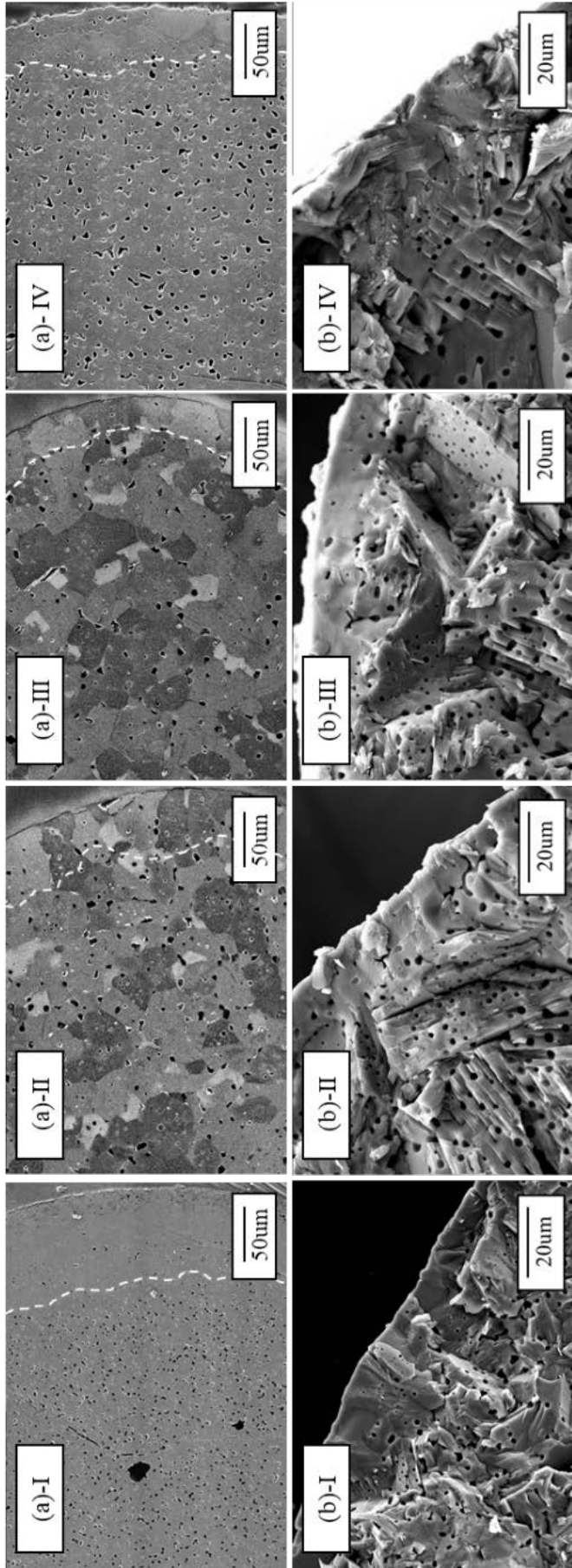


Figure 5.17 Morphology of sintered Li_2TiO_3 pebbles at $10\text{ }^\circ\text{C}/\text{min}$ rate with different temperature, atmosphere : (a) cross section, (b) fracture surface, (I) $900\text{ }^\circ\text{C}$ in air, (II) $1000\text{ }^\circ\text{C}$ in air, (III) $1100\text{ }^\circ\text{C}$ in air, (IV) $900\text{ }^\circ\text{C}$ in $\text{He} + 1\%\text{H}_2$

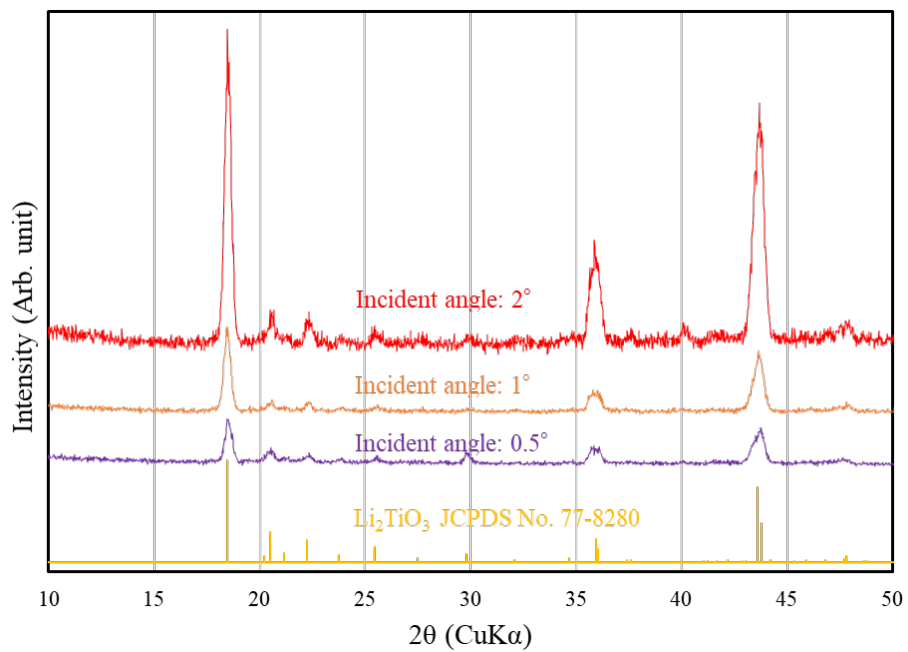


Figure 5.18 GIXRD patterns of sintered Li_2TiO_3 pebble collected at different incidence angles.

Angle ($^\circ$)	0.5	1	2
Depth (um)	0.2	0.3	0.7

Table 5.4 Penetration depth with incidence angles.

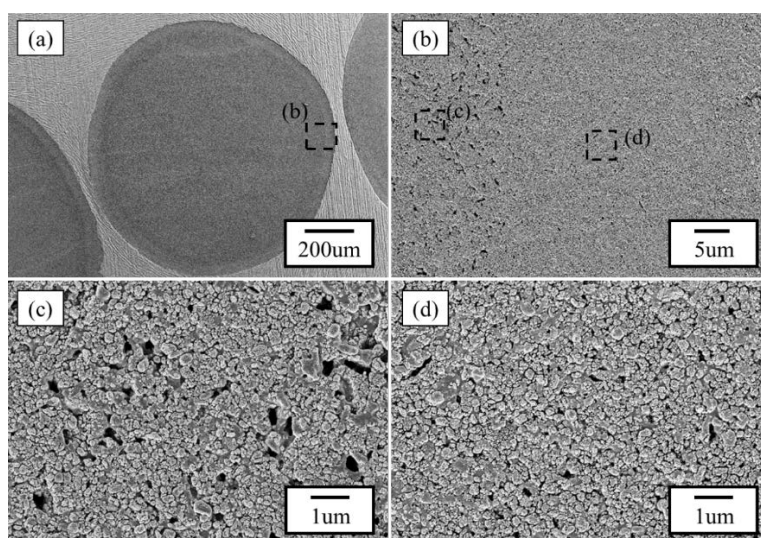


Figure 5.19 Cross-section of green pebble

In case of the sintered pebbles in the He + 1%H₂, the micro-crack is observed on the surface. Figure 5.20 is shown the cross-section of pebbles sintered at 900 °C, 1h, 10°C/min in the He + 1%H₂ atmosphere. The shell was observed, which is a relatively dense area compared to the core. The shell is expected to generate unnecessary pressure in the pebble during the sintering process. Therefore the point of occurring cracks is assumed at the boundary between the shell and the core area, which will be propagated both of the core and surface. The cracks can be lead that the generation of the dust and fracture of pebbles, etc. are connected to the problem of fuel circulation, decreasing TBR, and so on. The detail of the shell is discussed in the next section.

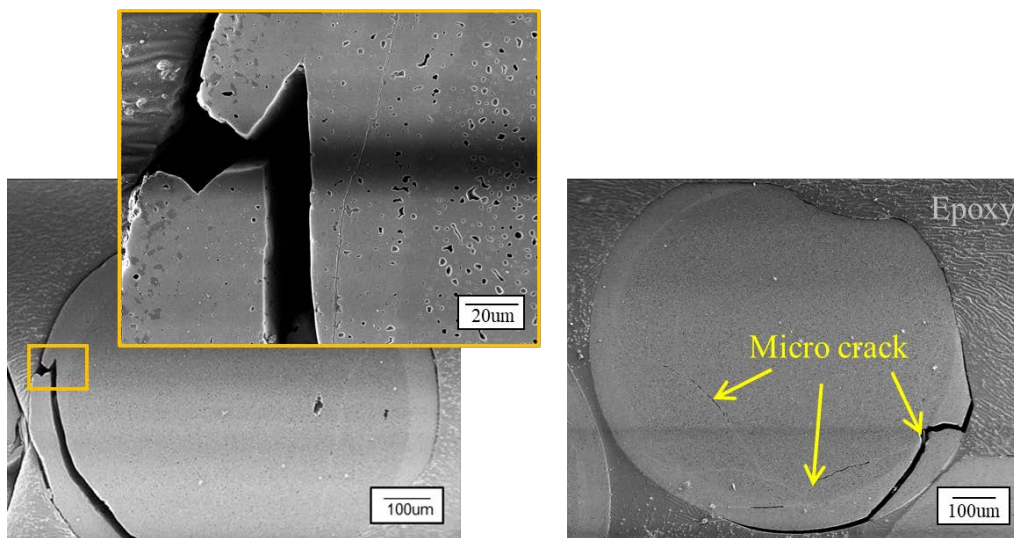


Figure 5.20 Cross-section of sintered pebbles at 900°C, 1h, 10°C/min.

One of the key issues for ceramic breeder blankets is tritium release. The tritium generated in the ceramic breeder by neutron reactions with ⁶Li and/or ⁷Li is believed to be transported out of the breeder through a number of mechanisms [30]. For tritium transport behavior in ceramic breeder materials in a typical fusion environment, the potential number of contribution mechanisms may be very large. The limited amount of experimental data acquired so far leads to the following tentative step description:

1. Production of tritium gas within the grain, primarily by ⁶Li(*n,α*)T reactions.
2. Migration of atomic tritium to the grain boundaries by intragranular diffusion.
3. Motion of the gas along the grain boundaries to the network of interconnected pores within the solid breeder.

4. Adsorption, desorption and surface reaction of tritium and tritium compounds at the solid/gas interface.
5. Diffusion of tritium and tritium compounds along the interconnected pores and release to the purge flow.
6. Convective transfer out of the breeder by the helium purge stream.

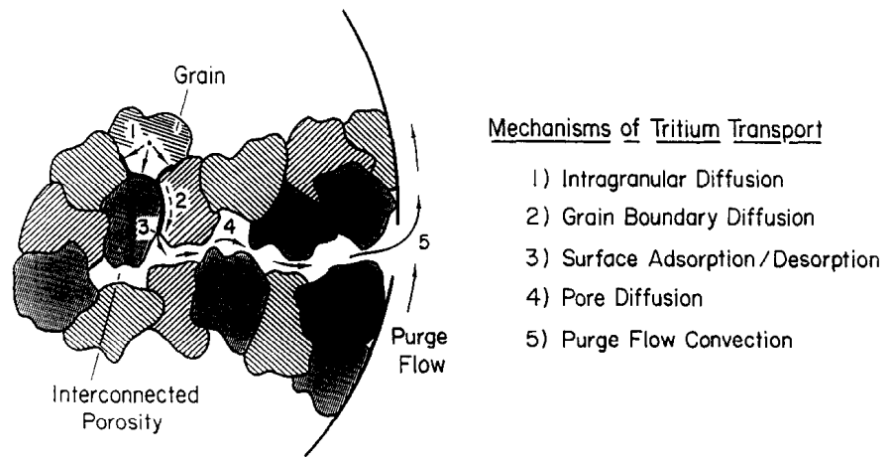


Figure 5.20 Schematic of tritium transport mechanisms in lithium ceramics [31].

As shown in figure 5.20 [31], the bred tritium diffuses through the bulk in atomic form; it then diffuses along grain boundaries to the solid/gas interface where a number of surface processes occur, including desorption to and adsorption from the pores. The desorbed tritium then percolates along the open interconnected porosity to be finally convected away by the purge gas [31]. The shell can be disturbing the tritium transport such as figure 5.20. Therefore, the shell have to remove for the TBR.

The Chia-Chang Lin et al. is suggested the degradation of PVA according to the pH [32]. The effect of pH on degradation of PVA is shown in figure 5.21. In figure 5.21, the E of x-axis is meaning of the degradation efficiency of PVA. The E can be show as

$$E (\%) = \frac{C_o - C}{C_o} \times 100$$

Where C_o is the initial PVA concentration and C is the concentration of PVA at time t . A higher E value represents a higher degradation efficiency of PVA.

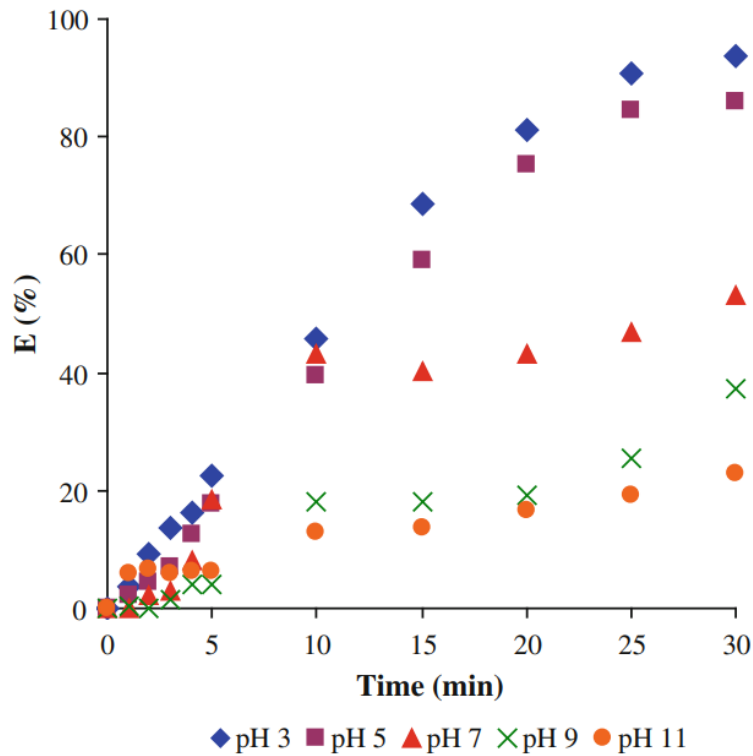


Figure 5.21 Effect of pH on degradation of PVA [32].

We have to consider pH in slurry droplet wetting method because of the PVA is added the Li_2TiO_3 slurry in shaping process. Where, the degradation of PVA is meaning of the hardening of slurry. The pH of Li_2TiO_3 and glycerin and boric acid compound is pH 14 and 2, respectively. The degradation of PVA is assumed when the slurry drop in the glycerin and boric acid compound. This degradation of PVA can be occurred the gradient of hardening velocity in green pebbles. Namely, the hardening velocity is higher on the surface of green pebble compared with core area. This gradient of hardening velocity according to the different pH is assumed the formation of the shell.

The LiOH layer is adopted instead of acetone layer for confirmation effect of different pH. The pH of LiOH layer were conducted 2 and 14 on the glycerin and boric acid compound such as acetone layer. The figure 5.22 is shown the LiOH layer and shaping process of green pebbles.

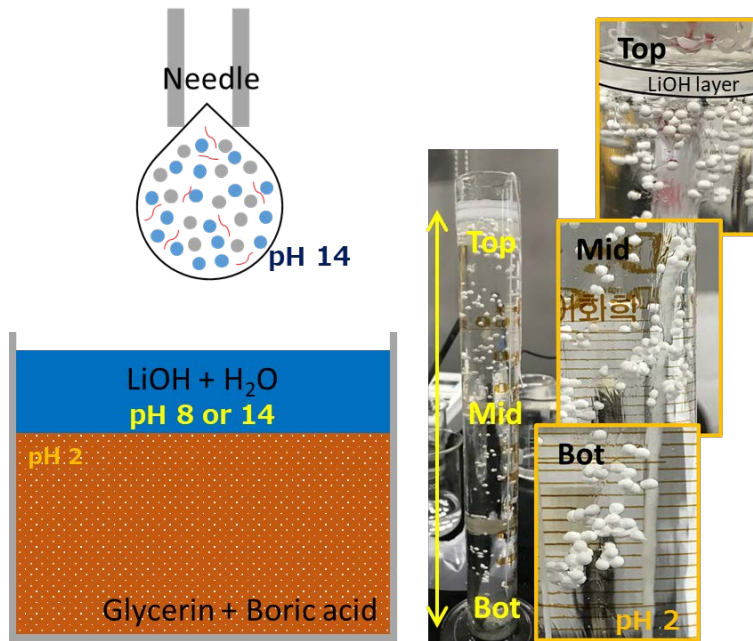


Figure 5.22 Schematic for adoption of LiOH layer and shaping process of green pebbles.

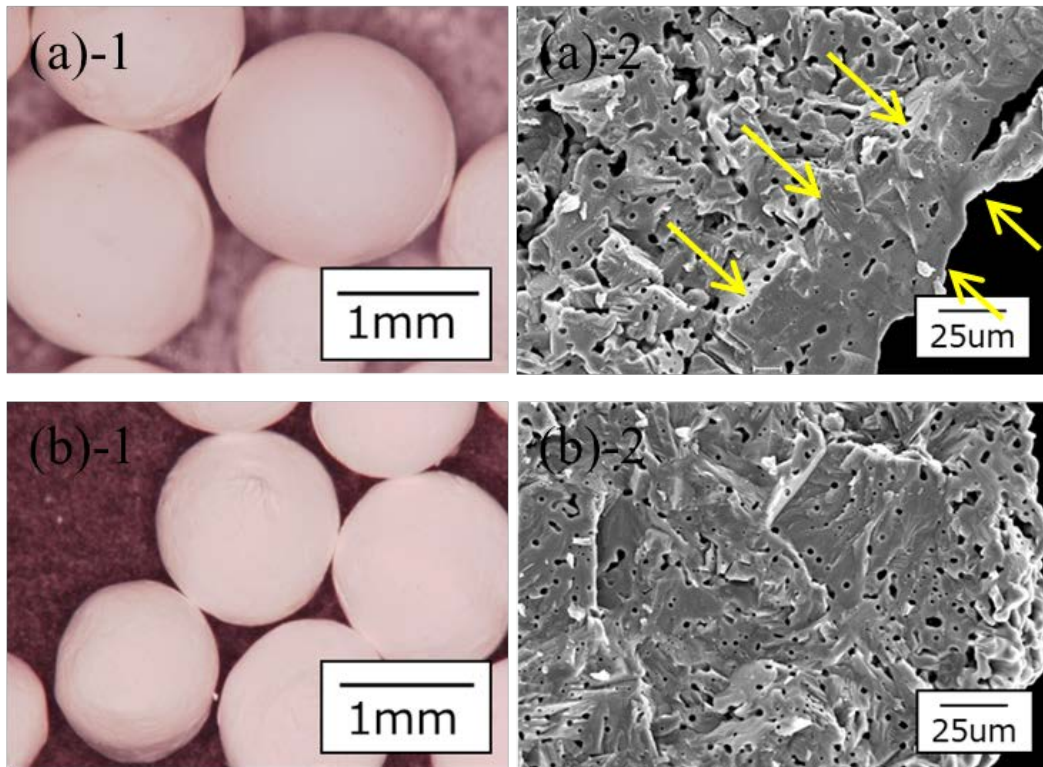


Figure 5.23 the morphology of Li_2TiO_3 pebbles fabricated with different pH of LiOH layer. The case of pH 8 is (a). (a)-1: green pebbles, (a)-2: fracture surface of sintered body. The pH 14 is (b). (b)-1: green pebbles, (b)-2: fracture surface of sintered body.

The shaping of fabricated green pebbles through LiOH layer with different pH is presented almost sphere such as figure 5.22. the pH of LiOH layer were controlled by ratio LiOH / H₂O. The LiOH layer is performed a role the acceleration for penetration of slurry into the glycerin and boric acid compound. The figure 5.23 is presented the morphology of Li₂TiO₃ pebbles fabricated with different pH of LiOH layer. In case of pH 8, the shaping of green pebbles is satisfied the sphere. However, the shell is observed on the surface, which can be confirmed the (a)-2 in figure 5.23. In case of the pH 14, the shaping of green pebbles and the homogeneous microstructure were observed the (b) of figure 5.23. The degradation of PVA according to the pH is expected the formation of the shell.

The Kathirvel Ganesan et al. is performed about the pH-induced gelation using the polysaccharide [33]. They are suggested that the gelation of alginate and pectin solution is due to intermolecular hydrogen bonding between protonated groups (carboxyl, hydroxyl) at low pH [33]. In the case of pectin, gelation is also stabilized by hydrophobic interactions of methylated groups. Increasing the pH leads to deprotonation of acidic groups which prevents aggregation of chains and eventually gelation. For example, alginic acid gels can be prepared by protonating the sodium salt of carboxylate functional groups in acidic solution [34,35]. Herein the sodium salt of carboxylate functional groups becomes carboxylic acid promoting the hydrogen bonding and network formation. It should be kept in mind that polymer degradation may occur in solutions at pH \leq 1.

5.3.4 Proposal of suitable heat-treatment conditions for Li₂TiO₃ pebbles

To date, a lot of studies has been done on the Li₂TiO₃ breeder materials towards enhancing characteristics. The breeder materials are recommended to have homogeneous microstructure with small grain size [14]. The homogeneous microstructure with grain size is a fundamental property in the main function of tritium breeding materials, it directly affects breeding. In general, the microstructure of the sintered body can be strongly affected by the sintering parameters. Therefore, the sintering parameters are generally determined to achieve a homogeneous microstructure. In addition, the understanding of sintering behavior is important. In this section, the effects of sintering conditions on the microstructure of sintered Li₂TiO₃ pebbles were discussed.

The effect of pyrolysis time with residual carbon were investigated for removal carbon in the green pebbles. The weight reduction rate and amount of carbon in the pebbles according to the different pyrolysis time are shown in Figure 5.24. The weight reduction rate is increased with increasing pyrolysis time. While the carbon content is decreasing with increasing pyrolysis time. The pyrolysis time need to be above 20h for removal residual carbon into pebble. Therefore, the suitable pyrolysis time is above 20h at 600 °C for removal residual carbon. The phase of Li_2TiO_3 pebbles can be occurred the transition phase, if the residual carbon is existed in the pebbles before the sintering process.

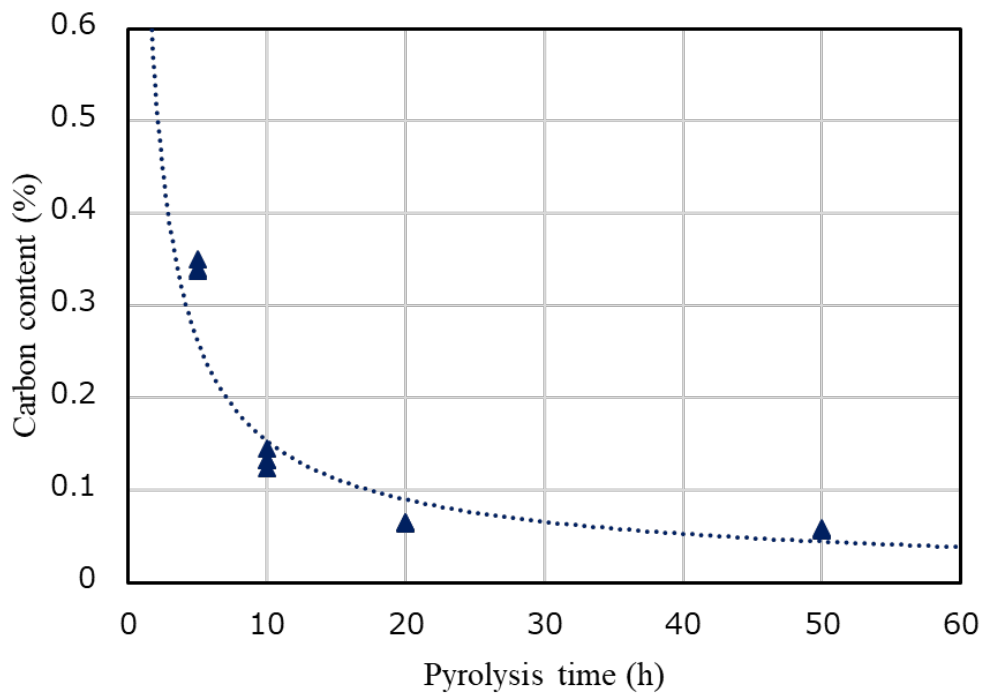


Figure 5.24 Carbon content and weight reduction rate with different pyrolysis time in 600 °C.

The Li_2TiO_3 pebbles will be applied in the atmosphere of mixed gas between He and H_2 . The mixed gas is occurred the reduction reaction with pebbles. Therefore the Li_2TiO_3 pebbles have to be stable in the reduction atmosphere for practice application. The figure 5.25 is shown the stable state with different pyrolysis time in the different atmosphere.

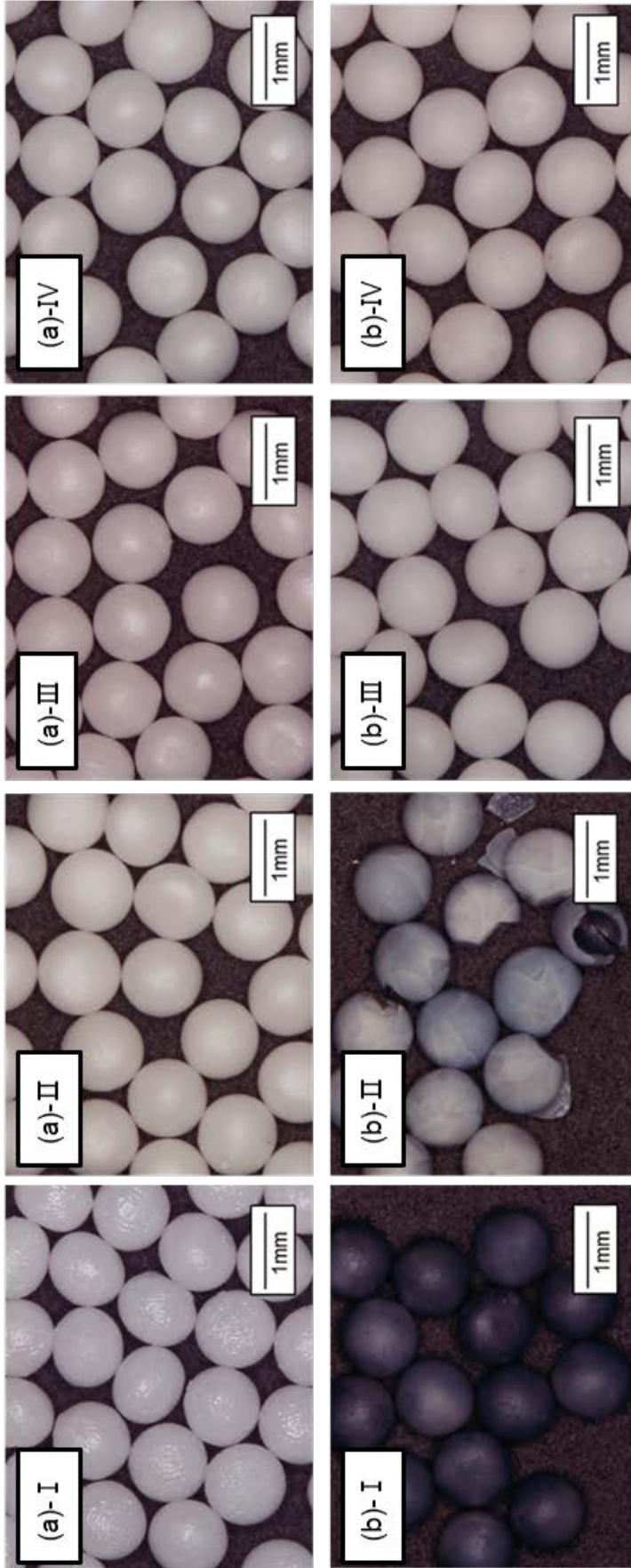


Figure 5.25 Li_2TiO_3 pebbles sintered at 900°C , 1h, $10^\circ\text{C}/\text{min}$ with different pyrolysis time and atmosphere.
 (a) Air, (b) $1\% \text{H}_2$, Pyrolysis time 5h (I), 10h(II), 20h (III), 50h (IV).

The figure 5.25 is shown the sintered pebble at the 900°C, 1h, 10°C/min with different atmosphere and pyrolysis time. Sintered pebbles with 5h pyrolysis time is shown different colour (dark-blue) depending on the sintering atmosphere. Currently, a few of data known about the colour change of the breeding materials depending on the heat-treatment atmosphere. T. Hoshino et al. suggested that the change color coincide cause of the oxygen deficiency with the conversion from Ti^{4+} to Ti^{3+} due to a reduction atmosphere [1]. According to Kleykamp, it is suggested that $LiTiO_2$ containing Ti^{3+} is produced by a reduction of Li_2TiO_3 [2]. The other sides, the sintered pebble in He + 1% H_2 atmosphere were observed different color (dark blue → white) with increasing the time of pyrolysis. It could be assumed that the insufficient oxidation reaction between carbon and oxide in the green pebble due to the insufficient pyrolysis time. Therefore, the residual carbon can be combined with lithium and inner oxygen, which generate products such as CO_2 , Li_2CO_3 , Li_2O , O_2 and LiO . The products were detected by the quantitative mass spectrometry (QMS) during the heating process. the mass of green pebbles and detected compositions with temperature are shown in Figure 5.26. the green pebbles are heated from room temperature (RT) to 900 °C in the helium atmosphere. The mass of the green pebble is strongly influenced by the evaporation of H_2O up to 270 °C. The compositions of Li_2CO_3 , LiO_2 , Li_2O , O_2 , and CO_2 is detected from the 300 °C. the reaction between residual carbon and oxygen will accelerate the volatility of lithium, which is lead to detect the lithium-containing composition.. After sintering process, the pebbles of dark-blue colour was performed heat-treatment at 900 °C, 1h with air atmosphere which is presented in figure 5.27. The colour of pebble were recovered from dark-blue to white. Namely, the number of residual carbon decreases due to the increasing pyrolysis time, which can be expected a decrease in the generation for oxygen vacancies of the materials. However, the vacancies of oxygen is unclear about that the how can be work in practice application. It is have to study for the application.

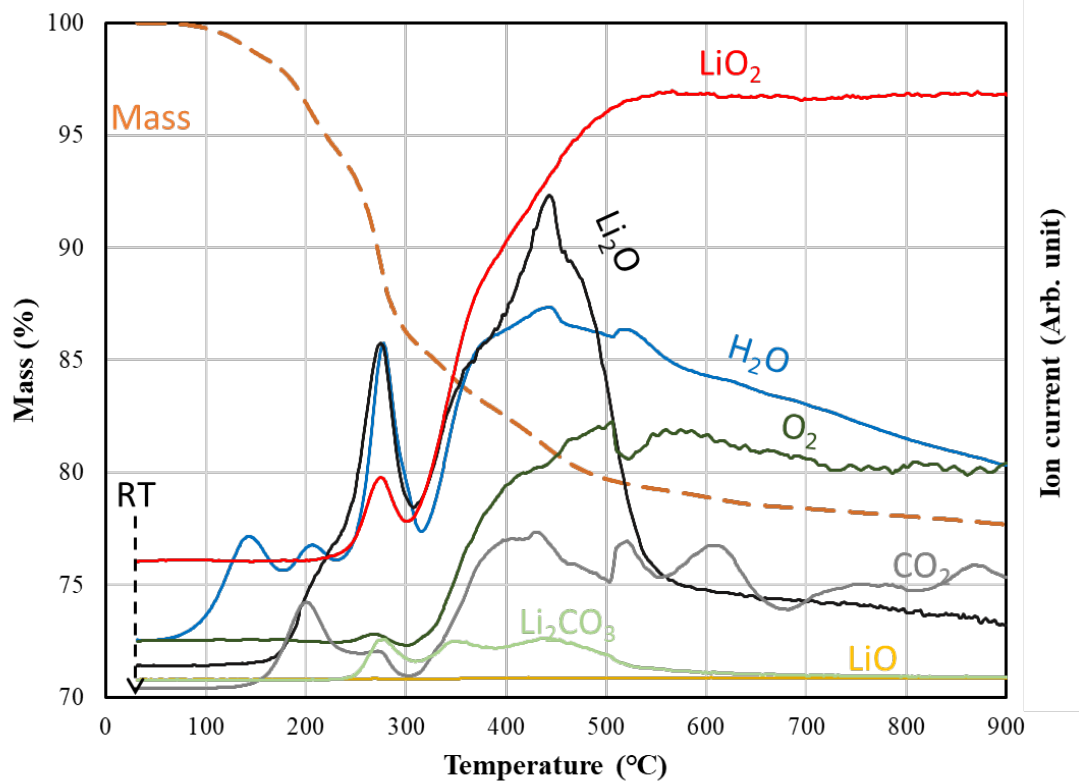


Figure 5.26 Mass and detecting ion spectrometry of Li_2TiO_3 green pebbles during the heating.

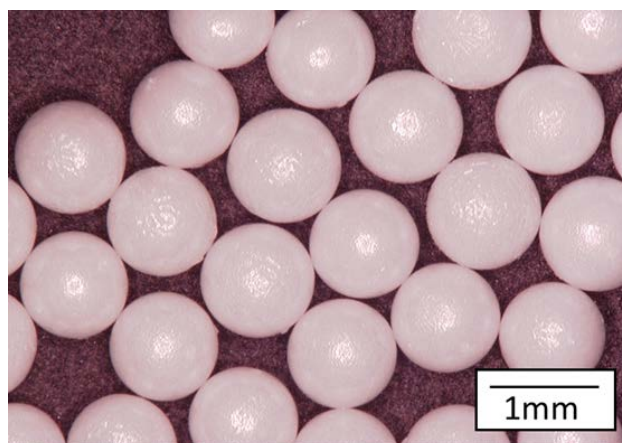


Figure 5.27 Pebbles (sintered in He +1% H_2 atmosphere with 5h pyrolysis time) after heat-treatment at 900°C, 1h in air atmosphere.

The XRD patterns of sintered Li_2TiO_3 pebbles at different temperatures in atmospheres are shown in Figure 4.8. All XRD patterns were identified as Li_2TiO_3 from the JCPDS No. 01-077-8280. During the heat treatment of the green pebble (in Figure 4.7), lithium-containing compositions were detected.

It was concerned that the generation of the secondary phase ($\text{Li}_4\text{Ti}_5\text{O}_{12}$) in the sintered Li_2TiO_3 pebbles from lithium evaporation but it was not detected. It is expected that the evaporated lithium is very small or generated secondary phase is less than the resolution (0.2%) of the XRD equipment.

Figure 4.10 shows the average grain size of the sintered Li_2TiO_3 pebbles at 900, 1000, and 1100°C for 1h with the different heating rate (2, 10°C/min) and atmosphere (Air, He + 1% H_2). Average grain sizes at each temperature in air atmosphere were 10.6 μm , 32.1 μm and 41.2 μm with 10°C/min while, 13.2 μm , 41.2 μm and 50.8 μm with 2°C/min in air. In case of He + 1% H_2 atmosphere, the grain sizes with the heating rate 2°C/min and 10°C/min were given and average value of 12.6 μm and 9.2 μm , respectively. The sintering process is sensitive to the temperature because it occurs based on the thermally activation process. In the sintering procedure of ceramics, a free energy reduction by the grain growth is the driving force, and the growing up of grains stabilizes the system. The system is expected to obtain greater driving force at higher temperature, and then, grains in a sintering body are considered to be larger. Hence, the average grain sizes in figure 4.10 increased with increasing of the sintering temperature. Figure 4.10 is indicated the typical microstructure of sintered Li_2TiO_3 pebbles on 1000°C in air with different heating rate. In the case of the heating rate, average grain sizes increased with decreasing the heating rate. Solid-state sintering has a competitive relationship with grain growth and densification during the process. Brook et al. suggested fast-firing sintering as a method to inhibit grain growth because grain growth and densification are inversely proportional to each other [8,9].

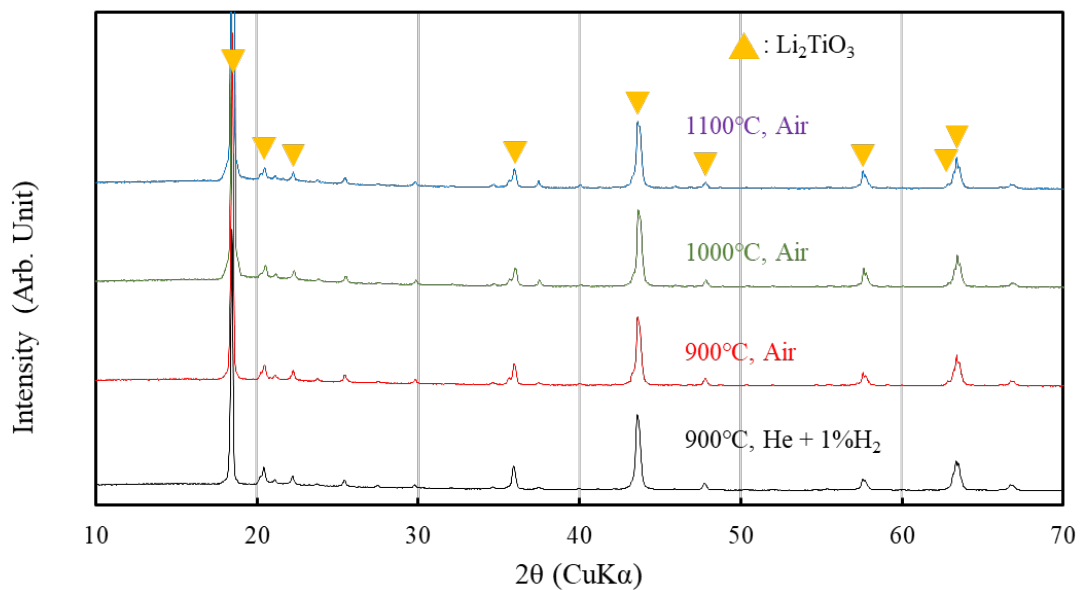


Figure 4.9 XRD patterns of the sintered pebbles by different temperature and atmosphere.

Fast-firing sintering is one of the sintering methods with a faster heating rate than conventional sintering. When the activation energy of the densification is greater than the activation energy of the grain growth, the relative ratio of (densification rate)/ (grain growth rate) is lower at lower temperatures and higher at higher temperatures. Therefore, it was confirmed that the grain growth was relatively controlled under the temperature rising rate condition of 2 °C/min, which is exposed relatively longer time at the high-temperature region than that of 10 °C/min. Generally, the reducing atmosphere during the sintering process is used to inhibit grain boundary and improving sintering density during the process. However, the sintered pebble in the He + 1%H₂ atmosphere shows similar grain size compared with the condition of air at 900 °C.

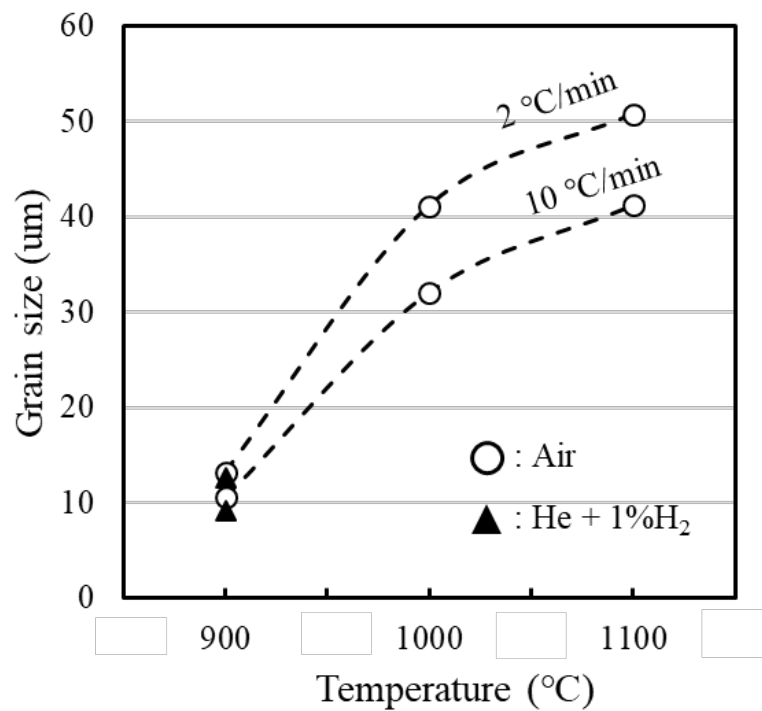


Figure 4.10 Grain growth behavior of sintered Li₂TiO₃ pebbles with various sintering conditions.

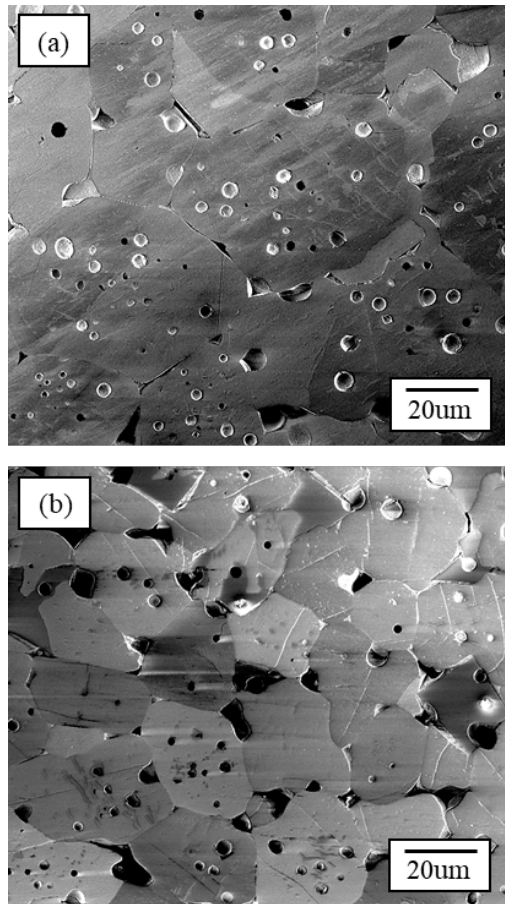


Figure 4.11 Typical microstructure sintered Li_2TiO_3 pebbles with different heating ratio.
(a) 2 °C/min, (b) 10 °C/min

5.4 Summary

In this chapter, the slurry droplet wetting method for tritium breeding materials were improved focusing to the improving the shaping and homogeneous microstructure of Li_2TiO_3 pebbles. The improvement of method were performed. The improvement of the fabrication method was carried out in two steps: shaping and heat-treatment steps. In the shaping step, a suitable mixing ratio of the Li_2TiO_3 slurry was Li_2TiO_3 (43.3%), PVA (5%), H_2O (71.7%), which were found through repeated experiments. However, the shell structure was observed in the sintered pebbles with regardless of the sintering conditions, which is confirmed the Li_2TiO_3 phase by the GIXRD method. It is expected that the formation of the shell structure will be affected on the tritium release properties and dust formation of the pebbles. The formation of shell is expected the gradation of PVA according to the different pH

between Li_2TiO_3 slurry and glycerin + boric acid compound. The shell can be remove the LiOH layer with pH 14 on the glycerin and boric acid compound. The shaping and homogeneous microstructure of Li_2TiO_3 pebbles are obtained by improvement of shaping step.

The green pebbles are heated under various heat-treatment conditions, which can be divide the two step: pyrolysis step and sintering step. The sintered pebbles with various pyrolysis time are show that the changing the color according to the sintering atmosphere. It is assumed the residual carbon in the pebbles because of not enough the pyrolysis time. The sintered pebbles with above 10h pyrolysis time is showed the white color in reducing atmosphere. The change color form white to black white is occurred by oxygen vacancies [5, 36]. Therefore, the residual carbon can be accelerate the generation of oxygen vacancies in the reducing atmosphere. Unfortunately, the fusion reactor using the He gas including the x % of H_2 for the transport bred tritium from the breeding materials. The carbon have to remove to be reasonable amount when considering the application atmosphere. And the homogeneous microstructure with grain size is a fundamental property in the main function of tritium breeding materials, it directly affects breeding. In general, the microstructure of the sintered body can be strongly affected by the sintering parameters. The grain size tends to increase with increasing temperature and decreasing the heating rate. In order to obtain a smaller grain size and homogeneous microstructure, the sintering temperature of 900 °C with the fast firing were optimal sintering conditions.

At present the sintering reactor or method were developed with various technology. Generally used reactor such as induced-heating method are applied in this thesis. Therefore, the heat-treatment conditions can not identified the optimal conditions.

References

- [1] Yi-Hyun Park et al., Li₂TiO₃ powder synthesis by solid-state reaction and pebble fabrication for tritium breeding material, *Fusion Engineering and Design* 124 (2017) 730-734.
- [2] Yi-Hyun Park et al., Fabrication of Li₂TiO₃ pebbles using PVA-boric acid reaction for solid breeding materials, *Journal of Nuclear Materials* 455 (2014) 106-110.
- [3] Georgina Izquierdo, Anthony R. West, Phase equilibria in the system Li₂O-TiO₂, *Materials Research Bulletin*, 15 (1980) 1655-1660.
- [4] J. C. Mikkelsen Jr., Pseudobinary phase relations of Li₂Ti₃O₇, *Journal of the American Ceramic Society*, 63 (1980) 331-335.
- [5] H. Kelykamp, Phase equilibria in the Li-Ti-O system and physical properties of Li₂TiO₃, *Fusion Engineering and Design*, 61-62 (2002) 361-366.
- [6] Joon-Soo Park, Jong-Il Kim, Naofumi Nakazato, Hirotsu Kishimoto, Shunsuke Makimura, Oxidation resistance of NITE-SiC/SiC composites with/without CVD-SiC environmental barrier coating, *Ceramics International*, 44 (2018) 17319-17325
- [7] Yi-Hyun Parka, Kyung-Mi Min, Mu-Young Ahn, Seungyon Cho, Young-Min Lee, Sang-Jin Park, Rehan Danish, Chul-Hwan Lim, Yong-Dae Jo, Optimization of mass-production conditions for tritium breeder pebbles based on slurry droplet wetting method, *Fusion Engineering and Design*, 109-111 (2016) 443-447.
- [8] M. P. Harmer and R. J. Brook, Fast firing-microstructural benefits, *Journal of the British Ceramic Society*, 80 (1981) 147.
- [9] H. Mostaghaci and R. J. Brook, Production of dense and fine grain size BaTiO₃ by fast firing, *Journal of the British Ceramic Society*, 82 (1983) 167.
- [10] P. Colombi, Glancing-incidence X-ray diffraction for depth profiling of polycrystalline layers, *Journal of Applied Crystallography*, 39 (2006) 176-179.
- [11] Q. Zhou, Preparation of Li₂TiO₃ by hydrothermal synthesis and its structure evolution under high energy Ar⁺ irradiation, *Journal of the European Ceramic Society*, 15 (2017) 4955-4961.
- [12] Suk-Joong L. Kang, Grain growth and densification in porous materials, *Densification, grain growth, and microstructure*, (2005) 145-170.
- [13] Morteza Ohgbaei, Omid Mirzaee, Microwave versus conventional sintering: A review of fundamentals, advantages and applications, *Journal of Alloys and Compounds*, 494 (2010) 175-189.
- [14] Alford NM, Breeze j, Penn Sj, Poole M. Layered Al₂O₃-TiO₂ composite dielectric resonators with tunable temperature coefficient for microwave application, *Measurement and Technology*, 147 (2000) 269-273.
- [15] A. V. Grosse, W. M. Johnston, R. L. Wolfgang, W. F. Libby, Tritium in nature, *Science*, 113, 1-2 (1951)
- [16] Yi-Hyun Park, Kyung-Mi Min, Mu-Young Ahn, Seungyon Cho, Young-Min Lee, Sang-jin Park, Rehan Danish, Chul-hwan Lim, Yong-Dae Jo, Optimization of mass-production conditions for tritium breeder pebbles based on slurry droplet wetting method, 109-111, 443-447 (2016)
- [17] Kathirvel Ganesan, Tatiana Budtova, Lorenz Ratke, Pavel Gurikov, Victor Baudron, Imke

- Preibisch, Philipp Niemeyer, Irina Smirnova, Barbara Milow, Review on the production of Polysaccharide aerogel particles, *Materials* (Basel), 11,11 (2018)
- [18] Chan, E.-S., Lee, B.-B., Ravindra, P., Poncelet, D., Prediction models for shape and size of alginate macrobeads produced through extrusion dripping method, *Journal of Colloid interface Science*, 338, 63-72 (2009)
- [19] Henry G. Barbour, William F. Hamilton, The falling drop method for determining specific gravity, *Journal of Biological Chemistry*, 69, 625-640 (1926)
- [20] J.D. Lulewicz, N. Roux, Fabrication of Li_2TiO_3 pebbles by the extrusion spheronisation sintering process, *Journal of Nuclear Materials*, 307–311, 803-806 (2002)
- [21] D. Mandal, M.R.K. Sheno, S.K. Ghosh, Synthesis & fabrication of lithium-titanate pebbles for ITER breeding blanket by solid state reaction & spherodization, *Fusion Engineering and Design*, 85, 819-823, (2010)
- [22] D. Mandal, D. Sathiyamoorthy, V.G. Rao, Preparation and characterization of lithium-titanate pebbles by solid-state reaction extrusion and spherodization techniques for fusion reactor, *Fusion Engineering and Design*, 87, 7-12 (2002)
- [23] X. Wu, Z. Wen, J. Han, X. Xu, B. Lin, Fabrication of Li_2TiO_3 pebbles by water-based sol-gel method, *Fusion Engineering and Design* 83, 112-116, (2008)
- [24] K. Tsuchiya, H. Kawamura, K. Fuchinoue, H. Sawada, K. Watarumi, Fabrication development and preliminary characterization of Li_2TiO_3 pebbles by wet process, *Journal of Nuclear Materials*, 258–263 (1998) 1985-1990
- [25] D. Mandal, et al., Preparation and characterization of lithium-titanate pebbles by solid-state reaction extrusion and spherodization techniques for fusion reactor, *Fusion Engineering and Design*, 87 (2012) 7-12
- [26] Sang-Jin Lee, et al., Fabrication of Li_2TiO_3 pebbles by a freeze drying process, *Fusion Engineering and Design*, 88 (2013) 3091-3094
- [27] Yi-Hyun Park, In-Keun Yu, Mu-Yung Ahn, Seungyon Cho, Duck Young Ku, Fabrication of Li_4SiO_4 pebbles using slurry droplet wetting method for solid breeding material, *Fusion Science and Technology*, 62 (2012) 185-189
- [28] David, E. Handbook of Polymer Foam; Rapra Technology Limited: Shrewsbury, (2004)
- [29] Yi-Hyun Park, Seungyon Cho, Mu-Young Ahn, Fabrication of Li_2TiO_3 pebbles using PVA–boric acid reaction for solid breeding materials, *Journal of Nuclear Materials*, 455 (2014) 106-110
- [30] G. Federici, A.R. Raffray and M-A. ABDOU, MISTRAL: A comprehensive model for tritium transport in lithium-base ceramics Part I: Theory and description of model capabilities, *Journal of Nuclear Materials* 173 (1990) 185-213.
- [31] A. Raffray, Seungyon Cho, A. Abdou, Modeling of tritium transport in ceramic breeder single crystal, *Journal of Nuclear Materials* 210 (1994) 143-160.
- [32] Chia-Chan Lin, Li-Ting Lee, Ling-Jung Hsu, Degradation of polyvinyl alcohol in aqueous solutions using UV-365 nm/ $\text{S}_2\text{O}_8^{2-}$ process, *International for Environment Science Technology*, 11 (2014) 831-838.
- [33] Kathirvel Ganesan, Tatiana Budtova, Lorenz Ratke, Pavel Gurikov, Victor Baudron, Imke Preibisch, Philipp Niemeyer, Irina Smirnova, Barbara Milow, Review on the production of polysaccharide aerogel particles, *Materials*, 11 (2018) 2144 10.3390/ma11112144

- [34] Robitzer M., Renzo F.D., Quignard, Physisorption methods for the characterization of the texture and surface of polysaccharide aerogels. *Microporous Mesoporous Mater*, 140 (2011) 9–16
- [35] Robitzer M., Tourrette A., Horga R., Valentin R., Boissière M., Devoisselle J.M., Di Renzo, Quignard F., Nitrogen sorption as a tool for the characterisation of polysaccharide aerogels. *Carbohydr. Polym.* 85 (2011) 44–53.
- [36] T. Hoshino, M. Dokiya, T. Terai, Y. Takahashi, M. Yamawaki, Non-stoichiometry and its effect on thermal properties of Li_2TiO_3 , *Fusion Engineering and Design*, 61-62 (2002) 353-360.

6. Proposal maximum operating temperature of Li_2TiO_3 pebble bed

6.1 Introduction

In the solid-type breeding blanket for a fusion reactor, the tritium breeder material is used as pebble bed forms [1,2]. The tritium is one of the fuels for the fusion reactor and generated in the breeding blanket by the nuclear reaction between the neutron from fusion plasma and the lithium in breeder material. The bred tritium is extracted by the purge gas flow through the empty spaces inside the pebble bed [3,4]. Therefore, the securing of stable flow path of the purge gas inside the pebble bed is important to maintain the function of breeding blanket. The integrity of the pebble bed can be affected by the sintering and the creep phenomena of the breeder pebble bed according to the temperature increase. The path flow of purge gas can be clogged by the sintering behavior and the creep phenomena of the pebble bed when we considering application environment in the solid breeding blanket. The maximum temperature of the lithium metatitanate (Li_2TiO_3) breeder region in the solid-type breeding blanket is assumed to be about 900 °C [5,6]. However, the Li_2TiO_3 pebbles in the breeding blanket during the operation conditions can be sintered with neighbored pebbles and it can affect the flow path of purge gas and the tritium extraction from the pebble bed. In the case of a solid breeder, the high-energy neutrons will penetrate the pebbles, leading to tritium being generated throughout the ceramic matrix. Therefore, it is essential that all generated tritium be extracted from the breeder material to ensure the maximum possible TBR. For recovery, this tritium must diffuse to the surface, as illustrated in figure 6.1 [13]. Because the Li_2TiO_3 pebbles have been manufactured by the sintering at about 850 °C - 1200 °C [7-11]. In practice, the sintered Li_2TiO_3 pebble bed during the high temperature experiments has been reported [12]. Accordingly, the maximum operating temperature of Li_2TiO_3 pebble bed should be determined for the stable tritium extraction by the purge gas flow inside the pebble bed. This study aims to propose the maximum operating temperature of the Li_2TiO_3 pebble bed in the solid-type breeding blanket through the investigation of the starting temperature of sintering on the Li_2TiO_3 pebble bed and the creep deformation behavior of the Li_2TiO_3 pebble bed at various conditions.

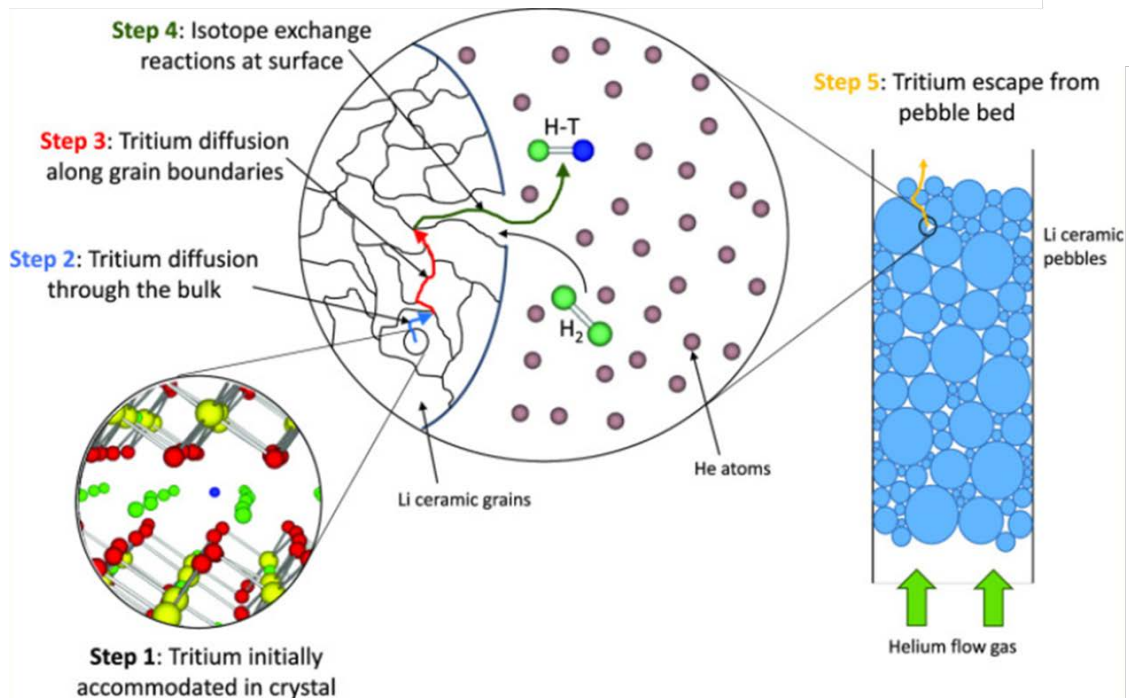


Figure 6.1 Schematic of the tritium release process from lithium ceramic pebbles in the breeder blanket [13].

6.2 Experimental

The sintering and creep test of the Li_2TiO_3 pebble bed were performed using the hot-press system. The Li_2TiO_3 pebbles with 1 mm of diameter were fabricated by the slurry droplet wetting method [7]. Figure 6.2 shows the hot-press system and the schematic diagram of the inside of the environmental chamber for sintering and creep test of the pebble bed. The Li_2TiO_3 pebbles were filled in the graphite mold. The dimension of the filled pebble bed was 22 mm(w) x 22 mm(l) x 10 mm(t). The weight of the Li_2TiO_3 pebble bed was about 10 g. The graphite mold including the pebble bed was located in the inside of the chamber. The pressure on the pebble bed was applied using the piston of the hot-press system. The shrinkage and densification of the pebble bed were evaluated by the displacement change of the piston, which was measured by the linear variable displacement transformer (LVDT) sensor.

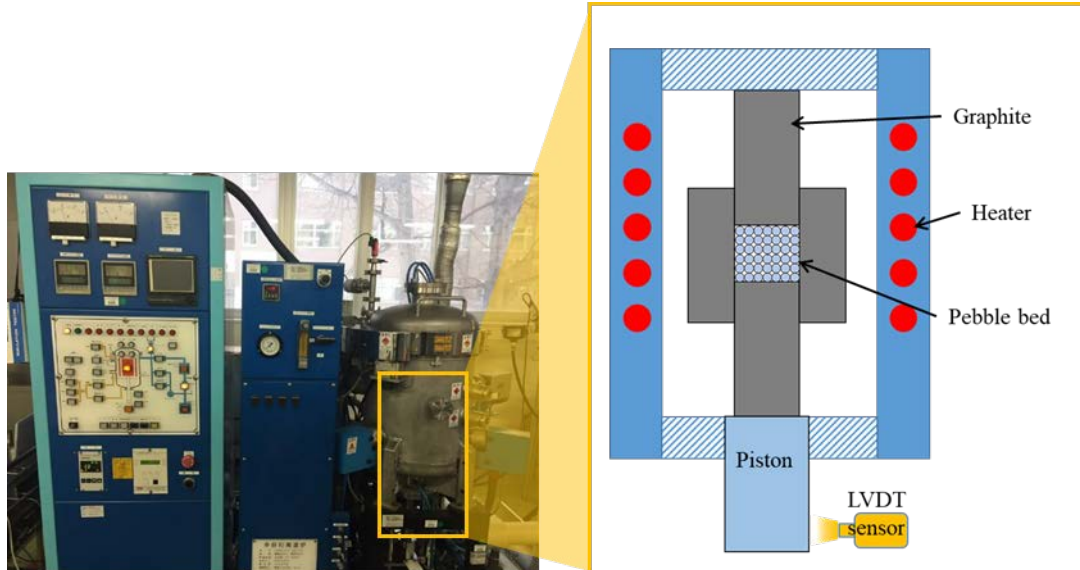


Figure 6.2 Hot-press system for sintering and creep test of pebble bed

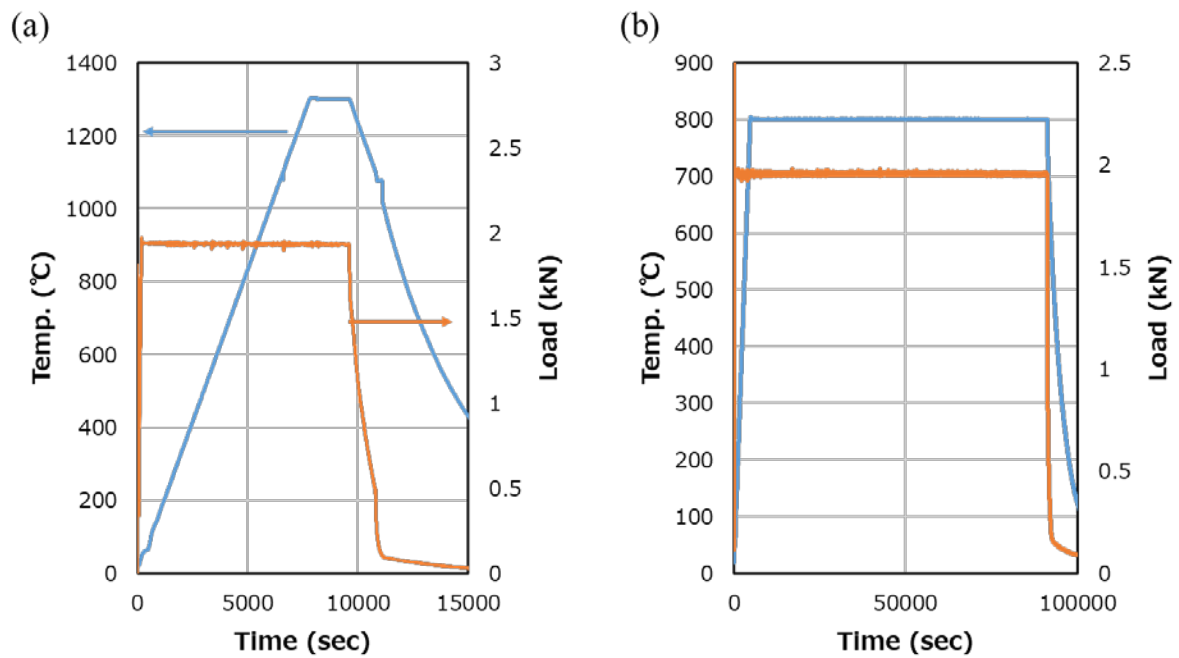


Figure 6.3 Thermal and pressure history of the hot-press system.

(a) sintering test, (b) creep test

The figure 6.3 is shown the thermal and pressure history of the hot-press system for (a) sintering test and (b) creep test of the Li_2TiO_3 pebble bed. The Li_2TiO_3 pebble bed was heated up to 1300 °C with a 10 °C/min of heating rate in Ar atmosphere during the sintering test. The applied pressures were 1 MPa and 4 MPa, respectively. The temperature and pressure for the creep test of the Li_2TiO_3 pebble bed were 800 °C with different pressure (1 MPa ~ 4 MPa) and the holding time of the temperature and pressure on the pebble bed was 24 hours.

6.3 Results & Discussion

6.3.1 Sintering phenomena of Li_2TiO_3 pebble bed

The densification of the pebble bed is able to re-plot as shown in figure 6.4, which is the densification curve of the Li_2TiO_3 pebble bed under the applied pressure of 4 MPa. The sintering of the Li_2TiO_3 pebble bed under the applied pressure of 4 MPa was started from about 800 °C.

In general, the sintering behavior can be divided typically three stage by the particle compaction, where three stage is initial (0~3 %), intermediate (4~92%), final (93~100%) stage. The less than 3% shrinkage of initial stage is shown the necking phenomena such as figure 6.6 (a). In the view-point of the tritium breeding materials, the necking phenomena can be rewrite that the flow path of purge gas to extract the bred tritium inside the pebble bed will be changed smaller. Indeed the shrinkage of initial stage on the Li_2TiO_3 pebble bed can be ignored on the tritium breeding ratio. The initial stage of the Li_2TiO_3 pebble bed sintering under the applied pressure of 4 MPa was estimated at from 800 °C to 850 °C. In addition, the starting temperature of sintering on the Li_2TiO_3 pebble bed was dependent on the applied pressure. Figure 6.5 shows the densification curve of the Li_2TiO_3 pebble bed under the applied pressure of 1 MPa. The sintering temperature of the pebble bed under the applied pressure of 1 MPa was about 850 °C. And the initial stage of the pebble bed sintering under the applied pressure of 1 MPa was estimated at from 850 °C to 900 °C.

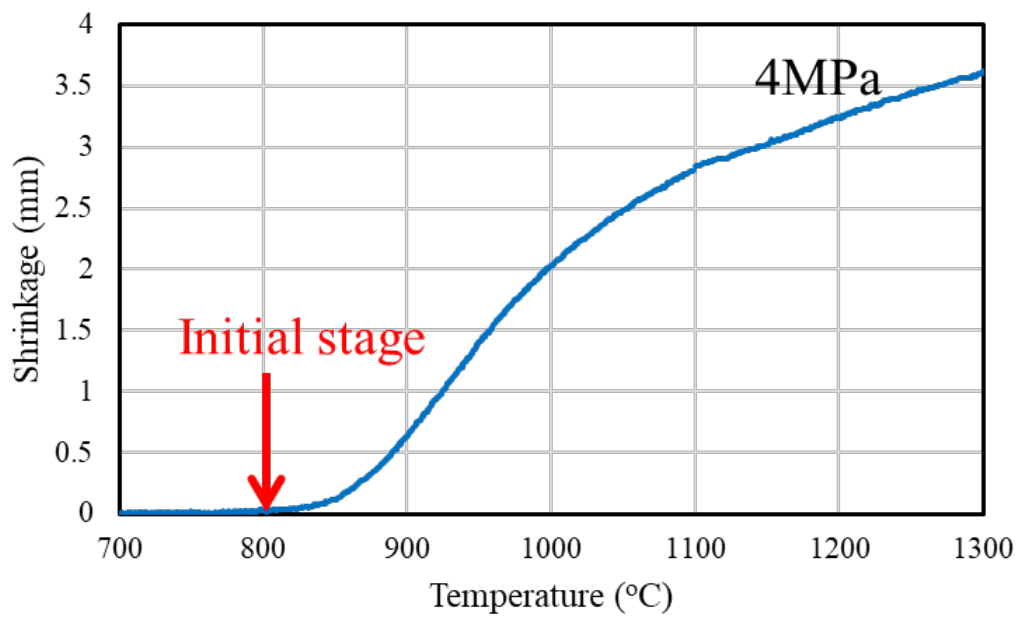


Figure 6.4 Densification curve of Li_2TiO_3 pebble bed under the applied pressure of 4 MPa

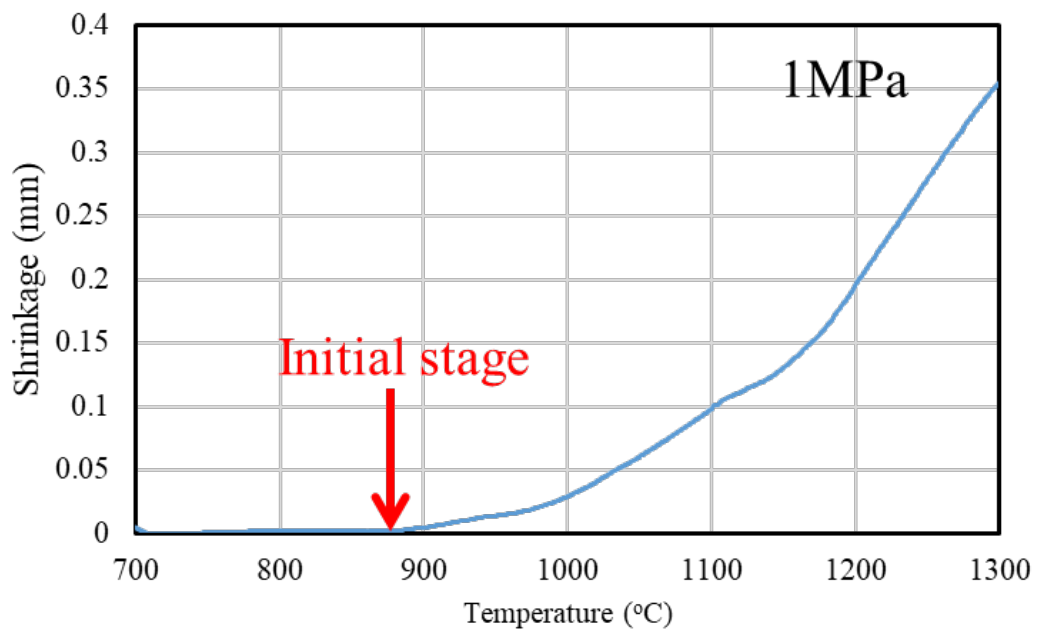


Figure 6.5 Densification curve of Li_2TiO_3 pebble bed under the applied pressure of 1 MPa

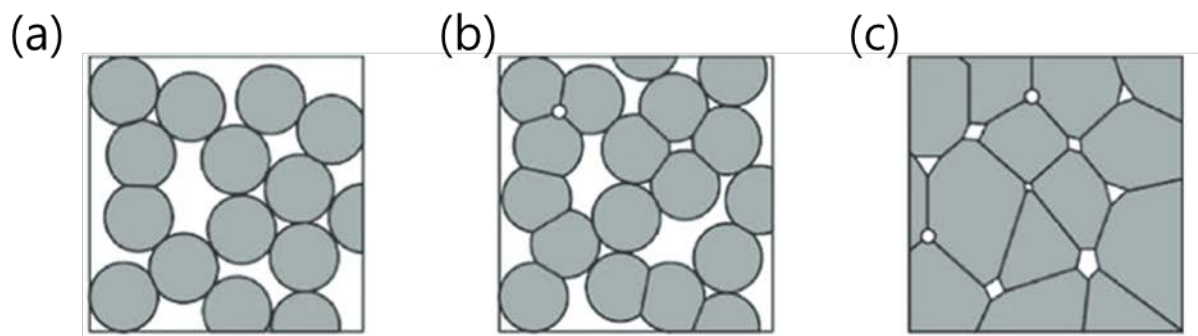


Figure 6.6 Schematic of sintering particles according to the sintering stage. (a) initial, (b) intermediate, (c) final.

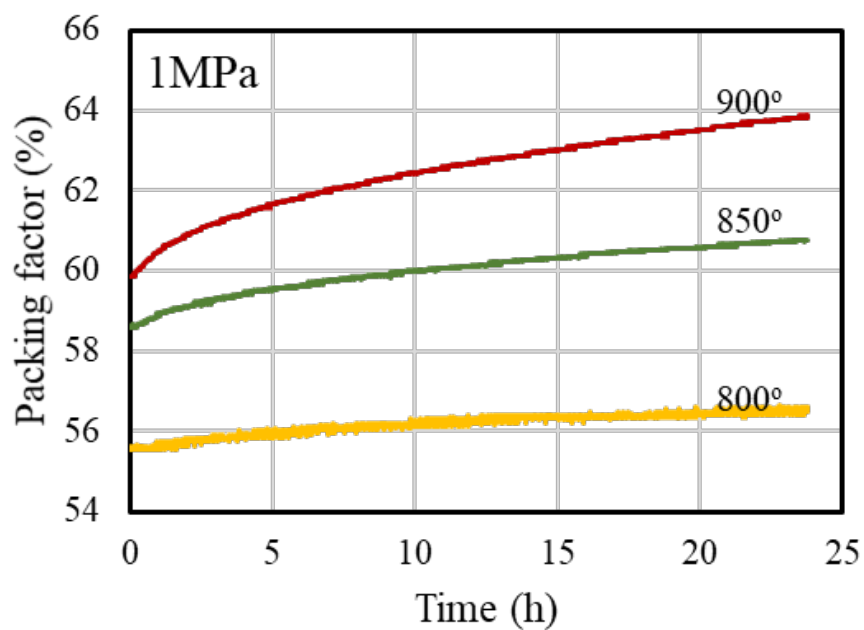


Figure 6.7 Effects of temperature on densification of Li_2TiO_3 pebble bed under the applied pressure of 1 MPa

6.3.2 Creep phenomena of Li_2TiO_3 pebble bed

In the case of high-temperature materials, it should be considered not only sintering but also creep phenomena. Figure 6.7 shows the effects of temperature on the densification of Li_2TiO_3 pebble bed under the applied pressure of 1 MPa. The vertical axis represents the packing factor of the Li_2TiO_3 pebble bed, which was able to be calculated from the shrinkage of the pebble bed. Where the holding time was 24 hours at the target temperature. In the figure 6.6, the shrinkage of pebble bed under the applied pressure of 1 MPa at the temperature of 800 °C after 24 hours was only less than 2 % with the densification of pebble bed had a trend of saturation after 24 hours. However, the densification of the pebble bed at more than 800 °C under the 1 MPa has been still progressed even if the holding time was after 24 hours. The temperature of 900 °C or under is the initial stage of the sintering on the Li_2TiO_3 pebble bed under the applied pressure of 1 MPa, as shown in figure 6.5. Therefore, the creep deformation is one of important parameters on the maximum operating temperature of the pebble bed.

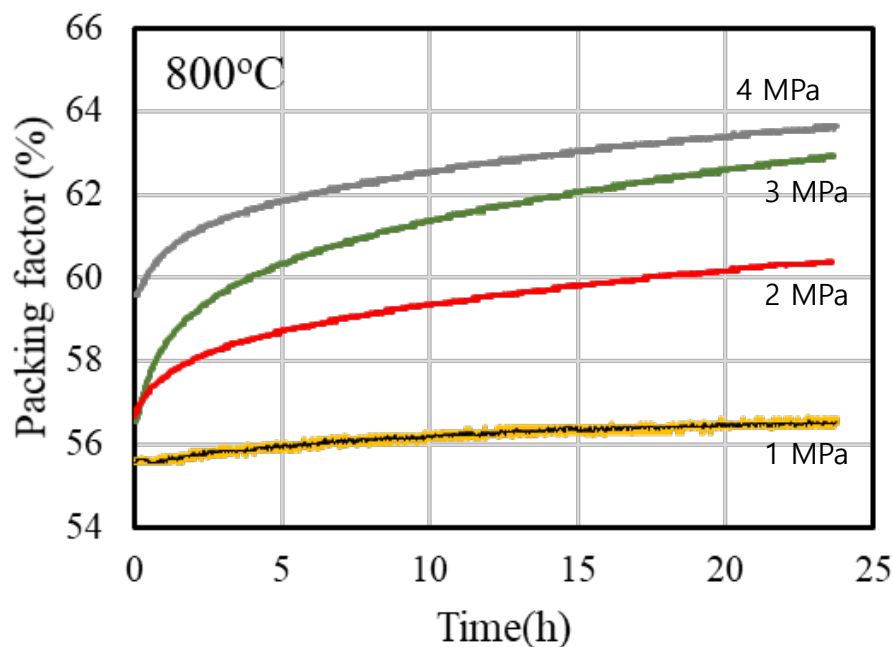


Figure 6.8 Effects of applied pressure on the densification of Li_2TiO_3 pebble bed at the temperature of 800 °C

The densification behavior of Li_2TiO_3 pebble bed at the temperature of $800\text{ }^\circ\text{C}$ were investigated with different pressure, which as shown in figure 6.8. These conditions corresponded to the initial stage of the sintering on the Li_2TiO_3 pebble bed. The densification of the pebble bed caused by creep deformation under more than the 2 MPa was still ongoing even if the holding time was after 24 hours. The appearances of the pebble bed after the creep test at each condition were shown in figure 6.9. The shape of the sintered pebble bed was observed under more than the applied pressure of 2 MPa after 24 hours. However, under the applied pressure of 1 MPa, the pebble bed was not able to be kept the shape of the pebble bed after the creep test. In case of 1 MPa, the pebbles can be divided easily after creep test. It is expected the necking phenomena between pebble and neighbor pebble.

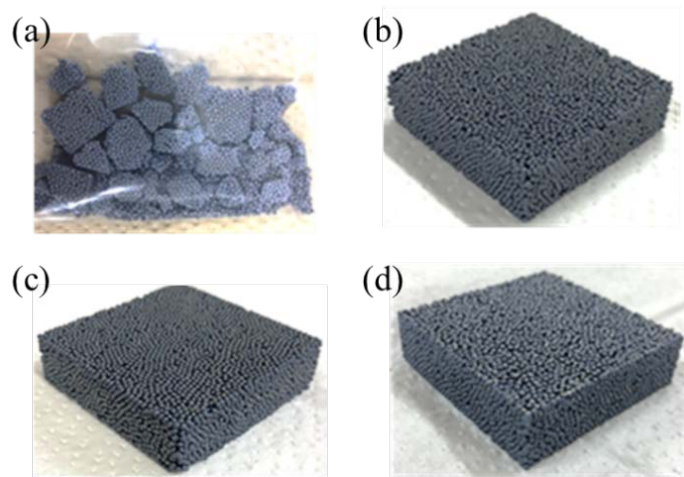


Figure 6.9 Morphology of Li_2TiO_3 pebble bed after creep test at the $800\text{ }^\circ\text{C}$.

(a) 1MPa, (b) 2MPa, (c) 3MPa, (d) 4MPa

6.4 Summary

In this chapter, the maximum operating temperature and pressure of the Li_2TiO_3 pebble bed were proposed by the investigation of the sintering and creep behavior of the Li_2TiO_3 pebble bed. The initial stage of the sintering phenomena on the Li_2TiO_3 pebble bed under the applied pressure of 1 MPa and 4 MPa were estimated at from 850 °C to 900 °C and from 800 °C and 850 °C, respectively. However, even though the Li_2TiO_3 pebble bed was located in the initial stage of sintering, it was confirmed that the densification of a pebble bed caused by creep deformation was progressed. From the viewpoint of stable extraction of bred tritium from the breeder pebble bed, it was recommended that the maximum operating temperature and pressure of the Li_2TiO_3 pebble bed were 800 °C and 1 MPa to keep the uniform flow path of purge gas inside the pebble bed.

Reference

- [1] P.J. Gierszewski, J.D. Sullivan, Ceramic sphere-pac breeder design for fusion blankets, *Fusion Eng. Des.* 17 (1991) 95-104.
- [2] A. Ying, et al., Status and perspective of the R&D on ceramic breeder materials for testing in ITER, *J. Nucl. Mater.* 367–370 (2007) 1281-1286.
- [3] F. Franza et al., Tritium transport analysis in HCPB DEMO blanket with the FUS-TPC code, *Fusion Eng. Des.* 88 (2013) 2444-2447.
- [4] M. Ahn Furudate, S. Cho, Study on equilibrium compositions of HTO/H₂ mixture in purge gas flow in tritium breeding blanket, *Fusion Sci. Technol.* 71 (2017) 514–519.
- [5] L. M. Ciancarli, et al., Overview of the ITER TBM Program, *Fusion Eng. Des.* 87 (2012) 375-402.
- [6] Mu-Young Ahn, et al., Design change of Korean HCCR TBM to vertical configuration, *Fusion Eng. Des.* 88 (2013) 2284-2288.
- [7] Yi-Hyun Park, et al., Fabrication of Li₂TiO₃ pebbles using PVA-boric acid reaction for solid breeding materials, *J. Nucl. Mater.* 455 (2014) 106-110.
- [8] Yi-Hyun Park, et al., Li₂TiO₃ powder synthesis by solid-state reaction and pebble fabrication for tritium breeding material, *Fusion Eng. Des.* 124 (2017) 730-734.
- [9] Jong-il Kim, et al., Effect of sintering conditions on the microstructure of Li₂TiO₃ tritium breeding materials, *Fusion Eng. Des.* 156 (2020) in press.
- [10] Tsuyoshi Hoshino, Optimization of sintering conditions of advanced tritium breeder pebbles fabricated by the emulsion method, *Fusion Eng. Des.* 98-99 (2015) 1788-1791.
- [11] Mao Yang, et al., Fabrication of Li₂TiO₃ ceramic pebbles with fine microstructure by microwave sintering, *J. Nucl. Mater.* 509 (2018) 330-334.
- [12] Yi-Hyun Park, et al., Measurement of thermal conductivity of Li₂TiO₃ pebble bed by laser flash method, *Fusion Eng. Des.* 146 (2019) 950-954.
- [13] Kamal N. Goswami and Samuel T. Murphy, Influence of lithium vacancy defects on tritium diffusion in *B*-Li₂TiO₃, *Journal of Physical Chemistry Nanomaterials and Interfaces* 124 (2020) 12286-12294

7. Chemical Compatibility between Conceptual Design of Li_2TiO_3 Pebbles bed and Structure Materials

7.1 Introduction

The challenge is to develop structural materials which maintain high performance during prolonged exposure to high thermal and radiation flux. In addition to their structural properties, they may need chemical compatibility with coolants and be relatively easy to manufacture. The thermo-mechanical properties must not be degraded significantly due to damage and activation by 14 MeV neutrons. Heat conductivity should be maintained as well as low swelling and void formation, despite high levels of helium and hydrogen production. The structure material have been required some of conditions, which is summarized in chapter 2.1.1. The compatibility among the requirements is important when consider the operating conditions. Considering the structural material such as a part of the first wall, the tritium breeding material will be formed a pebble bed in which pebbles are stacked, it is in point-contacted with the structure material (figure 7.1). If there is no evaluation of compatibility between structural and functional materials, the application of each material is essentially impossible. Therefore, it is necessary to evaluate the compatibility of each structural material with the practical application environment. Typically, the candidates of structure material in fusion reactor are reduced activation ferritic/martensitic (RAFM) steels, vanadium-based alloys, tungsten (W), fiber-reinforced composites based on silicon carbides.

The RAFMs have the most advanced technological and industrial development due to the experience acquired in fossil and nuclear energy technology. They show reasonably good thermo-physical and mechanical properties, adequate resistance to radiation-induced swelling and helium embrittlement, and good compatibility with major cooling and breeder materials. Moreover, industrial batches have already been produced such as the F82Hs of Japan [1-3], the EUROFER of Europe [4-6], the ARAA of Korea [7-9], and further studies towards super-clean steels are in progress. Development is required in several critical areas. Material with further reduced activation is needed, their radiation-induced hardening and embrittlement in a fusion relevant environment needs to be better understood. To enlarge their range of application to higher temperature, possible improvements using the technique of oxide dispersion strengthening is under investigation.

The fiber- reinforced composites based on the silicon carbide have been conceived and developed

mainly for aerospace applications and fossil power generation plants due to their potential for high temperature operation and high corrosion resistance which allows thermodynamic efficiency to be maximized. In addition for use in fusion, they exhibit very low short and medium term induced radioactivity and afterheat. The key issues to be addressed include the irradiation performance, the scaling up of fabrication techniques for large components, the lack of suitable techniques for joining parts since welding is not possible, the effect of matrix porosity and micro-cracking on coolant hermetic sealing capacity, the need for standardization and (at present) the high cost[10, 11]. Silicon Carbide and SiC/SiC composites have become widely used as promising candidate for structural and functional materials of advanced nuclear systems due to their excellent mechanical and thermal properties at high temperatures, low induced activity in the case of high purity and resistance for irradiation, high chemical stability and high heat resistance.

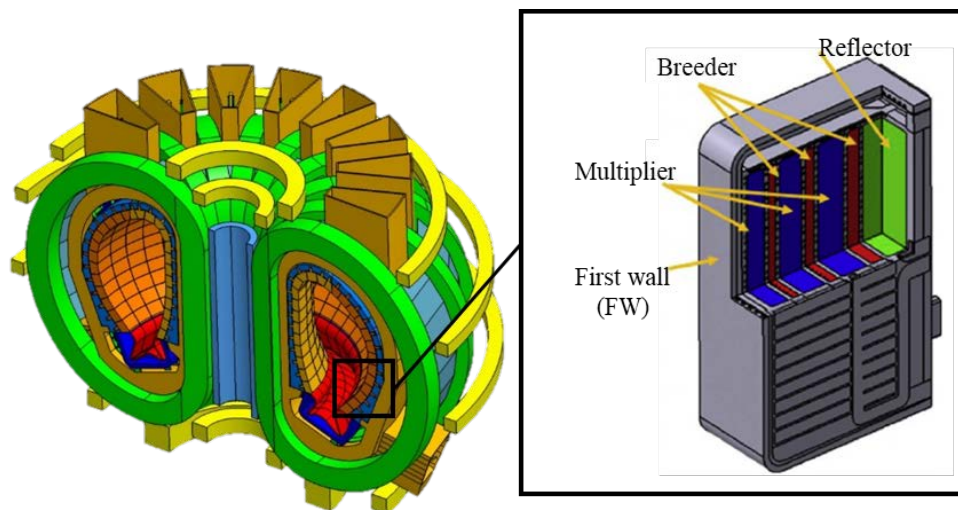


Figure 7.1 schematic of solid-breeding blanket

Lithium-based oxide ceramics are being considered as tritium breeder materials in the blanket of nuclear fusion reactors. One of the anticipated advantages of ceramic materials lies in avoiding the corrosive attack on vessels and pipework which is expected when liquid lithium (or a liquid lithium-lead eutectic) is used as breeding material. But even with the use of solid oxide breeder materials substantial corrosive attack of the metallic cases or SiC/SiC composites, e.g., the cladding tubes of breeder materials rods, may occur [12]. A number of compatibility tests have been performed elsewhere [13-18] to study the chemical reaction behavior of oxide breeder materials (Li_2O , LiAlO_2 , Li_2SiO_3 , Li_4SiO_4 , Li_2TiO_3 , Li_2ZrO_3) with various materials in closed systems. Compatibility studies have been intensively carried out for the liquid blanket design employing molten salt, especially in Li-Pb [19].

Alves et al. studied the compatibility between EUROFER and the ceramic breeder materials (Li_2TiO_3 and Li_4SiO_4) by heating them at 873 K and for up to 2000 h in He + 0.1% H_2 , yet, mainly focused on changes of breeder pebble surface [21]. They reported the contamination of the surface of Li_4SiO_4 pebbles by the constituent elements of EUROFER, while the contamination of the Li_2TiO_3 pebble was not clearly seen. A series of compatibility studies between EUROFER and lithium silicate were carried out by Hernandez et al. by heating them at 823 K for up to 120 days [22-24]. It is reported that the corrosion attack resulted in the formation of a double oxide corrosion layer on the surface of EUROFER where the outer and the inner layer contained Fe- and Cr-rich compositions, respectively. For the solid blanket concept, conversely, there is only a limited number of researches on compatibility between SiC/SiC composite and ceramic breeder, though comparable works using stainless steel and RAFMs such as F82Hs, EUROFER can be found [19, 20].

In this chapter, the compatibility of the SiC-based composite material and the Li_2TiO_3 tritium breeding material was evaluated in consideration of the practical application environment. From the results of this chapter, it is possible to accumulate data on the compatibility of SiC/SiC composites and Li_2TiO_3 tritium breeding materials. We also can be propose an optimal environment for the fusion reactor, when two materials are applied at the same time.

7.2 Experimental

7.2.1 Materials

The SiC/SiC composites are adopted as structure materials. NITE-SiC/SiC composites is made in Muroran Institute of Technology in Japan. The fiber reinforcing architecture was the CP. (the detailed described in chapter 3.) All of the specimens adopted as structure materials are machined the diameter of 7 mm with thickness 2 mm.

We prepared Li_2TiO_3 pebbles from the solid state reaction between titanium oxide and lithium oxide as the functional materials. Stoichiometric amounts of lithium and titanium of analytical grade were used as raw materials [25]. These two oxides were mixed homogeneously and ball-milled in alcohol. This mixed powder was dried in a vacuum oven and heat-treated at 700°C for 3 h in air. Li_2TiO_3 powder

and the sintered Li_2TiO_3 pebbles (chapter 5) at 900 °C, 1h, 10 °C/min, in air confirmed the Li_2TiO_3 phase by the X-ray diffraction. And the size of Li_2TiO_3 pebbles was 1.1mm of diameter.

7.2.2 Method

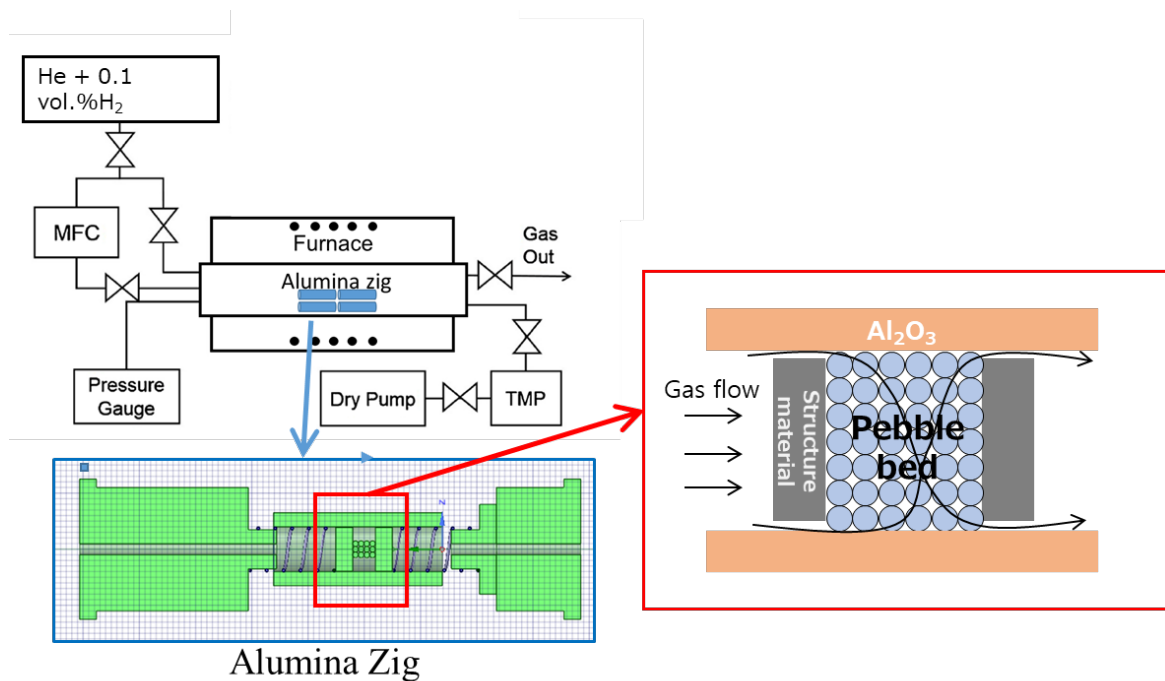


Figure 7.2 Schematic diagram of the alumina zig and the tubular furnace.

The samples were placed in the center of specially fabricated alumina zig inserted in a tubular furnace. In the alumina zig, a pebble bed was sandwiched between two structure materials by using an Inconel spring. The figure 7.2 is shown the image of the alumina zig and the tubular furnace. A dry vacuum pump and a turbo-molecular pump (TMP) operated until the internal pressure of the furnace reached 1.33×10^{-4} Pa. The purge gas composed of He with/without a 0.1 vol.% H_2 mixture was fed into the furnace until the internal pressure of the furnace reached standard atmospheric pressure. Then, the valve in the gas outlet line opened. The controlled purge gas directly flowed into the samples during the experiment. The purge gas was measured by a mass flow controller (MFC). The value was 200 cc/min. The furnace was heated to 675~800°C with heating rate of $10 \text{ }^\circ\text{C} \cdot \text{min}^{-1}$ and was kept for 7, 14, and 21. After completion of various heating times, the samples were removed from the furnace and

kept in a vacuum desiccator.

7.3 Results & Discussion

7.3.1 Compatibility between SiC & SiC/SiC composites and Li_2TiO_3 Pebble Bed

The figure 7.3 is shown the morphology of Li_2TiO_3 pebbles and NITE-SiC/SiC composites after evaluation at 675 °C for 7days (168). The Li_2TiO_3 pebble was located the upper, and the NITE-SiC/SiC composite was located the bottom in the figure 7.3. After evaluation of compatibility testing, the NITE-SiC/SiC composites show the satisfied status. The F/M interface was still existed in the face of the contacted Li_2TiO_3 pebble. The oxygen in the Li_2TiO_3 pebbles can not be affect the oxidation of F/M interface.

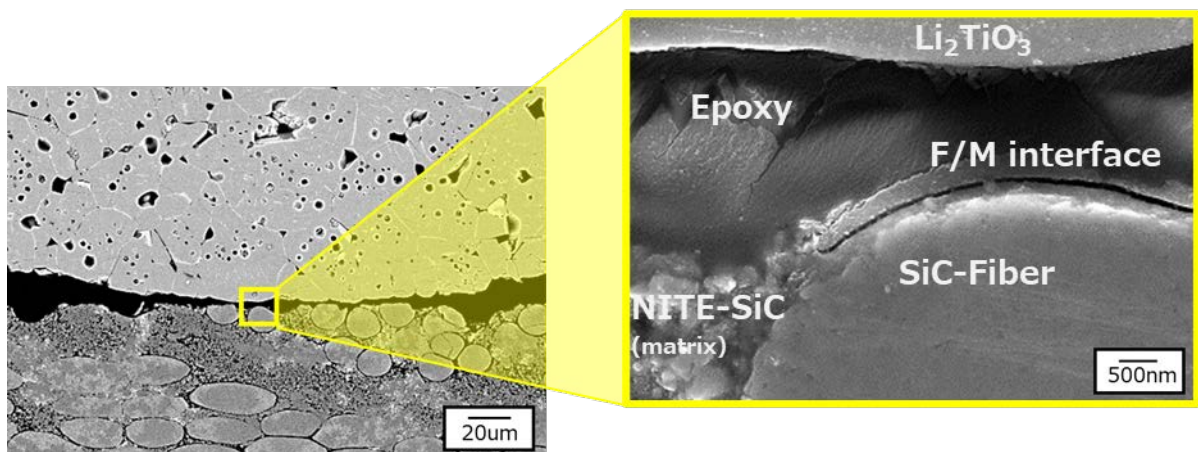


Figure 7.3 Morphology of Li_2TiO_3 pebbles and NITE-SiC/SiC composites after evaluation at 675 °C for 7days (168).

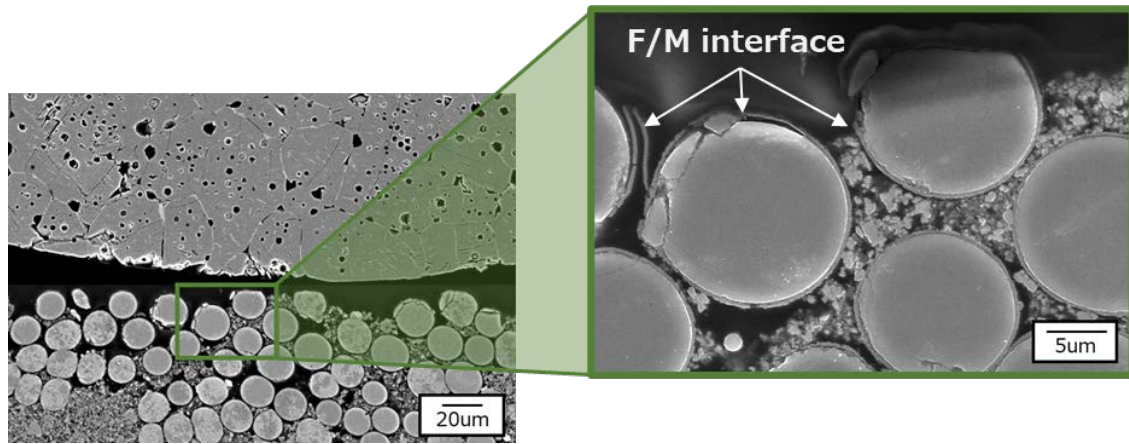


Figure 7.4 Morphology of Li_2TiO_3 pebbles and NITE-SiC/SiC composites after evaluation at 675 °C for 21days (504).

Figure 7.4 is shown the morphology of Li_2TiO_3 pebbles and NITE-SiC/SiC composites after evaluation at 675 °C for 21days (504). The micro structure of Li_2TiO_3 pebble and NITE-SiC/SiC composites were not changed. F/M interface still existed in the face of the 21days. The condition of 675 °C not be occurred the oxidation of NITE-SiC/SiC composites. However, the 800 °C was different compared to the condition of 675 °C. Figure 7.5 is shown the morphology with EDS mapping of Li_2TiO_3 pebbles and NITE-SiC/SiC composites after evaluation at 800 °C for 21days (504). After evaluation at 800 °C for 7days, the Li_2TiO_3 pebble and the NITE-SiC/SiC composites were shown the different microstructure.

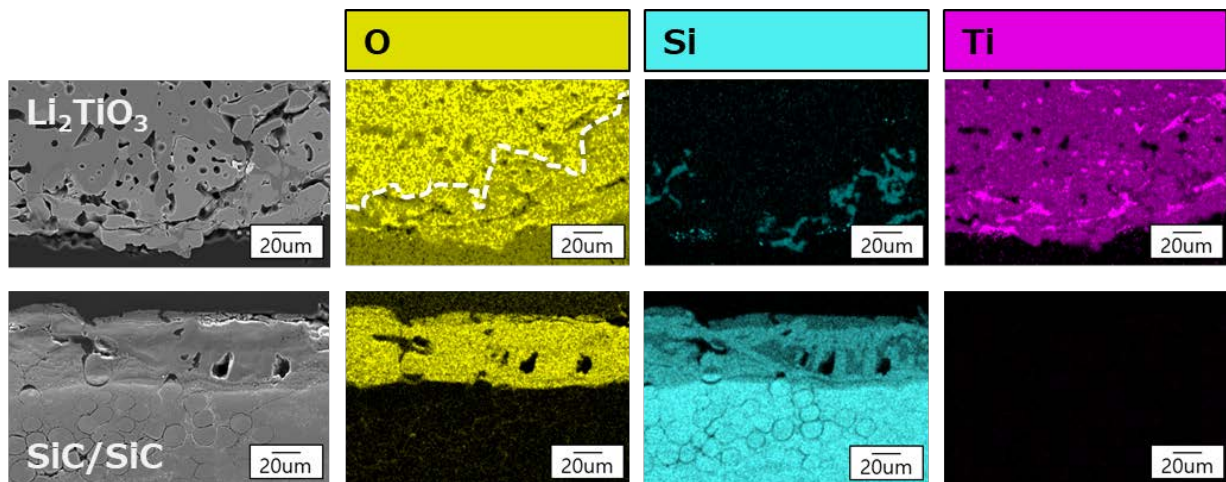


Figure 7.5 Morphology with EDS mapping of Li_2TiO_3 pebbles and NITE-SiC/SiC composites after evaluation at 800 °C for 7days (168h).

The Li_2TiO_3 pebbles was shown the decreasing of the oxygen with increasing the silicon a partially. Also, the NITE-SiC/SiC composite was shown the layer with oxygen and silicon. The changing of the chemical components is expected the migration of element by the temperature. The layer is expected the Li-Si-O system. However, the furthermore analysis about the layer are required.

7.4 Summary

In this chapter, the compatibility of the SiC-based composite material and the Li_2TiO_3 tritium breeding material was evaluated with the consideration of the practical application environment. The NITE-SiC/SiC composite material shows excellent coexistence with the Li_2TiO_3 breeding material up to 675 °C and 500 h. It is stable up to high temperatures compared to the operating temperature of blanket systems that use low emissivity steel (RAFMs).

Under the condition of 800 °C, interatomic diffusion of elements from the growth material and structural material and oxides on the surface of the NITE-SiC/SiC composite material is produced. The growth material exhibits microstructure changes and microcracks as the temperature rises.

From the results in this chapter, when NITE-SiC/SiC composite material is applied to the structural material and Li_2TiO_3 is applied to the growth material, it is considered that the temperature can be safely used up to 675 °C in the environment of He + 0.1% H_2 . A more detailed evaluation is required for the determination of the upper limit of the stable temperature and the coexistence above 800 °C.

From the results of this chapter, it is possible to accumulate data on the compatibility of NITE-SiC/SiC composites and Li_2TiO_3 tritium breeding materials. We also can propose an optimal environment for the fusion reactor, when two materials are applied at the same time.

References

- [1] Hideo Sakasegawa, Hiroyasu Tanigawa, Takanori Hirose, Taichiro Kato, Takashi Nozawa, Material strength standard of F82H for RCC-MRx, *Fusion Engineering and Design*, 161 (2020) 111952.
- [2] Takanori Hirose, Taichiro Kato, Hideo Sakasegawa, Hiroyasu Tanigawa, Takashi Nozawa, Evaluation of fatigue properties of reduced activation ferritic/martensitic steel, F82H for development of design criteria, *Fusion Engineering and Design* 160 (2020) 111823.
- [3] Yoshiyuki Watanabe, Hirotomo Iwakiri, Norihiko Murayoshi, Daiji Kato, Koichi Sato, Hiroyasu Tanigawa, Hydrogen retention behavior of primary precipitates in F82H steel: Atomistic calculation based on the density functional theory, *Fusion Engineering and Design* 159 (2020) 111788.
- [4] Eric Daum, Ulrich Fischer, Long-term activation potential of the steel eurofer as structure material of a demo breeder blanket, *Fusion Engineering and Design*, 49-50 (2000) 529-533.
- [5] L Giancarli, M Ferrari, M. A Fütterer, S Malang, Candidate blanket concepts for a European fusion power plant study, *Fusion Engineering and Design* 49-50 (2000) 445-456.
- [6] G. Aiello, J. Aktaa, F. Cismondi, G. Rampal, J.-F. Salavy, F. Tavassoli, Assessment of design limits and criteria requirements for eurofer structures in TBM components, *Journal of Nuclear Materials* 414 (2011) 53-68.
- [7] Jae Sung Yoon, Suk-Kwon Kim, Eo Hwak Lee, Hyung Gon Jin, Dong Won Lee, Seungyon Cho, Mechanical properties of ARAA steel after electron beam welding, *Fusion Engineering and Design* 124 (2017) 774-778.
- [8] Y. B. Chun, S. H. Kang, D. W. Lee, S. Cho, Y. H. Jeong, A. Żywczak, C. K. Rhee, Development of Zr-containing advanced reduced-activation alloy (ARAA) as structural material for fusion reactor, *Fusion Engineering and Design*, 109-111 (2016) 629-633.
- [9] Y. B. Chun, C. K. Rhee, D. W. Lee, Y. H. Park, Enhanced high-temperature mechanical properties of ARAA by thermos-mechanical processing, *Fusion Engineering and Design* 136 (2018) 883-890.
- [10] Waleed A. Mohrez, Hirotatsu Kishimoto, Yutaka Kohno, S. Hirotaki, Akira Kohyama, Behavior of W-SiC/SiC dual layer tiles under LHD plasma exposure, *Journal of Nuclear Materials* 442 (2013) 382-388.
- [11] Aljaž Iveković, Saša Novak, Goran Dražić, Darina Blagoeva, Sehila Gonzalezde Vicente, Current status and prospects of SiCf/SiC for fusion structural applications, *Journal of the European Ceramic Society* 33 (2013) 1577-1589.
- [12] P. HOFMANN and W. DIENST, Chemical compatibility between lithium-based oxide ceramics and stainless steels, *Journal of Nuclear Materials* 141-143 (1986) 289-293.
- [13] Toshimasa Kurasawa, Hidefumi Takeshita, Susumu Muraoka, Shoichi Nasu, Masanobu Miyake, Tadao Sano, Reaction of several iron and nickel based alloys with sintered Li₂O pebbles, *Journal of Nuclear Materials* 80 (1979) 48-56.
- [14] Toshimasa KURASAWA, Hidefumi TAKESHITA and Shoichi NASU, Compatibility between several heat resistant alloys and sintered Li₂O in static helium gas environment, *Journal of Nuclear Materials* 92 (1980) 67-72.
- [15] P. A. Finn, S. R. Breon, N. R. Chellew, Compatibility study of solid ceramic breeder materials, *Journal of Nuclear Materials* 103 (1981) 561-566.

- [16] O. K. Chopra, D. L. Smith, Interactions of solid ceramic breeding materials with structural alloys, *Journal of Nuclear Materials* 103 (1981) 555-560.
- [17] L. Yang, R. Medico, W. Baugh, K. Schultz, Irradiation study of lithium compound samples for tritium breeding application, *Journal of Nuclear Materials* 103 (1981) 585-589.
- [18] D. L. Porter, J. R. Krsul, M. T. Laug, L. C. Walters, M. Tetenbaum, Neutron irradiation and compatibility testing of Li₂O, *Journal of Nuclear Materials* 123 (1984) 929-933.
- [19] Keisuke Mukai, Fernando Sanchez, Regina Knitter, Chemical compatibility study between ceramic breeder and EUROFER97 steel for HCPB-DEMO blanket, *Journal of Nuclear Materials* 488 (2017) 196-203.
- [20] Keisuke Mukai, Maria Gonzalez, Regina Knitter, Effect of moisture in sweep gas on chemical compatibility between ceramic breeder and EUROFER97, *Fusion Engineering and Design* 125 (2017) 154-159.
- [21] L. C. Alves, E. Alves, M. R. da Silva, A. Paúl, A. La Barbera, Li ceramic pebbles chemical compatibility with EUROFER samples in fusion relevant conditions, *Journal of Nuclear Materials* 329-333 (2004) 1295-1299.
- [22] T. Hernández, P. Fernández, Corrosion susceptibility comparison of EUROFER steel in contact with two lithium silicate breeders *Fusion Engineering and Design* 89 (2014) 1436-1439.
- [23] Teresa Hernández, Pilar Fernández, Rafael Vila, Corrosion susceptibility of EUROFER97 in lithium ceramic breeders *Journal of Nuclear Materials* 446 (2014) 117-123.
- [24] Teresa Hernández, Pilar Fernández, Effect of the environment on the corrosion of EUROFER97 by solid lithium breeders, *Journal of Nuclear Materials* 447 (2014) 160-165.
- [25] K.M. Min, Y.H. Park, S. Cho, Synthesis of Li₂TiO₃ powder with high crystalline structure for tritium breeding material by ion-exchange process, *Fusion Eng.Des.* 109–111 (2016) 326–329.

8. Summary and conclusions

Ceramics is a promising candidate as structural/functional materials of the solid-breeding blanket, which is expected that effectively increase in terms of energy production efficiency of nuclear fusion reactors. In this study, the ceramics were adopted SiC/SiC composites as structural materials and Li_2TiO_3 breeder as functional materials.

SiC/SiC composites can be applied as structural materials such as first wall and side wall of blanket and tritium breeding zone, which enables generation energy at higher temperature than metals. Despite advantages of SiC/SiC composites over metals, composites with complicated shapes have own properties depending on their fiber reinforcing architectures. The strength such as in-plan, inter-laminar shear strength was similar approximate but the elastic modulus of specimens was different with fiber reinforcing architecture. From the comparison of a fracture surface and load-displacement curve analysis, the cross points of longitudinal or transverse direction fibers were suggested to behave as obstacles for both deformation and crack propagation. Although potential applications of SiC/SiC composites for fusion reactor is applied under very high vacuum environment ($\sim 10^{-5}$ Pa), it is required to consider their oxidation resistance for the prediction of accident tolerance at the loss of vacuum accident (LOVA) as well as the adulation of proper lifespan at long-term normal operation. NITE-SiC/SiC composites represented an extremely low amount of weight loss without any change of shape and size, even if these materials exposed at the severe oxidation environment under the forced flow of oxidative gas. The weight change speed of NITE-SiC/SiC composites clearly decreased with increasing the oxidation holding time. We suggested barrier SiC coat for resistance oxidation. It was confirmed that the CVD-SiC outer coating could be regarded as an effective environmental barrier for the oxidation proof resistance of NITE-SiC/SiC composites.

Li_2TiO_3 is Li-containing ceramics, which is a promising candidate for tritium breeding materials. The most important among the breeding materials is high tritium breeding ratio. In chapter 5 & 6, It was possible to obtain a spherical shape with a diameter (1mm), suitable grain boundary (5~10um), and a homogeneous microstructure under the required to efficiently produce the tritium by improvement of fabrication method. Also we are proposed that the optimal operation conditions from the sintering behavior with creep behavior of pebble bed. Because of the Li_2TiO_3 pebbles in the breeding blanket during the operation conditions can be sintered with neighbored pebbles and it can affect the flow path of purge gas and the tritium extraction from the pebble bed.

Finally, we are evaluated compatibility between SiC/SiC composites and Li_2TiO_3 tritium breeding materials. It was possible to predict that the oxidation behavior each of structure material and ion diffusion in both of the materials. Also, these results can be applied as a prediction of a lifetime and suggestion the optimal operation conditions when applicate the SiC/SiC composites and Li_2TiO_3 breeder as structural and functional material.

A design with the improved structural integrity of the breeding blanket is expected from the evaluation of the mechanical properties of the SiC/SiC composite material with a different fiber reinforcing architecture. Furthermore, the Li_2TiO_3 tritium breeding materials with suitable physical properties were fabricated by improvement fabrication method, which is expected to increase the efficiency of the fusion power reactor applied to the breeding blanket concept.

Research Activity

- Jong-Il Kim, Joon-Soo Park, Naofumi Nakazato, Hirotatsu Kishimoto, NITE-SiC/SiC複合材料の面内強度に及ぼす繊維強化構造の影響, 日本金属学会両北海道支部合同サマーセッション in Japan.
- Jong-Il Kim, Joon-Soo Park, Naofumi Nakazato, Hirotatsu Kishimoto, NITE-SiC/SiC複合材料の層間せん断強度に及ぼす繊維強化構造の影響、金属学会-2017 in Japan.
- Joon-Soo Park, Jong-Il Kim, Naofumi Nakazato, Hirotatsu Kishimoto, Shunsuke Makimura, Akira Kohyama, CVD方法によるSiCコーティングに及ぼすNITE-SiC/SiC複合材料の酸化挙動、金属学会-2017 in Japan.
- Jong-Il Kim, Joon-Soo Park, Naofumi Nakazato, Hirotatsu Kishimoto, Akira Kohyama, 多様な繊維強化構造を有するNITE-SiC/SiC複合材料の強度特性, Graduate of Muroran Insitute of Technology in Japan.
- Jong-Il Kim, Joon-Soo Park, Naofumi Nakazato, Hirotatsu Kishimoto, NITE-SiC/SiC複合材料の層間せん断特性、金属学会-2018 in Japan.
- Jong-Il Kim, Joon-Soo Park, Hirotatsu Kishimoto, Naofumi Nakazato, Takashi Nozawa, Inter-laminar strength of NITE-SiC/SiC composites with various fiber reinforcing architectures, 18th International Conference on Fusion Reactor Materials (ICFRM-18) in Japan .
- Joon-Soo Park, Jong-Il Kim, Naofumi Nakazato, Hirotatsu Kishimoto, Shunsuke Makimura, Akira Kohyama, Oxidation Resistance of NITE-SiC/SiC composites with CVD-SiC environmental barrier coat, 18th International Conference on Fusion Reactor Materials (ICFRM-18) in Japan.
- Jong-Il Kim, Joon-Soo Park, Byung-Min Kim, Naofumi Nakazato, Hirotatsu Kishimoto, Effects of fiber volume fraction and fiber reinforcing architecture on in-plane/inter-laminar strength of NITE-SiC/SiC composites, JCS-14 in Japan.
- Mu-Young Ahn, Seungyon Cho, Youngmin Lee, Soon Chang Park, Seok-Kwon Son, Yi-Hyun Park, Duck Young Ku, Chang-Shuk Kim, Jong-Il Kim, Dong Won Lee, Cheol Woo Lee, Seong Dae Park, Progress of HCCR TBM and its tritium extraction system development, 12th Internatinal Conference on Tritium Science & Technology (Tritium-12) in Korea.
- Yi-Hyun Park, Jong-Il Kim, Duck Young Ku, Mu-Young Ahn, Youngmin Lee, and Seungyon Cho, Fabrication of Li₂TiO₃ pebbles using nano-powder for tritium breeding material, 12th Internatinal Conference on Tritium Science & Technology (Tritium-12) in Korea
- Jong-Il Kim, Yi-Hyun Park, Mu-young Ahn, YoungMin Lee, Seungyon Cho, Effects of pyrolysis process on microstructure of Li₂TiO₃ tritium breeding materials during the sintering process, KCERS-2019, autumn in Korea.

- Jong-Il Kim, Yi-Hyun Park, Mu-young Ahn, YoungMin Lee, Seungyon Cho, Study on sintering conditions for Li_2TiO_3 tritium breeder pebbles, KCERS-2019 in Korea.
- Yi-Hyun Park, Jong-Il Kim, Mu-young Ahn, YoungMin Lee, Seungyon Cho, study of operating temperature of Li_2TiO_3 pebble bed for solid-breeding blanket according to the sintering phenomena, KCERS-2019 in Korea.
- Jong-Il Kim, Yi-Hyun Park, Mu-young Ahn, YoungMin Lee, Seungyon Cho, Effects of fiber reinforcing architecture on the inter-laminar strength of NITE-SiC/SiC composites, KCERS-2020, autumn in Korea.
- Jong-Il Kim, Yi-Hyun Park, Mu-young Ahn, YoungMin Lee, Seungyon Cho, Improvement in the slurry droplet wetting method, KCERS-2020, autumn in Korea.
- Jong-Il Kim, Yi-Hyun Park, Mu-young Ahn, Hirotatsu Kishimoto, YoungMin Lee, Seungyon Cho, Effects of Sintering Conditions on the Microstructure of Li_2TiO_3 Tritium Breeding Materials, 14th International Symposium on Fusion Nuclear Technology (ISFNT-14) in Hungary.
- Yi-Hyun Park, Jong-Il Kim, Mu-young Ahn, YoungMin Lee, Seungyon Cho, Maximum operating temperature for Li_2TiO_3 pebble bed by sintering phenomenon, 19th International Conference on Fusion Reactor Materials (ICFRM-19) in United States.
- Seungyon Choa, Mu-Young Ahn, Youngbum Chun, Hyung Gon Jin, Bum-Seok Kim, Chang-Shuk Kim, Jong-Il Kim, Suk Kwon Kim, Duck Young Ku, Cheol Woo Lee, Dong Won Lee, Eo Hwak Lee, Hyoung-Yon Lee, Youngmin Lee, Seong Dae Park, Soon Chang Park, Yi-Hyun Park, Chang Wook Shin, Seok-Kwon Son, Jae Sung Yoon, Sunghwan Yun, Status of HCCR TBM program for DEMO blanket, 31st Symposium on Fusion Technology (SOFT2020) in Online.

